

# **A THREE-DIMENSIONAL SPATIO- TEMPORAL VIEW OF MAJOR AEROSOL TYPES OVER INDIAN REGION**

WARIS HOODA  
September 2021

SUPERVISORS:  
Dr. Manu Mehta, ISRO  
Dr. Frank Osei Badu, ITC

# **A THREE-DIMENSIONAL SPATIO- TEMPORAL VIEW OF MAJOR AEROSOL TYPES OVER INDIAN REGION**

WARIS HOODA

Enschede, The Netherlands, September 2021

Thesis submitted to the Faculty of Geo-Information Science and Earth Observation of the University of Twente in partial fulfilment of the requirements for the degree of Master of Science in Geo-information Science and Earth Observation.

Specialization: Geo-Information Science and Earth Observation (Geoinformatics)

**SUPERVISORS:**

Dr. Manu Mehta, ISRO

Dr. Frank Osei Badu, ITC

**THESIS ASSESSMENT BOARD:**

Dr. Ir. A. (Alfred) Stein, ITC

Dr. Milap Punia, JNU

#### DISCLAIMER

This document describes work undertaken as part of a programme of study at the Faculty of Geo-Information Science and Earth Observation of the University of Twente. All views and opinions expressed therein remain the sole responsibility of the author, and do not necessarily represent those of the Faculty.

## ABSTRACT

Tiny particles suspended in air impact the Earth's atmosphere in direct and indirect ways; directly in terms of alteration of solar radiation and indirectly by modifying the cloud properties. The aerosols are of both natural and anthropogenic origin. The sources of natural aerosols are pretty much identified, and the transport mechanism is also well understood. However, a large uncertainty is found for anthropogenic aerosols both in terms of source and transport mechanism and is still an area of research. Because aerosols have a shorter atmospheric life, assessing their contribution to climate change is difficult. A complete 3-dimensional spatio-temporal view of aerosols can aid in a better understanding of climatic dynamics and climate change. The Indian region is most suited for such research due to its diversified terrain, high aerosol concentrations, and seasonal fluctuation. The study outlines seasonal and zonal variability along with trends of aerosol vertical distribution over India (which is one of the major aerosol hotspots), in terms of major aerosol types, i.e., dust, polluted dust and smoke. Specific analysis over the selected zones is also reported, along with two special cases, one each for dust and smoke aerosols. To study the three-dimensional spatio-temporal aerosol distribution, the Cloud-Aerosol Lidar and Infrared Pathfinder Satellite Observation (CALIPSO) datasets from 2007 to 2020 are used. Strict screening checks like Aerosol Layer Fraction, Atmospheric Volume Description, etc are applied to the CALIPSO dataset for quality retrieval. The work is supplemented by the Modern-Era Retrospective analysis for Research and Applications Version 2 (MERRA 2) reanalysis for comparison purposes. In general, higher extinction coefficients are observed to be concentrated close to the ground (above  $\sim 1$  km). Columnar trends of extinction profiles varied in the different regions, however, in general, found to be increasing in the higher altitudes regime, except during monsoons. The decreasing trend of extinction profiles during the monsoonal period could be primarily related to the decreasing trend of dust aerosols observed in the study area. Meteorological conditions and transit from the Thar Desert or the Arab region have heavily influenced dust dominance in the northern part of the Indian region during monsoon, as evidenced by Hybrid Single-Particle Lagrangian Integrated Trajectory Model (HYSPPLIT). During the pre-monsoon and monsoon, polluted dust has increased over the Indian region. An increasing trend of smoke aerosols is seen over the study area during December-February. In particular, changes in aerosol vertical distribution were also studied during the COVID-19 lockdown period of April-May 2020 in the Indian region, wherein a decrease in total extinction profiles has been observed over the majority of the Indian region.

## ACKNOWLEDGEMENTS

First and foremost, I want to express my appreciation to my esteemed supervisor, Dr. Manu Mehta, for her continuous support, patience, vast knowledge, and timely inspiration during my master's thesis research. Though, due to the lockdown, almost all of her research work was done virtually, it was because of her extra efforts, even after hours, that environment seemed much more real. Since graduation, I've had an interest in climate science and urban science. I had a reasonably steady hand at programming, but I am a newbie in the subject of climate science. It was because to my supervisor that I was able to gain a foothold in the field of climate research. Her smart approach and decisions to the complex problem during the research work will be lifelong learning for me.

I'd also want to thank my second supervisor Dr. Frank for his support and for adding a new perspective to the research. His teaching will be appreciated not only in the current study, but also in any future applications in the field of Earth Observation.

Special thanks to my best buddy Pradeep Yadav, who supported me right from under graduation through difficult times, encouraged me up, and celebrated each achievement with me. Thankyou Pradeep for being just one call away. I'd want to express my gratitude to everyone who helped me complete this research work. I am deeply grateful to my seniors for their timely advice

My sincere thanks to Dr. Sameer Saran for his support during the master's program. I really appreciate his support and extra efforts in managing the course when situation was difficult due to COVID in India as well as in The Netherlands.

I am grateful to my parents for their love, care, prayers, and struggles in order to provide me with a better life and a bright career. I'd want to express my gratitude to my mother for going above and beyond, even late at night, to ensure that I could work without disruption. It doesn't matter how much I thank her, it's still not enough.

# TABLE OF CONTENTS

---

Abstract.....	i
Acknowledgements.....	ii
Abbreviations.....	iv
List of figures.....	v
List of tables.....	vii
1. Introduction.....	1
1.1. Background.....	1
1.2. Research objective.....	3
1.3. Outline of thesis.....	4
2. Literature review.....	5
2.1. Background.....	5
2.2. Spatial distribution.....	9
2.3. Aerosol optical properties.....	9
2.4. Quantification of aerosols.....	10
2.5. Validation of CALIPSO data with other datasets.....	11
2.6. Current scenario of aerosols in India.....	11
3. Study area.....	14
3.1. Indian region.....	14
3.2. Indo-Gangetic Plain.....	20
3.3. Desert region.....	20
3.4. South India region.....	20
3.5. Arabian Sea.....	21
3.6. Bay of Bengal.....	21
4. Data and methodology.....	22
4.1. Dataset.....	22
4.2. Workflow.....	29
5. Results and discussion.....	31
5.1. Vertical distribution of aerosols over Indian land surface.....	31
5.2. Percentage fraction of aerosols over land surface.....	42
5.3. Vertical distribution of Aerosols over Oceanic Region.....	46
5.4. Percentage fraction of aerosols over ocean surface.....	50
5.5. AOD and MERRA2 comparison.....	53
5.6. Trend analysis.....	55
5.7. Trend analysis in altitude bins.....	59
5.8. Special Case: April-May 2020 COVID-19 lockdown case study.....	61
5.9. Special Case: Smoke cases of India.....	65
5.10. Vertical spatial autocorrelation:.....	67
6. Conclusion.....	68
List of references.....	73
Appendix - I.....	88
Appendix - II.....	89
Appendix - III.....	91
Appendix - IV.....	92

## ABBREVIATIONS

---

<b>Abbreviation</b>	<b>Expansion</b>
AERONET	Aerosol Robotic Network
ALF	Aerosol Layer Fraction
AOD	Aerosol Optical Depth
ARFINET	Aerosol Radiative Forcing Network
AVD	Atmospheric Volume Description
AVHRR	Advanced Very High-Resolution Radiometer
CAD	Cloud Aerosol Discrimination
CALIOP	Cloud-Aerosol Lidar with Orthogonal Polarization
CALIPSO	Cloud-Aerosol Lidar and Infrared Pathfinder Satellite Observation
CCN	Cloud Condensation Nuclei
DEM	Digital Elevation Map
DJF	December January February
FT	Free Troposphere
GCM	Global Circulation Model
HERA	Hybrid Extinction Retrieval Algorithm
HYPLIT	Hybrid Single-Particle Lagrangian Integrated Trajectory Model
IGP	Indo-Gangetic Plain
IPCC	Intergovernmental Panel on Climate Change
JJA	June July August
LULC	Land Use Land Cover
MAM	March April May
MERRA	Modern-Era Retrospective analysis for Research and Applications
MISR	Multi-angle Imaging Spectro Radiometer
NOAA	National Oceanic and Atmospheric Administration
PBAP	Primary Biological Aerosol Particles
PBLH	Planetary Boundary Layer Height
PDF	Probability Density Function
RCM	Regional Climate Model
SCA	Scene Classification Algorithm
SIBYL	Selective Iterated Boundary Locator
SNR	Signal-to-Noise Ratio
SON	September October November
TOA	Top of Atmosphere
VFM	Vertical Feature Mask

## LIST OF FIGURES

<b>Figure 1</b> Aerosol particle size distribution .....	6
<b>Figure 2</b> Koppen classification scheme for India .....	14
<b>Figure 3</b> Seasonal wind speed and direction (a, c, e, g) at 850 hPa (b, d, f, h) at 500 hPa.....	16
<b>Figure 4</b> Averaged Indian monsoon dates (a) 1961-2019 Monsoon Onset Dates (b) 1971-2019 averaged Monsoon Withdrawal dates.....	17
<b>Figure 5</b> Seasonal precipitation pattern of Indian region (a) MAM (b) JJA (c) SON (d) DJF .....	18
<b>Figure 6</b> (a) LULC Map of India (b) Indian region DEM.....	18
<b>Figure 7</b> Zonal classification map of India .....	19
<b>Figure 8</b> Extinction retrieval process (Adapted from (M. H. Kim et al., 2018)) .....	23
<b>Figure 9</b> CALIPSO aerosol subtyping scheme (Adapted from (M. H. Kim et al., 2018)) .....	25
<b>Figure 10</b> Screening checks used in (a) frequency of occurrence (b) extinction coefficient retrieval.....	29
<b>Figure 11</b> Methodology .....	30
<b>Figure 12</b> Seasonal nighttime extinction coefficient 532 retrievals and frequency of occurrence plots (a-b) Indian region (c-d) IGP region (e-f) Desert region (g-h) South India region.....	31
<b>Figure 13</b> Seasonal Total Aerosol Extinction (MERRA-2) .....	32
<b>Figure 14</b> Dust seasonal nighttime extinction coefficient 532 retrievals and frequency of occurrence plots (a-b) Indian region (c-d) IGP region (e-f) Desert region (g-h) South India region.....	34
<b>Figure 15</b> Dust diurnal difference of frequency of occurrence plots (a) Indian region (b) IGP region (c) Desert region (d) South India region .....	34
<b>Figure 16</b> Seasonal dust extinction at 550 nm (a) MAM (b) JJA (c) SON (d) DJF .....	35
<b>Figure 17</b> Polluted dust seasonal nighttime extinction coefficient 532 retrievals and frequency of occurrence plots (a-b) Indian region (c-d) IGP region (e-f) Desert region (g-h) South India region.....	37
<b>Figure 18</b> Polluted dust diurnal difference of frequency of occurrence plots (a) Indian region (b) IGP region (c) Desert region (d) South India region .....	37
<b>Figure 19</b> Polluted continental seasonal nighttime extinction coefficient 532 retrievals and frequency of occurrence plots (a-b) Indian region (c-d) IGP region (e-f) South India region.....	39
<b>Figure 20</b> Dust diurnal difference of frequency of occurrence plots (a) Indian region (b) IGP region (c) South India region.....	39
<b>Figure 21</b> Smoke seasonal nighttime extinction coefficient 532 retrievals and frequency of occurrence plots (a-b) Indian region (c-d) IGP region (e-f) Desert region .....	40
<b>Figure 22</b> Dust diurnal difference of frequency of occurrence plots (a) Indian region (b) IGP region .....	40
<b>Figure 23</b> Smoke Injection Height in IGP region (a) MAM season (b) SON season .....	41
<b>Figure 24</b> 0-2 km seasonal diurnal percentage fraction of aerosols (a-b) Indian region (c-d) IGP region (e-f) Desert region (g-h) South India region.....	44
<b>Figure 25</b> 2-4 km seasonal diurnal percentage fraction of aerosols (a-b) Indian region (c-d) IGP region (e-f) Desert region (g-h) South India region.....	45
<b>Figure 26</b> Diurnal seasonal extinction coefficient 532 retrievals and frequency of occurrence plots (a-b) Arabian Sea (c-d) Bay of Bengal .....	46
<b>Figure 27</b> Marine seasonal nighttime extinction coefficient 532 retrievals and frequency of occurrence plots (a-b) Arabian Sea (c-d) Bay of Bengal .....	47
<b>Figure 28</b> Marine diurnal difference of frequency of occurrence plots (a) Arabian Sea (b) Bay of Bengal .....	47
<b>Figure 29</b> Dusty marine seasonal nighttime extinction coefficient 532 retrievals and frequency of occurrence plots (a-b) Arabian Sea (c-d) Bay of Bengal.....	48
<b>Figure 30</b> Dusty marine diurnal difference of frequency of occurrence plots (a) Arabian Sea (b) Bay of Bengal.....	48
<b>Figure 31</b> Dusty seasonal nighttime extinction coefficient 532 retrievals and frequency of occurrence plots (a-b) Arabian Sea (c-d) Bay of Bengal.....	49
<b>Figure 32</b> Dust diurnal difference of frequency of occurrence plots (a) Arabian Sea (b) Bay of Bengal .....	49
<b>Figure 33</b> 0-2 km seasonal diurnal percentage fraction of aerosols (a-b) Arabian Sea (c-d) Bay of Bengal.....	52
<b>Figure 34</b> 2-4 km seasonal diurnal percentage fraction of aerosols (a-b) Arabian Sea (c-d) Bay of Bengal .....	52
<b>Figure 35</b> CALIPSO and MERRA 2 seasonal nighttime AOD .....	53
<b>Figure 36</b> CALIPSO and MERRA 2 seasonal nighttime dust AOD .....	54

<b>Figure 37</b> CALIPSO and MERRA 2 seasonal nighttime polluted dust AOD .....	54
<b>Figure 38</b> CALIPSO and MERRA 2 seasonal nighttime smoke AOD .....	54
<b>Figure 39</b> Extinction coefficient nighttime during lockdown and before lockdown in (a) Indian region (b) IGP region (c) South India region.....	61
<b>Figure 40</b> Dust extinction coefficient and frequency of occurrence during nighttime during lockdown and before lockdown in (a) Indian region (b) IGP region (c) South India region.....	62
<b>Figure 41</b> Polluted dust extinction coefficient and frequency of occurrence during nighttime during lockdown and before lockdown in (a) Indian region (b) IGP region (c) South India region.....	63
<b>Figure 42</b> HYSPLIT back trajectory analysis for IGP region (a) 7 May 2018 (b) 8 May 2019 (c) 10 April 2020 (d) 8 May 2020 .....	64
<b>Figure 43</b> Extinction coefficient and frequency of occurrence for (a-b) Polluted continental (day-time) (c-d) Elevated Smoke (nighttime) .....	65
<b>Figure 44</b> Latitudinal Cross-section view of Vertical feature Mask for (a-b) Polluted continental (c-d) Elevated Smoke.....	66
<b>Figure 45</b> HYSPLIT back trajectory analysis for IGP region (a) 8 November 2013 (b) 7 November 2017 .....	66
<b>Figure 46</b> Variogram for seasonal extinction profiles.....	67

## LIST OF TABLES

---

<b>Table 1</b>	Aerosol key properties (Adapted from (O. Boucher et al., 2013))	7
<b>Table 2</b>	Seasons in timeline in India	14
<b>Table 3</b>	Zone Details	19
<b>Table 4</b>	Lidar Ratio for aerosol types (V4.10) (Adapted from Kim et. al, 2018)	24
<b>Table 5</b>	Total number of files in each season and region	26
<b>Table 6</b>	VFM Data Resolution	26
<b>Table 7</b>	VFM quality checks (CALIPSO, 2006)	27
<b>Table 8</b>	MAM AOD trend	55
<b>Table 9</b>	JJA AOD trend	55
<b>Table 10</b>	SON AOD trend	56
<b>Table 11</b>	DJF AOD trend	56
<b>Table 12</b>	MAM Dust AOD trend	56
<b>Table 13</b>	JJA Dust AOD trend	57
<b>Table 14</b>	Polluted dust AOD trend (MAM and JJA)	57
<b>Table 15</b>	Polluted dust AOD trend (SON and DJF)	57
<b>Table 16</b>	SON Smoke AOD trend	58
<b>Table 17</b>	DJF Smoke AOD trend	58
<b>Table 18</b>	MAM Oceanic Aerosol AOD trend	58
<b>Table 19</b>	JJA Oceanic Aerosol AOD trend	59
<b>Table 20</b>	SON Oceanic Aerosol AOD trend	59
<b>Table 21</b>	DJF Oceanic Aerosol AOD trend	59
<b>Table 22</b>	Seasonal AOD (Total) trend	60
<b>Table 23</b>	Dust AOD trend	60
<b>Table 24</b>	Polluted dust AOD trend	60
<b>Table 25</b>	Smoke AOD trend	60
<b>Table 26</b>	Oceanic aerosol AOD trend	60



# 1. INTRODUCTION

## 1.1. Background

Tiny organic and inorganic particles of size range  $0.001\ \mu\text{m}$ – $10\ \mu\text{m}$  suspended in the Earth's atmosphere are referred to as aerosols. These small particles continue to be the most uncertain in estimating the changing energy budget of the Earth. One of the primary causes of climate change is the nature of aerosol particles. Although the climate has changed in past years, the study of anthropogenic emissions on climate change is important with a rise in human-produced aerosols. Aerosols from natural and anthropogenic sources are continuously discharged into the atmosphere. The sources of natural aerosols like sea salt, dust, volcanic ash are seas, deserts, volcanic eruptions, etc.; while the sources of man-made aerosols like smoke, polluted continental particles, etc. are vehicular emissions, biomass burning, industries, etc. Over most land surfaces, the atmosphere is loaded primarily by dust and smoke amongst all aerosol types and possesses high variability over space and time. 90 per cent of total aerosols are natural by origin, while 10 per cent of total aerosols are anthropogenic aerosols (Holz et al., 2009). These aerosols impact public health, visibility, ocean fertilization, Earth energy budgets, cloud formation, climate forcing, radiation flow, and hydrological flow (Graf, 2004; Haywood & Boucher, 2000; Langmann, 2007; K. M. Lau et al., 2006; Menon et al., 2002; Schult et al., 1997; Shen et al., 2021; Thompson et al., 1987). Further, cloud formation is also attributed to hydrophilic aerosol particles. Aerosol particles accumulate together to produce cloud condensation nuclei (CCN). Water vapour condenses and forms clouds around these nuclei (Albrecht, 1989; MO et al., 2004; Rosenfeld et al., 2008; Twomey, 1974). These clouds then carry the weather and link different global climatic systems. Anthropogenic origin aerosol accounts for 20 - 40% of AOD and 25 - 66 % of cloud condensation nuclei concentrations on a global scale (Masson-Delmotte et al., 2019).

The Earth's atmosphere is affected by aerosols in both direct and indirect ways. Depending on its size and chemical composition, each aerosol can absorb or release radiation. The heating and cooling of the atmosphere have a significant direct and indirect influence on the earth's climate. The immediate impact is the absorption of shortwave solar radiation, which results in global heating. While the indirect impact works against greenhouse gases by releasing longwave radiation, the indirect impact of aerosols is one of the most important uncertainties in the global climate model (Nebojsa Nakicenovic and Rob Swart (Eds.), 2000). The aerosol also indirectly impacts the microphysics of the cloud. The indirect effect results from the uneven distribution of aerosols throughout the surface, which is mostly driven by human activities. Currently, aerosols exert a negative climatic forcing, however, the amount of that forcing is significantly unclear (Forster et al., 2007), although the confidence level of the aerosol–radiation interactions mechanism remained high amongst numerous forcing mechanisms in the climate system in IPCC AR5 (Masson-Delmotte et al., 2019).

Calculating aerosol radiative forcing is more challenging than estimating greenhouse gas radiative forcing because aerosol mass and particle number concentrations fluctuate substantially in space and time. Apart from these factors, much of the uncertainty in calculating the radiative forcing is due to the vertical distribution of the aerosols (Forster et al., 2007; Guan et al., 2010; Zarzycki & Bond, 2010). Aerosols have a shorter life in the atmosphere than the main greenhouse gases, which accounts for much of the unpredictability. The higher the altitude, the longer the lifetime of aerosols. The longer is the lifetime of the aerosols, the farther they can travel. Therefore, precise spatio-temporal information is crucial to validate models and to better estimate the aerosol radiative impact in the vertically resolved profiles. The capacity to differentiate between natural and anthropogenic aerosols is also required when calculating radiative forcing.

Globally, numerous attempts have been made to assess the warming effects of aerosol absorption through modelling and satellite/ground monitoring (Alpert et al., 1998; Quijano et al., 2000; Satheesh et al., 2008). Satellites such as Moderate Resolution Imaging Spectroradiometer (MODIS), Ozone Monitoring Instrument (OMI), Suomi NPP (National Polar-orbiting Partnership), etc could only give columnar characteristics, thus studies were mostly focused on those properties (R. Kahn et al., 2017; R. A. Kahn et al., 2005, 2010; R. C. Levy et al., 2010). Similarly, studies using ground-based instruments like AERONET also focused on columnar properties of aerosols (Li et al., 2014; Prasad et al., 2007). However, there have been several attempts to use in-situ measurements of aerosol vertical profiles, but they have been constrained in either the time or space domain (Eck et al., 1999; Ellsworth J. Welton et al., 2002; Ganguly et al., 2009; Holben et al., 1998; Pathak et al., 2016).

Based on a sample of big past, current, or predicted future emitting economies, the IPCC's regional climate regime established eight geographical areas. India and China are the current emitting economies in the categorization, which captures the responses to two contrasting monsoonal paradigms. Especially in India, the source and kind of aerosols have varied in recent years because of the region's increasing industrialization. As the economy expands, so do emissions, and the region is now dominated by anthropogenic aerosols. According to recent studies, increasing trends of AOD is documented over the Indian region which is in line with the previous studies that recorded increasing anthropogenic activities in the region (Babu et al., 2013; Dey & Girolamo, 2010, 2011; Hsu et al., 2012; Mehta et al., 2016a, 2019, 2020; Mehta, Khushboo, et al., 2021; Mehta, Singh, et al., 2018a). The most recent one in India is the Great Smog of Delhi in November 2017. Further, high seasonal variability of aerosols types was observed in the region and different zones (Mehta et al., 2020). Considering the Indo-Gangetic Plains (IGP), which is most polluted region has a lot of seasonal fluctuation in terms of dust and smoke. Due to prevailing climatic conditions and anthropogenic activity, this area has a greater aerosol burden than the rest of the country (Ritesh Gautam et al., 2010). Each aerosol type has a distinct impact on the climate. During the pre-monsoon season, dust aerosol loading rises across northern and central India (Middleton, 1986; Prospero et al., 2002).

People residing in the Indo-Gangetic Plains face significant hazards during dust storms due to a 50–100% rise in concentration of ground-level Particulate Matter (Hegde et al., 2007; Prasad et al., 2007). A recent dust storm was in May 2018. High aerosol loadings can reduce visibility, and dust breakouts can be dangerous in dust-prone areas. Many recent studies indicate that dust particles that scatter and absorb solar energy before re-emitting long-wave radiation not only delay but impede the Monsoon (Y. Sun et al., 2012). The Elevated Heat Pump hypothesis, on the other hand, claims that warming of the mid-upper troposphere over the Tibetan Plateau with absorptive aerosols like dust or black carbon can strengthen the monsoon by improving up draft movement and speeding up moist transport of air from nearby oceanic bodies into northern India (K. M. Lau et al., 2006). Because of their direct and indirect effects on climate, anthropogenic particles have been a focal point for researchers all around the world. Furthermore, according to the IPCC's recently published AR6 assessment, anthropogenic aerosols are still a major component of climate change with medium to high confidence. Researchers across the world agree that anthropogenic aerosol forcing is to blame for the decline in monsoon precipitation. The Northern Hemisphere is experiencing a decrease in anthropogenic aerosols, while the South Asia region is experiencing an increase. The rising trend is linked to a decrease in precipitation during the monsoon season. This uncertainty due to the poor characterization of smoke aerosols. In the lockdown time (April to May 2020), the area had an improvement in air quality and gave opportunity to the researcher to understand above mentioned fluctuations and atmospheric dynamic. The aerosol loading in the country and IGP was substantially reduced (Mehta, Hooda, et al., 2021; M. K. Mishra & Rathore, 2021a; Pathakoti et al., 2020a; Thomas et al., 2021). In the vertical distribution, a significant decrease was also noted (Mehta, Hooda, et al., 2021). However, the distribution of aerosol types still needs to be studied to better understand the region's atmospheric dynamics.

Although physical properties such as size, mass, absorption, and dispersion are well understood, the influence and feedback on the system are not well established. This is largely due to the nonlinear spatial and temporal distribution of aerosols. Several field studies have been conducted, resulting in both process-level and descriptive knowledge about aerosols in various areas. Furthermore, regional variations in aerosol properties have been observed using several aerosol networks and satellite studies (Alpert et al., 1998; Quijano et al., 2000; Satheesh et al., 2008). Much work and study have gone into understanding the columnar characteristics of aerosols, our understanding of the vertical structure of aerosols is still restricted. The study of columnar variation alone is insufficient to explain the variations in the earth's climate and extreme weather events, which are mostly dependent on aerosol altitude. The chemical processes and interactions of these aerosols are affected by changes in temperature and altitude, which impact atmospheric processes (Cohen et al., 2018; Hua Wang et al., 2018). Correct assessment of the vertical distribution of aerosol particles is a crucial aspect for atmospheric correction in the field of remote sensing. A proper evaluation of vertical aerosol distribution is necessary to further improve Global Climate Models (GCM) and Regional Climate Models (RCM) predictions. Since aerosols have shorter atmospheric life, small changes in these aerosol concentrations in the atmosphere have a huge impact on the climate system, causing bias and uncertainty in GCM and RCM (Laprise, 2008; Rummukainen et al., 2015). Because global scale models do not account for regional variability, they cannot be directly downscaled to RCM to forecast future climate and projections in the region. The uncertainty is primarily attributed to fluctuation in concentrations of aerosols in the atmosphere due to shorter life. As a result, a detailed region-specific investigation is needed to understand the aerosol consequences in the atmosphere.

The high spatial variability both in terms of columnar & vertical distribution and interaction of aerosols with the environment is still an area of research. Previously the studies only focused on columnar properties of aerosols with launch of CALIPSO satellite research were conducted on vertical distribution too especially in Indian region. However, such studies were on a shorter temporal scale. The current work of “Three-dimensional Spatio-temporal view of major aerosol types over the Indian Region” attempts to present a comprehensive detailed 3-D view of aerosol types. The study also determines the diurnal variability across different seasons and trends over different parts of the Indian region. The next section defines the work objectives.

## 1.2. Research objective

1. To analyse the decadal seasonal variability of dust and smoke in the Indian region on a spatio-temporal scale.

The objective will be focused on the analysis of day and night aerosol vertical profiles during the period 2007-2020 for major aerosol types. The findings could be biased during the daytime due to the high SNR which shall also be discussed. Also, some uncertainty could be due to the instrument calibration and lidar ratio for aerosol types. To this end, a comparative study is to be performed in the following objective.

2. To analyse seasonal changes in dust and smoke loadings from CALIPSO and comparison with previous findings and reanalysis datasets.

The results reflect the spatial-temporal vertical distribution of aerosols. The seasonal mean extinction (2007 - 2020) coefficients calculated for total aerosol and aerosol types are analysed. Some case studies like the comparison of aerosol loading over the Indo-Gangetic Plain during the lockdown period (April-May 2020) and April-May 2015-19 averaged data will also be attempted. The frequency of occurrence of different aerosol types will be analysed for different seasons in the

region and special cases. Later, the HYSPLIT model will be used to trace the source of aerosol particles during extreme loading periods. Finally, the results will be compared using MERRA 2 datasets.

3. To study the zonal distribution of the aerosols across different seasons.

The objective is to find the dominant aerosols in different regions of India. The work discusses the vertical distribution of different zones and then compares them with the Indian region distribution. Seasonal trends are presented for each zone.

### 1.3. Outline of thesis

**Chapter 2** gives detailed information on the present aerosol situation and its optical depth globally and in the study region through various satellites and ground measuring techniques. Some preliminary studies on prior attempts of aerosol vertical distribution are also discussed. Chapter 2 also provides a brief understanding of the aerosol properties. The area of study and the distinct zones are described in **Chapter 3**. Details such as geography, kinds of aerosols and potential sources of aerosols are discussed. **Chapter 4** discusses details of satellite data used in the research work. In addition, here you will find information regarding the data sets of reanalysis dataset. **Chapter 5** discusses the aerosol vertical distribution and its types using Level 2 data from CALIPSO. In the subsequent paragraphs in the chapter, the trend analysis is discussed. The vertical distribution and trend analysis are also discussed for various zones of the study area. Brief discussion on frequency of occurrence for different aerosol types in the study area and various zones in study region is there in the chapter. Later in the chapter, a comparison of CALIPSO AOD with MERRA 2 AOD is presented. For extreme events, a source trajectory is discussed. To the end of the thesis, a quick overview of the attempted study work and key points were noted in **Chapter 6**. The future scope of the current research work is also highlighted in the chapter.

## 2. LITERATURE REVIEW

### 2.1. Background

The atmosphere of the Earth is characterized as the layer of gases around the planet that is sustained by the Earth's gravity. The atmosphere of the Earth consists largely of two groupings. The first category comprises gases of almost stable concentrations, whereas the second group includes particles with fluctuating concentrations. Clouds and atmospheric aerosol particles vary widely in the Spatio-temporal domain are included among other atmospheric components. Aerosols are suspensions with significantly different chemical composition and distribution of size for fluid, solid or mixed particles, except for the pure form of water (Putaud et al., 2010). The atmospheric lifetime of these suspended particles is a minimum of 1 hour to be called aerosol. There are diverse chemical components present in particles in the environment. These components are peculiar to the development and the origin of particles and may develop rapidly during condensation, coagulation, and photochemical processes during atmospheric movement. The primary composition of atmospheric aerosols is inorganic particles, organic particles, black carbon, mineral particles, and PBAPs (O. Boucher et al., 2013). The inorganic species include particles such as nitrate, sulphate, ammonium, sea salt. Black Carbon is a specific kind of carbonaceous material produced by incomplete or partial combustion under particular conditions of fossil fuels and biofuels. Aerosols like sea salt, mineral dust, black carbon, and PBAPs are pumped into the atmosphere as primary particles while ammonium, sulphate, nitrate, and non-sea-salt are injected into the secondary aerosol particles formation process. These aerosols are injected into the atmosphere from multiple sources and can have a shorter or longer lifespan. Aerosol particles can be carried and transformed from one mode to another in the atmosphere as an outcome of physiochemical processes and climatic circumstances. Aerosol particle sizes vary dramatically, ranging from a few nanometres to several hundreds of micrometres. During the condensation phase, the gases in the environment are absorbed by aerosol particles, forcing them to grow bigger. Coagulation processes, in which two or more particles come into contact and aggregate together, can also cause particles to increase in size. Inverse processes, such as abrasion or evaporation, can result in a reduction in particle diameter. In general, multiple size modes describe the aerosol size distribution, each with its own set of sources, transformations, and removal processes. The primary distinction is between the fine and coarse modes (particle diameter  $D_p < 1 \mu\text{m}$  and  $D_p > 1 \mu\text{m}$ , respectively) (Olivier Boucher, 2015; Sundström et al., 2009). Gravitational settling is the most significant removal procedure for the coarse mode because of its bigger size and mass. As a result, brief residence periods in the environment are typical of this mode. Separation of the nucleation, aitenken, and accumulation modes is another split of the fine mode. The details are described in Figure 1 and Table 1. These particles may influence Earth's radiation budget, that is, if they have sizes larger than 100 nm in diameter, they can disperse solar radiation, or some can absorb and alter solar energy like black carbon. Aerosol particulates may form droplets at specific supersaturation circumstances by condensing the water vapour on their surface, which relies on the chemistry and the size of the aerosol particles (Andreae & Rosenfeld, 2008). If particles have a diameter of more than 50 nm, they can behave as CCN. An upsurge in the aerosol concentration in the atmosphere usually leads to higher levels of CCN and cloud droplets, leading to higher levels of cloud albedo. Understanding the aerosol particles chemical composition is essential, as it can significantly affect the particles optical properties. Many aerosol components are hygroscopic, and when relative humidity (RH) increases, aerosols absorb water, and due to the swelling effect, the diameter of aerosol particles increases (Cheng et al., 2008). As a result, relative humidity influences the optical characteristics of aerosol particles (Zieger et al., 2013). The impact of RH on aerosol scattering is determined by the size of the aerosol particle and the chemical composition, since

these two parameters affect the scattering characteristics and the of aerosol particles capacity to absorb water.

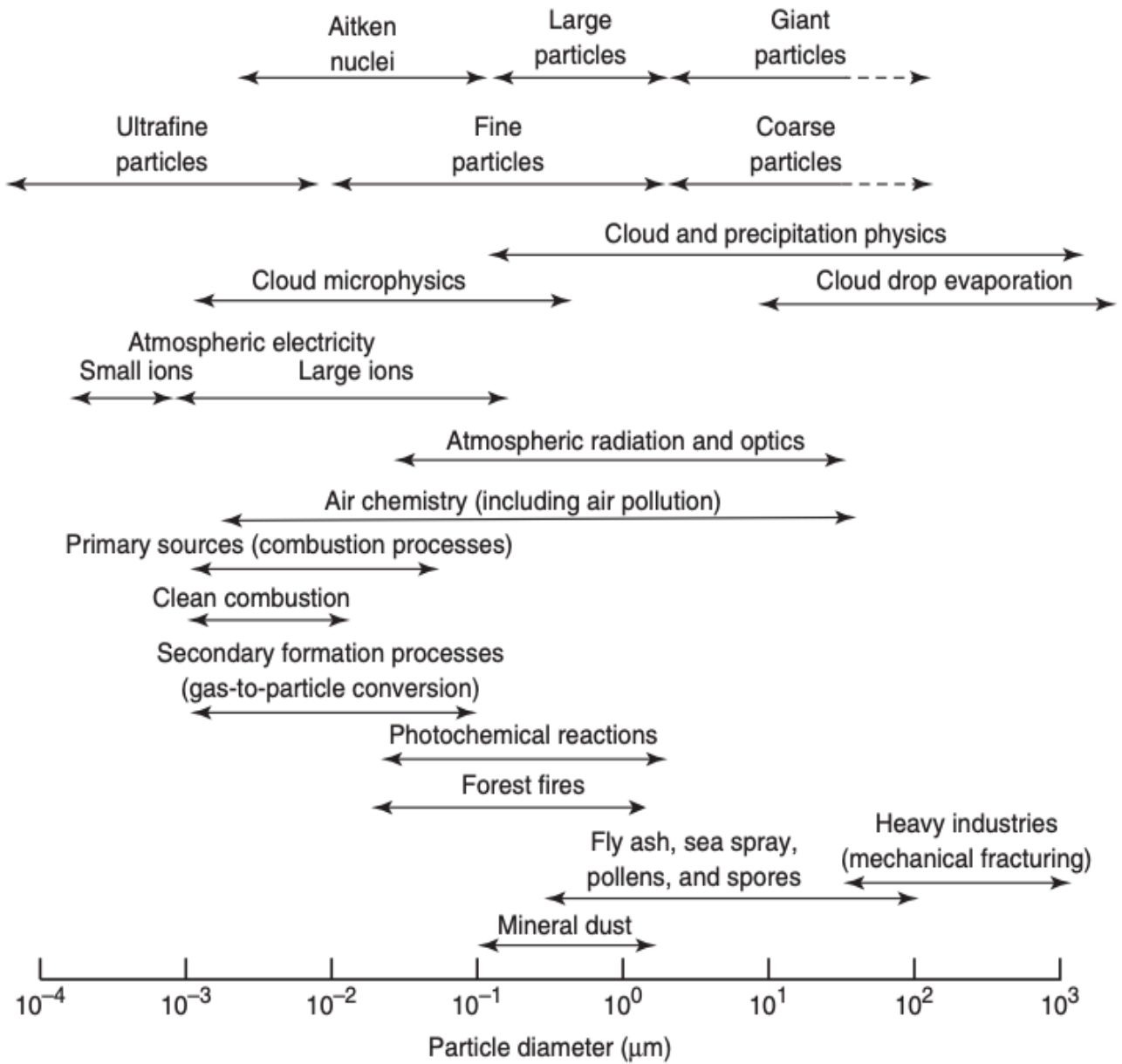


**Figure 1** Aerosol particle size distribution

(Adapted from (Tomasi et al., 2017) )

**Table 1** Aerosol key properties (Adapted from (O. Boucher et al., 2013))

Aerosol Type	Particle size	Major source	Main Sink	Atmospheric lifetime (Troposphere)	Key Climate Relevant Properties
Sulphate	Primary: Aitken, accumulation and coarse modes Secondary: Nucleation, Aitken, and accumulation modes	Primary: marine and volcanic emissions. Secondary: oxidation of SO <sub>2</sub> and other S gases from natural and anthropogenic sources	Wet deposition Dry deposition	~ 1 week	Light scattering. Very hygroscopic. Enhances absorption when deposited as a coating on black carbon. Cloud condensation nuclei (CCN) are active.
Nitrate	Accumulation and coarse modes	Oxidation of NO <sub>x</sub>	Wet deposition Dry deposition	~ 1 week	Light scattering. Hygroscopic. CCN active.
Organic aerosol	POA: Aitken and accumulation modes. SOA: nucleation, Aitken, and mostly accumulation modes. Aged OA: accumulation mode	Combustion of fossil fuel, biofuel, and biomass. Continental and marine ecosystems. Some anthropogenic and biogenic non-combustion sources	Wet deposition Dry deposition	~ 1 week	Light scattering. Enhances absorption when deposited as a coating on black carbon. CCN active (depending on aging time and size).
Black Carbon	Freshly emitted: <100 nm Aged: 0.1 - 2.5 μm	Combustion of fossil fuels, biofuels, and biomass	Wet deposition Dry deposition	1 week to 10 days	Large mass absorption efficiency in the shortwave. CCN is active when coated. May be ice nuclei (IN) active.
Mineral dust	Coarse and super-coarse modes, with a small accumulation mode	Wind erosion, soil re-suspension. Some agricultural practices and industrial activities (cement)	Sedimentation Dry deposition Wet deposition	1 day to 1 week depending on size	IN active. Light scattering and absorption. Greenhouse effect.
Sea spray	Coarse and accumulation modes	Breaking of air bubbles induced e.g., by wave breaking. Wind erosion.	Sedimentation Dry deposition Wet deposition	1 day to 1 week depending on size	Light scattering. Very hygroscopic. CCN active. Can include primary organic compounds in a smaller size range

## 2.2. Spatial distribution

Aerosol particles can change their physical and chemical characteristics in accordance with vertical and horizontal fluctuations. The horizontal variability in the lower layers of the atmosphere is significant because of the aerosol's highly variable lifespan (varying between a few days to weeks). The sources of these aerosols are spread unequally across the planet. The diverse atmospheric processes contribute to transport up to shorter and longer distances from the emission source. Depending on their size and weight, aerosol particles are therefore exposed to sedimentation or diffusion (dry deposits) or leaching, during precipitation (wet deposition). The aerosol's vertical variability is equally essential and determined by the atmospheric thermodynamic structure.

Depending on flux or temperature variations, the atmosphere might split into various strata. Therefore, we may divide between the troposphere (roughly 0 to 15 km), stratosphere (between 15 and 50 km), mesosphere (between 50 and 85 km), thermosphere (between 80 and 500 km), and exosphere beyond these layers. The troposphere thus contains the bulk of aerosol particles, where 80 per cent of the air mass is located (Seinfeld & Pandis, 2016). The troposphere can split into two distinct sub-layers: the Boundary Layer (BL) and Free Troposphere (FT). BL is near the Earth and therefore immediately affects the Earth's surface and responds to surface forcing within a time frame of less than an hour (Stull, 1988). In reaction to convection, the BL is formed in the daytime, normally known as a mixed convective layer. Before sunset, as turbulence diminishes, the mixed convective layer is converted to the residual layer (RL) (Hodzic et al., 2004). The RL has comparable characteristics to the mixed layer in terms of both mean state and concentration variables.

## 2.3. Aerosol optical properties

### 2.3.1.1. Extinction Coefficient E

Extinction Coefficient is the amount to which the light attenuates through the atmosphere because of aerosol particle dispersion and absorption. Lambert Beer's Law describes the impact of extinction (aerosols and molecules) in the atmosphere. Radiation intensity ( $I$ ) can be measured using the formula:

$$I = I_0 \exp(-El),$$

Where,

$I_0$  is the radiation intensity at the source  
 $l$  is the length of the medium.

The extinction coefficient is measured in  $m^{-1}$ .

### 2.3.1.2. Aerosol Optical Depth

Optical depth refers to the amount of light that is dispersed or absorbed by a medium from a beam. The integrated extinction coefficient is the summation of all extinctions in a column in a given cross-section.

The greater the AOD, the larger the number of aerosols in a column. AOD is a critical parameter in calculating and comprehending the variability of the energy budget of earth on a longer spatio-temporal scale. (O. Boucher & Haywood, 2001; O. Boucher & Tanré, 2000; Carslaw et al., 2013; Charlson et al., 1992; Miller et al., 2004; Ramanathan et al., 2001).

### 2.3.1.3. Angstrom Exponent

Angstrom Exponent ( $\alpha$ ) is a parameter that defines how the optical thickness of an aerosol usually varies with the light wavelength. Approximation of the spectral dependence on AOD is calculated using:

$$\tau = \beta \lambda^\alpha$$

Where  $\beta$  is the optical aerosol depth of  $1\mu\text{m}$ .

Inversely, the Angstrom Exponent is linked to the average size of the aerosol particles: the smaller the particles, the bigger the exponent. For example, cloud droplets are generally big, and so the Angstrom Exponent (almost nil) is very tiny in clouds, and the wavelength does not affect the optical depth. This is why it seems like the clouds are white or grey. This relationship may be used to determine an aerosol particle size by measuring its optical depth at various wavelengths.

## 2.4. Quantification of aerosols

### 2.4.1.1. Ground-based measurement

There have been numerous investigations all around the world using a variety of ground-based aerosol measurement instruments as part of global/regional networks like the Aerosol Robotic Network (AERONET), AFRINET, Micro-Pulse LIDAR Network (MPLNET) (Eck et al., 1999; Ellsworth J. Welton et al., 2002; Ganguly et al., 2009; Holben et al., 1998; Pathak et al., 2016). Ground-based measurements give more precise and continuous data though, they are spatially limited. However, investigations employing on-site equipment are crucial for satellite data validation.

### 2.4.1.2. Atmospheric research based on satellites

The increasing capability of satellite remote sensing gives an unparalleled opportunity to deepen our knowledge of the aerosol impact on the climate system. In-situ aerosol measurements are more accurate but are restricted to point observations (Sundström et al., 2009) (Sundström et al., 2012). On the other hand, satellite data offers complete planetary information. As a result, satellite data is critical for understanding the spatial variability of the climate system. With advancements in instrumentation, numerous satellites launched for various purposes. Some of those that focused on estimating aerosols in the atmosphere are Moderate-resolution Imaging Spectroradiometer (MODIS) onboard Terra/Aqua, Multi-Angle Imaging Spectroradiometer on Terra (MISR), Ozone Mapping Instrument (OMI) onboard Aura, and AVHRR on NOAA series (R. A. Kahn et al., 2005; Robert C. Levy et al., 2007; L. A. Remer et al., 2005). In satellite remote sensing, particularly aerosol optical depth (AOD) from passive sensors such as the Moderate-resolution Imaging Spectroradiometer (MODIS) and Multiangle Imaging Spectroradiometer (MISR), have resulted in strong observational constraints for the aerosols direct effect on solar radiation at the top-of-atmosphere (TOA) (Al-Saadi et al., 2005; Lorraine A. Remer et al., 2006; Yu et al., 2006). Aerosol optical depth estimations derived from satellite data have also been used in monitoring networks for air quality forecasting and give observation-based estimates of long-range aerosol transport. Passive sensors do nevertheless, in cloud-free settings, provide overall column amounts with no information on the vertical distribution of aerosols except the height of the plume (R. A. Kahn et al., 2007; Pierangelo et al., 2004). The measurements of passive sensors are affected by the surface conditions. Until the deployment of active space-borne sensors, the vertical distribution of aerosol could not be assessed systematically over the globe. One of the first fully operational active sensors is CALIOP onboard Cloud-Aerosol Lidar and Infrared Pathfinder Satellite Observations (CALIPSO) (David M. Winker et al., 2003). CALIOP is an excellent platform for aerosol investigation because of the high-resolution solution imaging vertical profiles and

precise depolarization measurements. It offers an opportunity to compare model simulations on global and yearly vertical aerosol distributions. The satellites are focussing on aerosols is aligned into a constellation to obtain coherent data for intercomparison. The “A-train” series of satellite sensors is one such example that brings the capability for detecting air pollution from space (Anderson et al., 2005). Presently, the A-train consists of several satellites (Aura, PARASOL, CALIPSO, CloudSat, Aqua) equipped with both passive (e.g. POLDER, TES, OMI, MODIS, CRES) active (e.g., CALIOP and CPR) sensors, which provide estimations of clouds, aerosols and trace gases. Moreover, there are variations due to the algorithm differing backscatter-to-extinction ratios. CALIOP correctly identifies the aerosol type, as evidenced by comparisons with the Angström Exponent and AERONET aerosol size distribution data.

## 2.5. Validation of CALIPSO data with other datasets

(Mielonen et al., 2009) reported that 70% of the daily mean aerosol types were agreed upon by the CALIPSO and AERONET sensors. Aerosols like polluted dust which is mixed absorbing and dust which is of coarse type shown the best agreement, 53 per cent and 91 per cent, respectively. However, it was more challenging to distinguish fine aerosols. For fine mode absorbing and non-absorbing aerosol types, the agreement was 37 per cent and 22 per cent, respectively. Giles et al. 2012 also statistically validated the V4 data of CALIPSO with ground-based instruments (Mielonen et al., 2009; Ali H. Omar et al., 2005) have used AERONET data extensively to classify aerosol types. The sensors data may be validated or compared using reanalysis models/datasets (Buchard, Randles, Silva, et al., 2017; Proestakis et al., 2018).

## 2.6. Current scenario of aerosols in India

Several investigations in the Indian region have been carried out in recent years to explore the optical properties of aerosols and effect evaluations (Aloysius et al., 2008; Badarinath, Kumar Kharol, et al., 2009; Dey & Di Girolamo, 2011; Gogoi et al., 2008; Kedia et al., 2014; Mehta, Sharma, et al., 2018; Mehta, Singh, et al., 2018b; Mehta et al., 2016a, 2019, 2020; Mehta, Hooda, et al., 2021; Mehta, Khushboo, et al., 2021; Moorthy et al., 2013; S. S. Prijith et al., 2013; Ramachandran & Kedia, 2010; Ramanathan et al., 2007; Satheesh et al., 2008; Satheesh & Krishna Moorthy, 2005). Due to diverse topography and recent high industrial development, the Indian region experiences high aerosol loading and intra-seasonal variability among aerosol subtypes. In terms of loading and aerosol subtypes, aerosols above the IGP experience considerable seasonality (Aloysius et al., 2008; Jethva et al., 2005; Kaskaoutis et al., 2014; Kedia et al., 2014; K.-M. Lau et al., 2008).

Mineral dust has a significant contribution to tropospheric aerosol loading, impacting the seasonal variability of global and regional radiative forcing (Tegen & Miller, 1998). The northwest side of the Thar Desert is a major source of mineral dust in the Indian atmosphere. Dust storms, a common climatic phenomenon in India, are also known to originate from this region (Middleton, 1986). Dust activity begins pre-monsoon and peaks in May, just before the arrival of the southwestern monsoon. The predominant western airmass generates substantial dust mineral aerosol flow from the Arab region to the Indian desert. The dust particles then mix with fine mode particles in the IGP (Middleton, 1986; Prospero et al., 2002). (R. Gautam et al., 2009) mapped the dust transport using MODIS, OMI, and TOMS data. Some researchers also reported that due to the transportability of dust particles to long distances, dust in India is transported from Afghanistan, Pakistan, and the Arabian Peninsula owing to prevailing wind conditions and impacts Indian climate system (Das et al., 2013; Dey et al., 2004; Middleton, 1986; Pandithurai et al., 2008). The high Himalayas make it difficult for dust storms to pass through and accumulate dust at the foothills of the Himalayas and in the IGP. Due to which there is high AOD in the region before monsoon (R. Gautam et al., 2009; Pant et al., 2006; Singh et al., 2004). However, (A. Pandey et al., 2017) reported a declining trend of dust in IGP. The inter-annual changes in dust distributions over source as well as the transported areas of the Gangetic Plain to net atmospheric aerosol loading are not precisely understood (Dey et al., 2004; Pandithurai et al., 2008; Prasad et al., 2007; Ram et al., 2010; Singh et al., 2004). Some recent studies suggest that mineral dust influence cloud microphysical properties and cloud lifetime. This in turn causes fluctuations to the radiative energy balance, may also potentially induce changes in the global hydrological cycle, particularly over the

Indian subcontinent, which receives the majority of the annual precipitation during the summer (K. M. Lau et al., 2006; Miller et al., 2004; PJ et al., 2006). Apart from the Indian landmass, the north-south difference is characteristic of the Arabian Sea aerosol distribution throughout the MAM season (Kaskaoutis et al., 2014; Satheesh & Srinivasan, 2002). Over the Indian subcontinent, a similar aerosol loading pattern prevails, with a higher gradient from north to south.

During the winter months and post-monsoon, the IGP region experiences extreme anthropogenic pollution, which is dominated by particles of fine mode. The Great Smog of Delhi in November 2017 was among the most recent and significant events. The major contribution during SON and DJF is from fine-mode pollution aerosols (such as sulfate and soot) to enhanced aerosol optical depth. In the Indian states of Punjab, Haryana, and western Uttar Pradesh, substantial paddy residue burning occurs each year in post-monsoon time (October-November) (Badarinath, Kharol, et al., 2009; Badarinath, Kumar Kharol, et al., 2009; Kaskaoutis et al., 2014; Kharol et al., 2012; A. R. Sharma et al., 2010). Emissions from the burning regions in IGP migrate from Punjab side to Bay of Bengal owing to meteorological conditions. MODIS AOD reported by (Kharol et al., 2012) during the biomass burning from mid-October to mid-November 2012 in the region was above 1.5 while the smoke plumes were carried within the BL and <2–2.5 km, according to CALIOP profiles. Several more studies have been carried out reporting a thorough analysis of AOD and vertical distribution over the IGP during JJA (Kaskaoutis et al., 2014; A. K. Mishra & Shibata, 2012a, 2012b). Sometimes the Arabian Sea and Central South India also have received a negative influence due to biomass burning from the IGP region, depending on wind speed and direction (Badarinath, Kharol, et al., 2009; Badarinath, Kumar Kharol, et al., 2009). In the past, Atmospheric Brown Clouds have been observed in the Indian region (Carmichael et al., 2009). The Atmospheric Brown Clouds consist of dust, soot, sulfates, organic substances, etc. that are formed due to the mixing of aerosols of anthropological and natural origin. Brown Clouds were found to have a significant role in solar dimming (Bollasina et al., 2008; Ramanathan & Ramana, 2005; Randles & Ramaswamy, 2008; Tripathi et al., 2007), and atmospheric heating as well as stability and hydro-hydrological cycles. The relationship between aerosol and cloud due to burning biomass, either on land or seas, is an unclear and intricate phenomenon that relies heavily on vertical distribution between aerosols and clouds, on their relative height (Koch & Del Genio, 2010)

There is a high variability of aerosols over the different regions within India due to local sources and prevailing meteorological conditions. Thorough research of seasonal variations of AOD across India, utilizing satellite-based sensors, such as MODIS, over the period 2001-2013, was given by (Mehta, 2015). For instance, throughout the winter in northern India, there has been a rising trend of aerosols. Similar trends were noted during the use of grounded instruments by (Babu et al., 2013). Again, a variable trend in the IGP region during monsoon was observed by both (Mehta, 2015) and (Babu et al., 2013). (Babu et al., 2013) used AOD from ARFINET and AERONET instruments. The variability is due to offset by the extensive wet removal through the monsoonal rainfall. The region's tropospheric column is loaded with natural sources such as aeoline transported dust via IGP and marine aerosols throughout India's peninsular region. In the pre-monsoon season, statistically significant increases in trends were observed for the parts of the south Indian region which was also reported by (Babu et al., 2013). Similar trends were reported over India during 2000-2010 using MISR (Dey & Di Girolamo, 2011). A few studies conducted over the Bay of Bengal and the Arabian Sea (Kedia & Ramachandran, 2009; Lakshmi et al., 2017; Sudhakaran Syamala Prijith et al., 2018; R. Srivastava, 2017) reported an increase in AOD while a decrease in dust concentration over the Bay of Bengal during pre-monsoon. (Sudhakaran Syamala Prijith et al., 2018) reported an increasing AOD trend in oceanic regions. In pre-monsoon and summer season, transportation of aerosols over the Arabian Sea has also increased and has helped to improve AOD. While in June, there is an increase in aerosol transport to the Arabian Sea from north-western continental regions up to 3 kilometres above sea level through the lower troposphere. It is noted that the transport is predominantly above 3 km in April.

All the studies discussed above and attempted by the researchers using column integrated values could not explain the vertical distribution of aerosol. Aerosol, depending upon the constituent material properties and meteorological conditions, can uplift to different altitude levels. For example, smoke from biomass burning tends to elevate to higher altitudes while particles of vehicular emission remain confined to lower altitudes depending upon the boundary layer conditions. The concentration of different aerosol types varies at different altitudes, depending upon which they play a significant role in the climatic process. Therefore,

understanding the variations in the columnar distribution along with vertical distribution of aerosol over a longer spatial-temporal scale is critical in the current changing climatic scenario (Huneeus et al., 2012; Nabavi et al., 2016; Schulz et al., 2006; D. M. Winker et al., 2013).

Several researchers in many parts of the world have used a combination of ground and aerial lidar sensors to study the vertical distribution of aerosols (Cavalieri et al., 2010; Jayaraman et al., 2006; Mona et al., 2012; Navas-Guzmán et al., 2013; Solanki & Singh, 2014). A few studies focused on the aerosol vertical distribution using CALIPSO satellite, considering both spatial and temporal aspects together. However, using space-borne instrument CALIOP on CALIPSO few studies have been conducted considering both spatial and temporal aspects together. Huang et al. (2013) used a 5-year CALIOP data but attempted for the whole Indian area as one domain utilizing level 3 data, at coarse spatial resolution. The seasonal fluctuation of the aerosol extinguishing patterns was reported. The gradient in the aerosol vertical distribution over India was shown by (S. S. Prijith et al., 2016), using CALIPSO data, during the period 2006 to 2013. (Mehta, 2015) also have documented worldwide trends in the primary aerosol categories using CALIOP lidar monthly level 3 datasets at rough resolution. In tropospheric section of atmosphere over India region, researchers observed a rise in yearly aerosol concentrations but did not consider seasonality. (Kulkarni & Sreekanth, 2020), however, also utilized the coarsest Level 3 data and trend estimates, to investigate further the seasonal variability of large kinds of aerosol throughout the various Indian regions.

A comprehensive study was undertaken by (Mehta et al., 2020) to study the decadal-scale vertical distribution of aerosol over the Indian Mainland. The work is validated with MODIS(Aqua/Terra). In the work, seasonal vertical distribution over five different cities in different regions was presented. Furthermore, the trends were presented in top altitudes and lower altitudes. For example, an increasing trend in lower altitudes in Delhi while in Patna an increasing trend was observed in both upper and lower altitudes. Size distribution of aerosols at upper and lower altitudes were also reported. For example, fine mode and spherical particles were more dominant during winter in both altitude bins, which is in line with the anthropogenic aerosol size emitted due to burning of biomass in the region.

As a result of a heterogeneous blending of the optical and physiochemical characteristics (CLAQUIN et al., 1998), and of their geographic, vertical, and time distributions, there is a considerable amount of ambiguity surrounding the part dust-aerosols play in climatic variability (Sarra et al., 2001; D. Sharma et al., 2012). There have been few investigations on the vertical profile of aerosols at a coarser resolution in oceanic areas. Therefore, to better understand the role of different aerosol type involvement in climate feedback, we need to simulate their vertical distribution over a longer time period in various areas.

In addition, the lockdown due to COVID-19 enabled the researchers to better explore the dispersion of natural and anthropogenic aerosols in the atmosphere. Multiple studies have been undertaken in terms of columnar distribution, i.e. AOD, and vertical distribution of these distributions, with substantial decreases in aerosol loading in the region observed (Mehta, Hooda, et al., 2021; Pathakoti et al., 2020b). In addition, diurnal variability of aerosol vertical distribution over India was presented. It is noted that there was a significant reduction in aerosol concentration at 0-0.5 km altitude. The paper also included an AOD inter-comparison of MODIS(Aqua), OMI(Aura), MERRA2, and CALIOP(CALIPSO) data for various areas. Few studies are done on vertical distribution of aerosol in the India region to estimate the dominance of natural aerosols without human intervention. However, vertical profiling of aerosol types over the different zones needs attention.

### 3. STUDY AREA

#### 3.1. Indian region

India occupies the Asian mainland's south-central peninsula. The Indian mainland is between a latitude of 8°4' N and 37°6' N and a longitude of 68°7' E and 97°25' E. The total area of India is 32,87,263 sq. km which is approximately 2.4% of the Earth surface. India is 3214 km north-south and 2933 km east-west. India is surrounded by three oceans. India on the west side is surrounded by the Arabian Sea, onto the east coast Bay of Bengal, and in the south by the Indian Ocean.

Based on the geomorphology of the landmass, India is divided into six physiographic regions. The regions are the Himalayas, Thar Desert, Peninsular Plateau, Indo-Gangetic plains, Coastal plains, and Islands. However, based on Köppen climate classification, India has nine climatic zones/subtypes, ranging from dry desert in the west to alpine tundra and glaciers in the north, and humid tropical areas sustaining rainforests in the southwest and island territories (Figure 2).

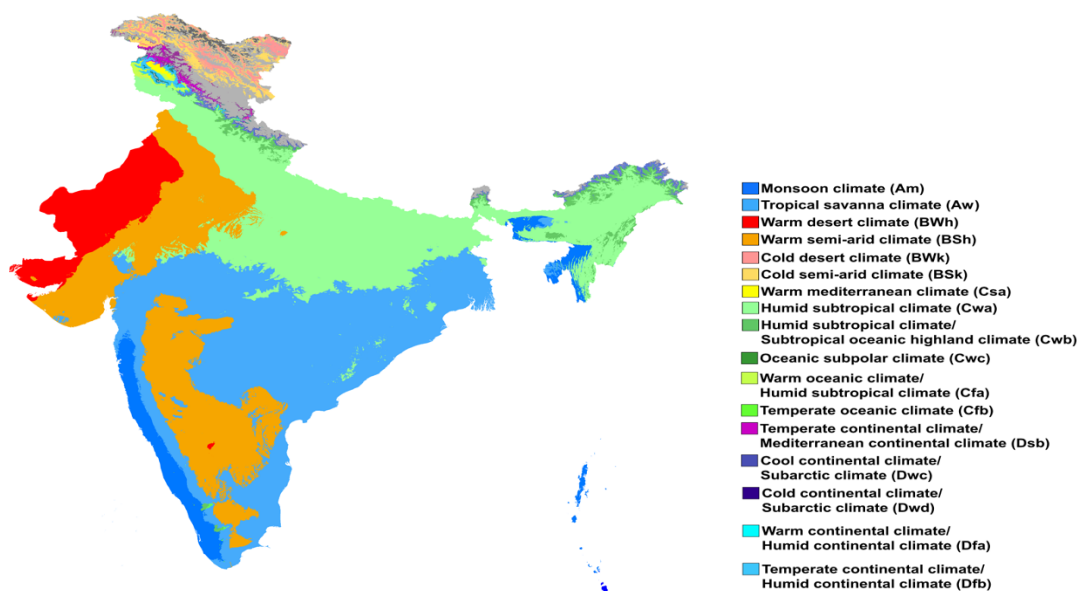


**Figure 2** Köppen classification scheme for India

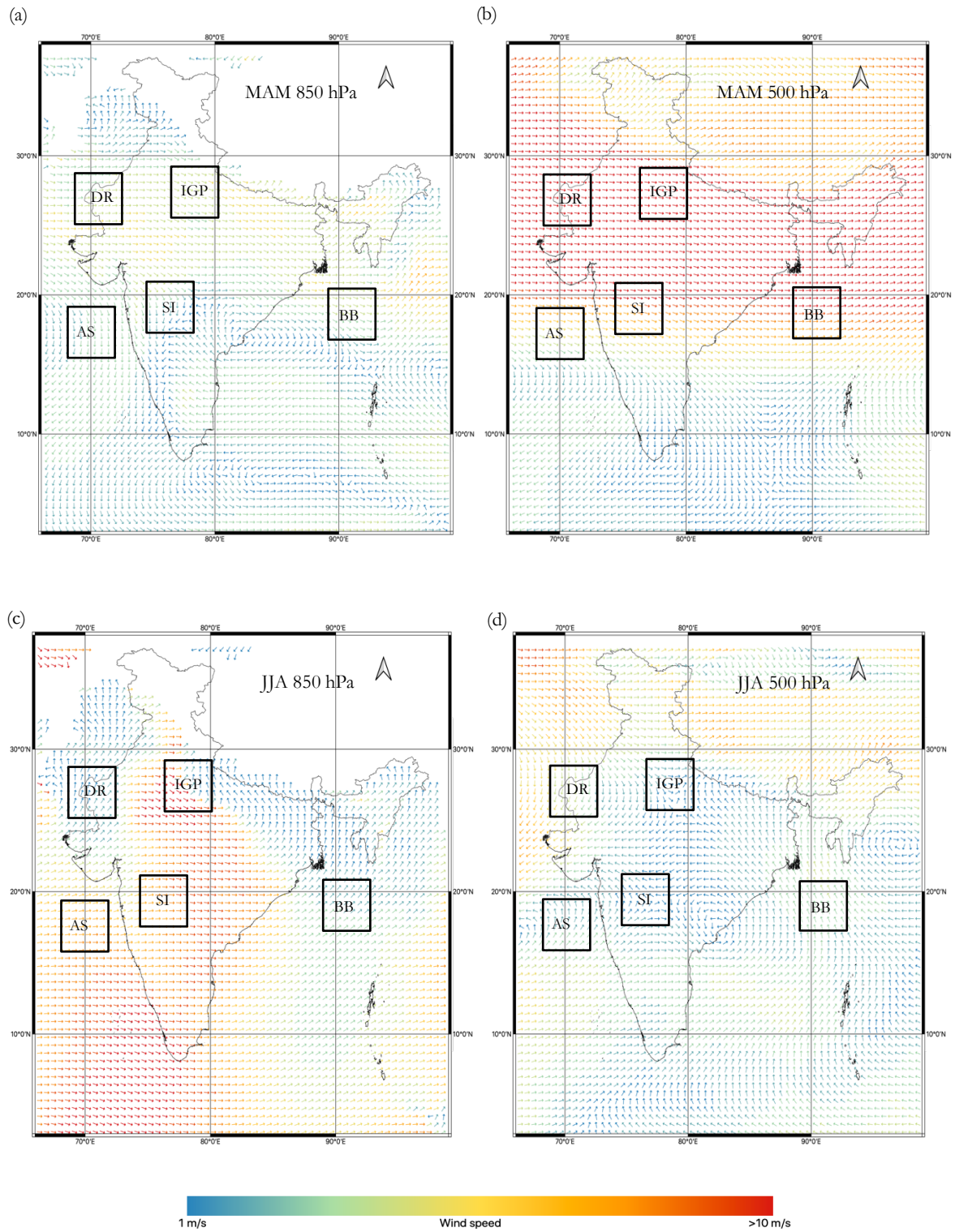
Seasons in India are classified based on the wind pattern (Figure 4) and precipitation (Figure 5). Seasonal description is listed in Table 1 as follows:

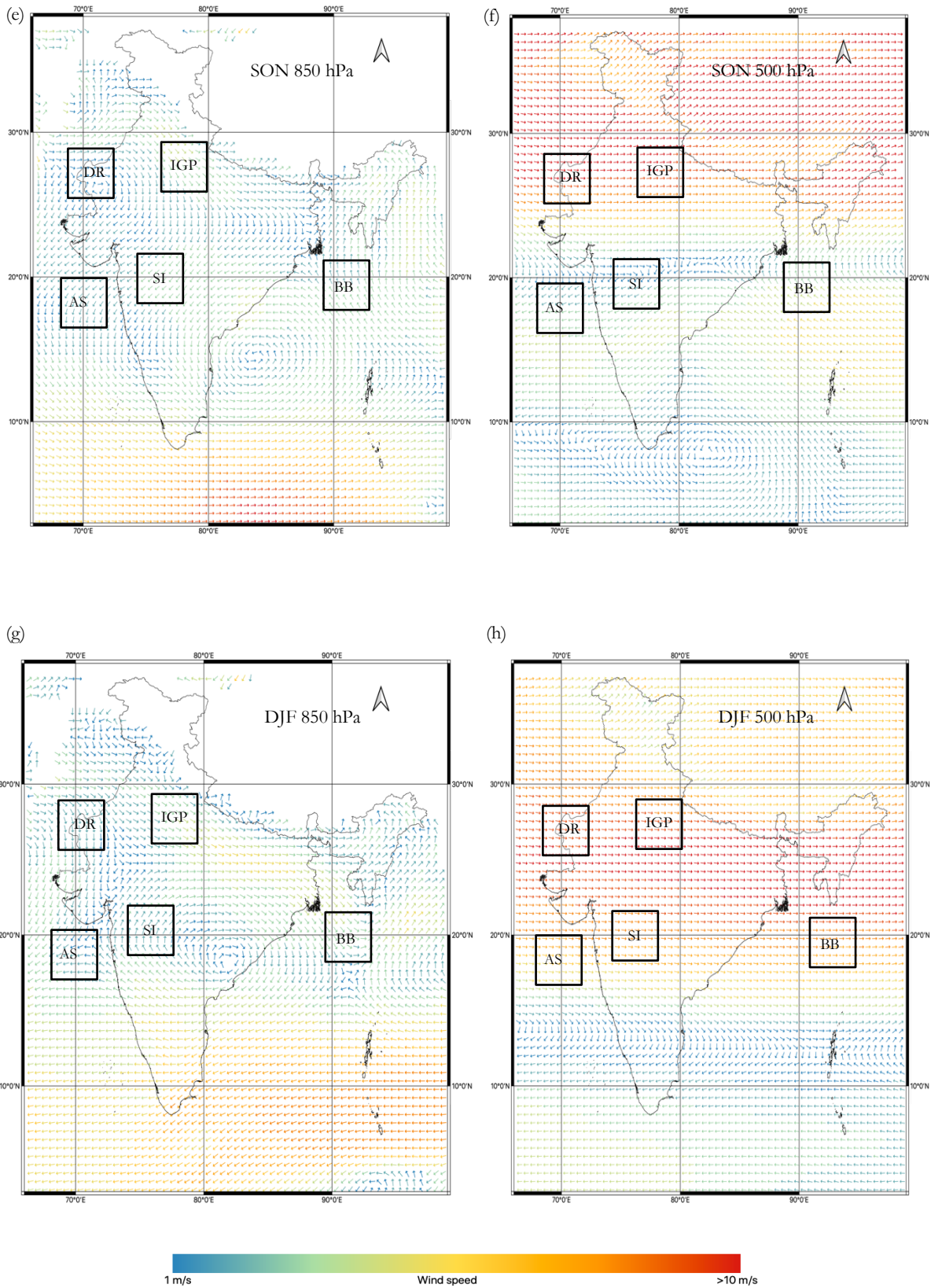
**Table 2** Seasons in timeline in India

Season	Months
Pre-Monsoon (MAM)	March, April, May
Monsoon (JJA)	June, July, August
Post Monsoon (SON)	September, October, November
Winters (DJF)	December, January, February

The physio-chemical characteristics and the geographical variability of aerosols throughout the Indian region are influenced by the synoptic meteorological process. The seasonally averaged wind pattern throughout the winter period, before-monsoon wind, during summer-monsoon, and post-monsoon across the Indian

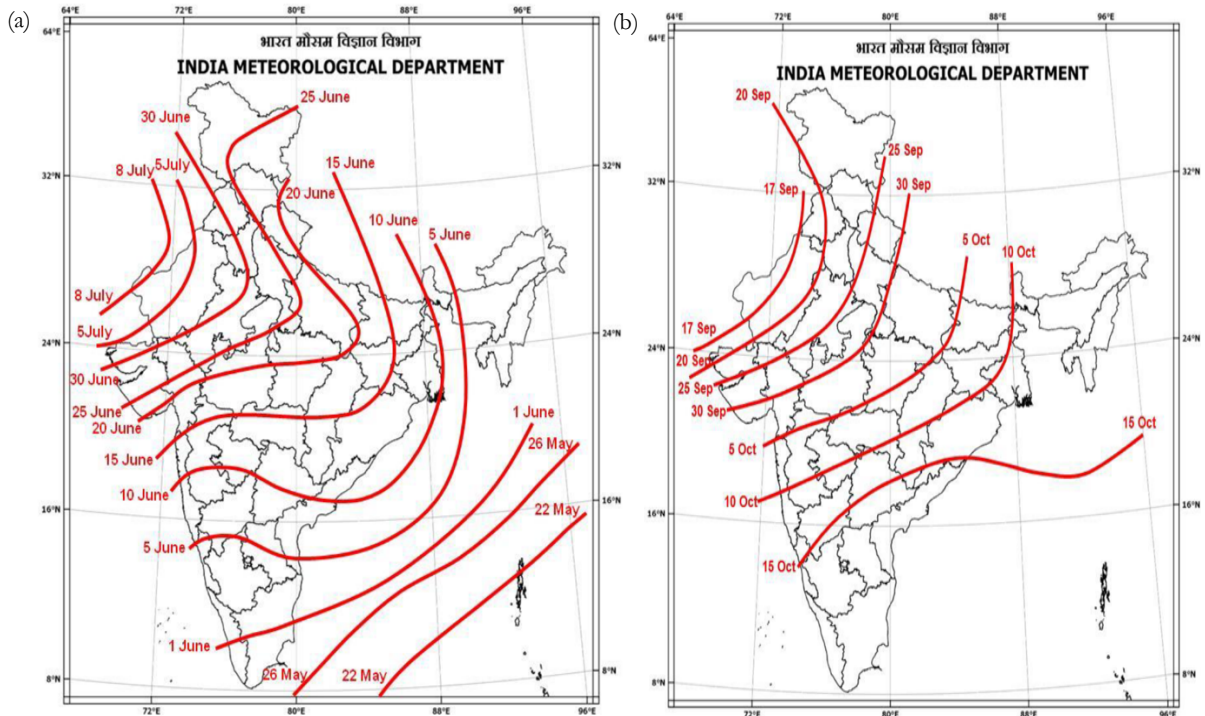
region at 850 hPa and 500 hPa are shown in Figure 3 prepared from MERRA 2 reanalysis data set (2007–2020).



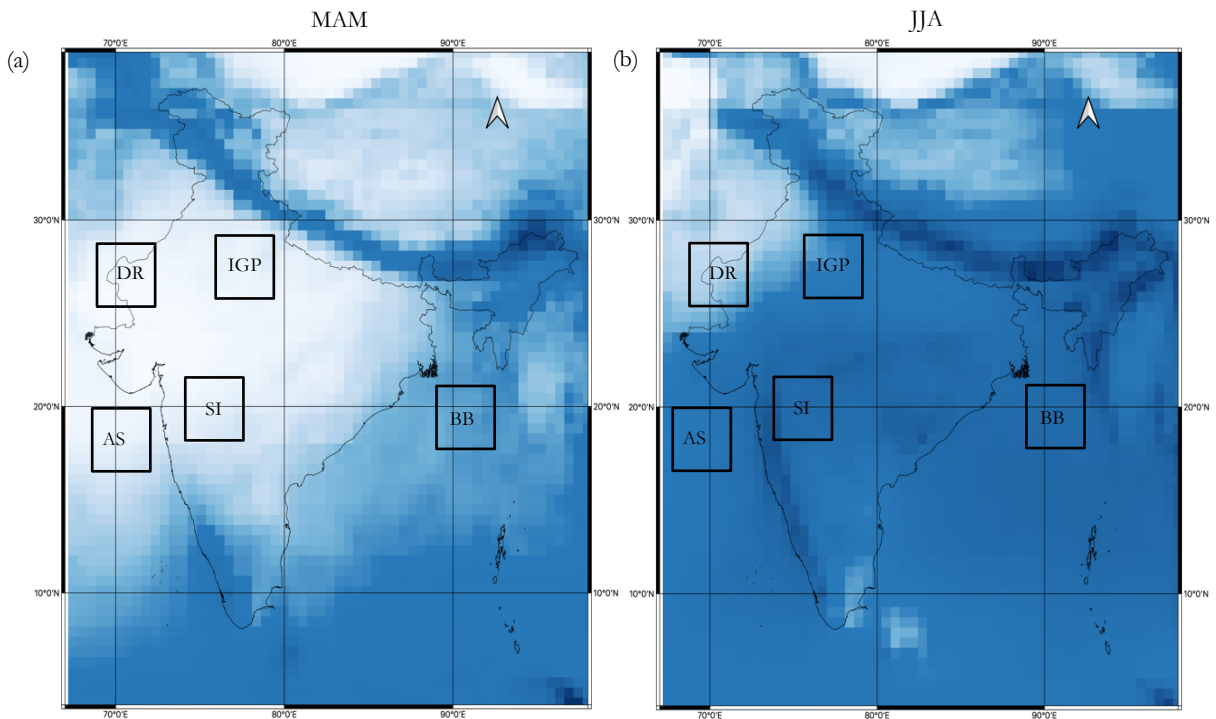


**Figure 3** Seasonal wind speed and direction (a, c, e, g) at 850 hPa (b, d, f, h) at 500 hPa

The categorization of seasons described in Table 2 is largely based on precipitation pattern, as shown in Figure 5. In different parts of India, there are significant variations in arrival times of monsoon, shown in Figure 4.



**Figure 4** Averaged Indian monsoon dates (a) 1961-2019 Monsoon Onset Dates (b) 1971-2019 averaged Monsoon Withdrawal dates



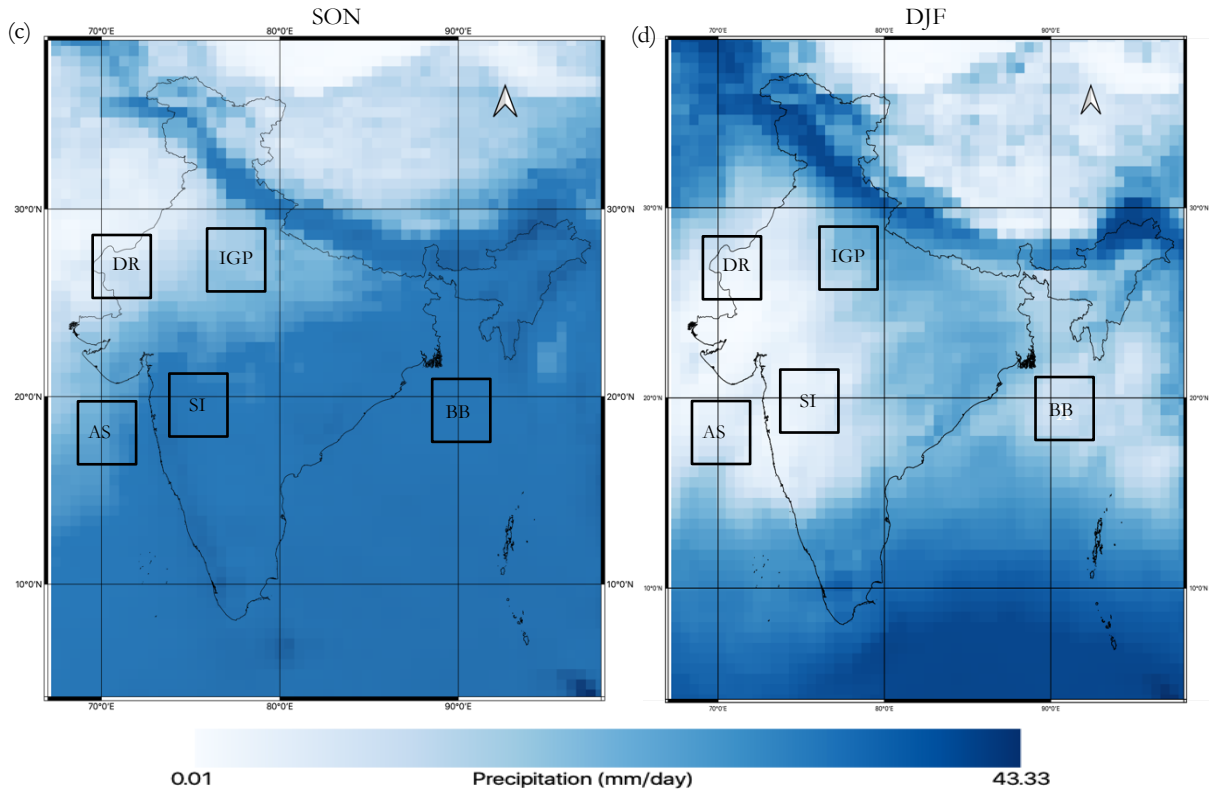


**Figure 5** Seasonal precipitation pattern of Indian region (a) MAM (b) JJA (c) SON (d) DJF

The digital elevation map (Figure 6 (a)) and the Land Use and Land Cover Classification maps (Figure 6(b)) are shown below:

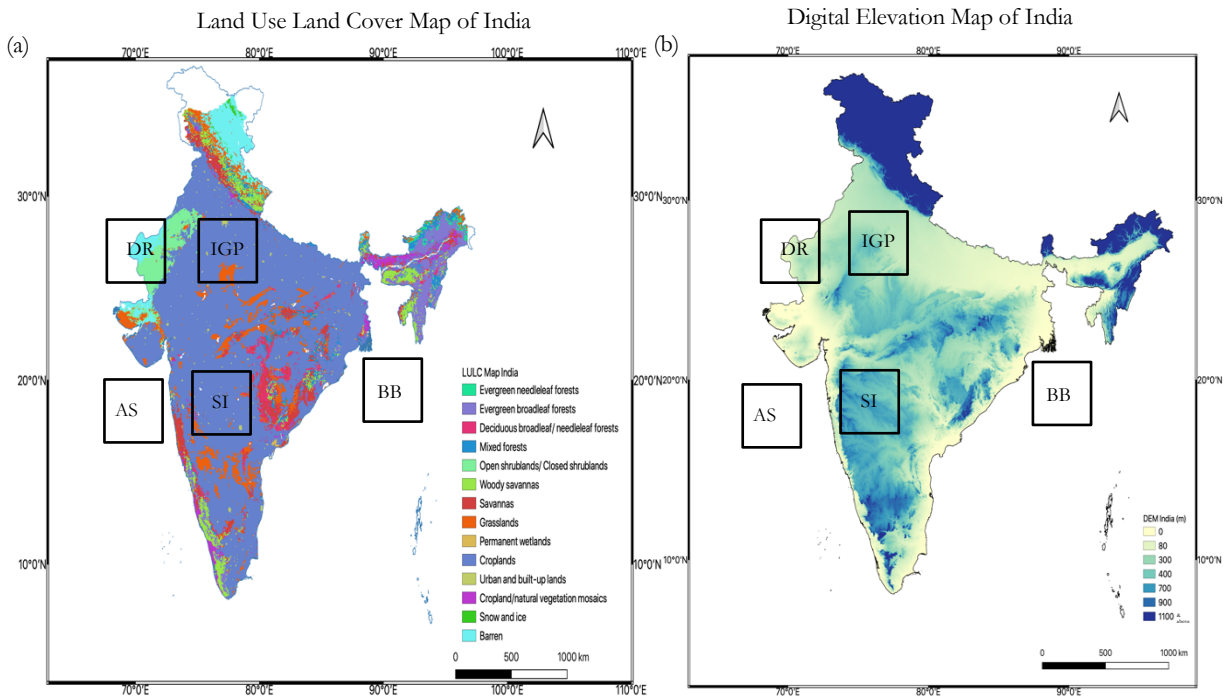


**Figure 6** (a) LULC Map of India (b) Indian region DEM

Based on the above-mentioned classification schemes like Köppen classification, wind pattern, precipitation, LULC, DEM following zones are created to keep homogeneity in results comparison. Other details about each zone are described in the following sections.

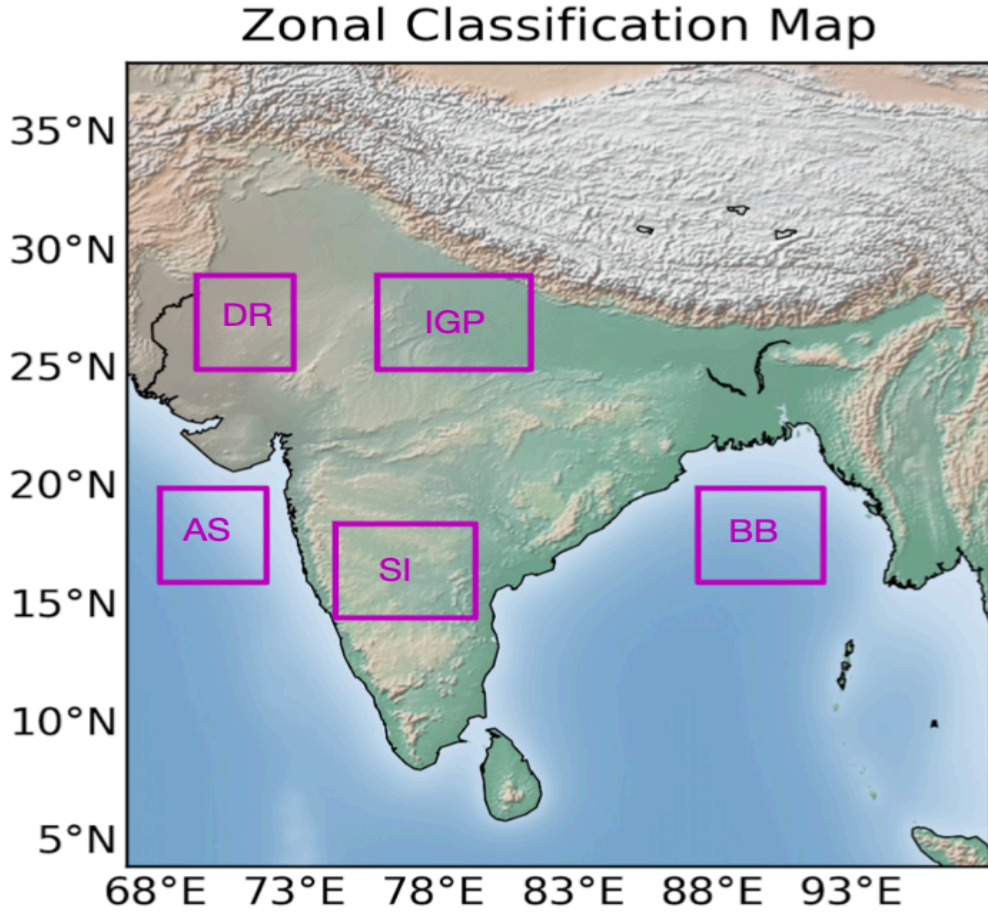


**Figure 7** Zonal classification map of India

The boundary description is given in the Table 3:

**Table 3** Zone details

Zone	Lat/ Long	Elevation Range (m)
Desert Region (DR)	TL: 29 N,69.5 E ; BR: 24 N,74 E	80-300
Indo-Gangetic Plain (IGP)	TL: 29 N,75 E ; BR: 24 N,80 E	80-300
South-India (SI)	TL: 19 N, 74 E; BR: 14 N, 79 E	400-700
Arabian Sea (AS)	TL: 20 N, 67.5 E; BR: 16 N, 72 E	-
Bay of Bengal (BB)	TL: 20 N, 87.5 E; BR: 16 N, 92 E	-

### 3.2. Indo-Gangetic Plain

Indo-Gangetic Plains (IGP) in the South Asian region is a highly significant agro-ecological area, and about one-fifth of the entire geographical area is occupied by the 4 nations of the Indian subcontinent (Pakistan, India, Nepal, and Bangladesh). The IGP alone produces 40% of total food grain output in India with 20% of the geographic area and has a population of approximately 40%. Paddy and wheat are the most commonly grown crops in the IGP's north-western region (A. R. Sharma et al., 2010). Farmers typically burn these crop leftovers in-situ to prepare the fields due to the short time gap between rice harvesting and wheat sowing, as well as the related increased costs of labour-based crop residue clearance from the fields. Due to this, IGP is one of the world's most contaminated river basins (Dey et al., 2004; Tripathi et al., 2007). Also, the IGP area includes many power generation and industries. India's recent economic boom has led to a considerable increase in industrial emissions in the region. Due to high emissions and biomass burning, the region has been an area of interest for researchers across the world (R. Gautam et al., 2009; Jethva et al., 2005; Mehta et al., 2020; Mehta, Sharma, et al., 2018; Mehta, Singh, et al., 2018a; Vinjamuri et al., 2020). The region also experiences varying intermixing of dust and smoke (Krishna Moorthy et al., 2007).

The region based on Köppen climate classification can be characterized as arid, steppe, hot which is denoted as bSh, and into temperate, dry winter, hot summer which is denoted as Cwa. In bSh classification the rainfall is low, the precipitation variability year by year is large, relative humidity is low, the evaporation rate is high (when the water is accessible), clear sky, and heavy sunlight. In the Cwa classification, the winters are mild, dry, and quite short. Summers are prolonged and quite hot, typically reaching temperatures above 40 °C from mid-April to peaks in May and early June. The region is exceedingly dry, with dust storms, characteristics that are generally associated with arid or semi-arid regions. Then monsoon, where the region nearly regularly gets significant rain. Due to the wind's directions in winters, the region acts as the gateway of aerosols to the Bay of Bengal (Figure 4). The region is dominated by both natural and anthropogenic aerosols and possesses high seasonality.

### 3.3. Desert region

The desert region in India is called the Thar Desert or the Great Indian Desert. It is the twentieth biggest desert in the world and the ninth largest hot subtropical desert in the world. The Thar Desert makes up around 4.56% of India's total geographical area. It spans a substantial region of West India, from 200,000 to 238,700 km<sup>2</sup>. The majority of the Thar Desert, 61 per cent of its geographical area, is located in Rajasthan (India). Sand dunes make up around 10 per cent of this region, with the other 90 per cent made up of jagged rock formations, compacted salt-lake bottoms, and interdunal and fixed dune regions. The Thar Desert on India's western side is a hot and arid region with a lot of aeolian activity and aerosol transport from the summer Southwest winds. During the pre-monsoon season, the area is prone to dust storms.

According to Köppen climate classification, the region is classified as BWh and Bsh. In Bsh temperature can range from 0 °C in the winter to more than 50 °C in the summer. The majority of the rainfall in this region is linked with the brief July–September southwest monsoon, which provides 100 to 500 mm of rain. Water is a scarce resource and is found at considerable depths, ranging from 30 to 120 meters below ground. Rainfall is unstable and unpredictable, ranging from less than 120 mm in the far west to 375 mm in the east. The desert region's soils are usually sandy to sandy-loam in nature.

### 3.4. South India region

The region of South India is confined to the West by the Arabian Sea, and to the south by peninsular India. The region includes urban areas, coastal regions and western ghats. The region has a transitional climate, with severe weather in the north, moderate and windy weather in the uplands, and warm and humid weather in the eastern, southern, and coastal areas. Based on Köppen classification, the region can consist of two types of classification, Aw and Bsh. The driest month in Aw climates has a precipitation of less than 60 mm of mean monthly precipitation. While the description of Bsh was explained earlier in the Desert Region

section. Some previous studies find that the region is predominantly occupied by smoke however a few discussed polluted dust and smoke.

### **3.5. Arabian Sea**

Arabian Sea is on the western side of India. Under favourable climatic circumstances, the Arabian Sea (AS; north-western portion of NIO), one of the most biologically productive marine areas, is subject to dust deposition from surrounding arid/semi-arid regions (Aswini et al., 2020; Shao et al., 2011). Due to the seasonal monsoon setting (summer and monsoon winter), the transport and deposition of dust display considerable seasonality (Tindale & Pease, 1999). The region also experiences frequent western disturbances and cyclones. Different regional oceanic processes, which include wind-driven coastal boosting (Barber et al., 2001) and convective mixing in the winter, lead to nutrient input to the surface of the Arabian Sea and considerably affect primary productivity (Barber et al., 2001). Furthermore, some research has suggested nutrition delivery via dust deposition (Srinivas et al., 2011). Several model studies in recent years have underlined the impact of dust-containing iron in improving primary productivity in the Arabian Sea (Banerjee & Kumar, 2014; Guieu et al., 2019).

### **3.6. Bay of Bengal**

Located east of Indian territory, the Bay of Bengal is restricted to latitude from 5°N to 22°N and longitude from 80°E to 100°E and has significant influence in ocean-atmosphere coupling and the Indian monsoon timings. The atmosphere in the Bay of Bay is often more turbulent than in the Arabian Sea and the Indian Ocean (Moorthy et al., 2009). Aerosols in the Bay of Bengal are extremely diverse, owing to variations in air mass influenced by densely inhabited surrounding areas (Satheesh et al., 2006). Aerosols of the Bay of Bengal are very heterogeneous because of the effect of diverse air masses from intensively populated lands in the surrounding (Satheesh et al., 2006). In this area, marine productivity is restricted by the low availability of nutrients from deep seas, and marine biodiversity mostly relies on nutrient transportation in the continental areas. The movement and deposition of mineral dust particles in the region are therefore of relevance concern due to the fertilization of iron ocean biota and subsequent changes in the marine aerosol system (Kumar et al., 2002; Nair et al., 2013). Several investigations were carried out around the region with ground instrumentation, aircraft, and ship-borne equipment. The study shows that aerosols above 1 km with the highest attenuation between 2 km and 4 km have contributed from 75% to 85% of the AOD. (Moorthy et al., 2010; Nair et al., 2010) also reported vertical heterogeneity. The aerosol distribution, in particular dust aerosols and their movement to the Bay of Bengal, which influence the regional climate and the monsoon system, are crucial for spatial and seasonal characterization.

## 4. DATA AND METHODOLOGY

The work focuses on the seasonal aerosol type vertical extinction patterns from 2007-2020. The CALIPSO data is the primary data, whereas MERRA 2 reanalysis data is used for comparison purposes. Chapter 3 already described the Indian with zonal description and the seasonal variation in the region. This chapter explains the CALIPSO data and the data collection and extraction algorithm. At the end of the chapter, the methods utilized to obtain the results are discussed.

### 4.1. Dataset

#### 4.1.1. CALIPSO

CALIPSO and CloudSat were launched on April 28, 2006. CALIPSO follows the Aqua and CloudSat satellites as part of NASA's afternoon constellation (Stephens et al., 2002). The  $98.2^\circ$  angle of the orbit covers  $82^\circ\text{N}$  to  $82^\circ\text{S}$  worldwide. The orbit on every sixteen days with cross-track errors below  $\pm 10$  km to repeat the same ground track. (D. M. Winker et al., 2010) presented a general overview of the CALIPSO mission, science goals, and instrumentation. A detailed overview of the program, objective, instrumentation, and retrieval algorithm is provided in (D. M. Winker et al., 2010; David M. Winker et al., 2009a). Furthermore, extensive explanations are provided elsewhere separately regarding CALIOP data packages and algorithms (Liu et al., 2009a; Ali H. Omar et al., 2009; Powell et al., 2009; S. A. Young & Vaughan, 2009a). There are three different tools in the payload of CALIPSO: the Cloud-Aerosol Lidar with Orthogonal Polarization (CALIOP) which is the primary instrument, an Imaging Infrared Radiometer (IIR), and a moderate spatial resolution Wide Field-of-view Camera (WFC) (David M. Winker et al., 2003). Extinction coefficients are derived from the backscatter profiles that are given at 532 and 1064 nm and two polarization components at 532 nm (parallel and perpendicular) (Hunt et al., 2009; David M. Winker et al., 2007).

It must be emphasized that processing spatial data from the satellite sensor requires dealing with a number of challenges that are not often found in surface or ground-based observations. Many air characteristics are tenuous, and the satellite's vast distance from these characteristics combined with the energy restrictions of the laser transmitter using the satellite power budget and visual safety standards can lead to low SNRs in recorded data. One of the primary issues leading to the uncertainty in estimating CALIOP aerosol is ambiguity related to the calculation of lidar S ratio. The issue gets worse during daytime operations, when weak backscatters like thick sandy surfaces, snow-covered or water clouds are viewed against highly lit backdrops. Spatial averaging multiple profiles is the conventional way to increase an SNR. Typically, the lidar ratio changes within a certain aerosol type by around 30%. Some aerosol types have slightly greater variability and some less variability. Another uncertainty is the fact of the misclassification of the aerosol type. The aforementioned concerns are addressed in the next section's discussion of retrieval methods.

##### 4.1.1.1. Retrieval algorithms: Level 2 processing

The extinction coefficient and backscatter coefficient in level 2 data are calculated using attenuated backscatter data acquired in level 1 data (David M. Winker et al., 2009b). The extraction procedure is depicted in Figure no. 9. Level 2 analysis has numerous steps and is detailed in the following subsections. M. A. Vaughan et al., 2009; S. A. Young & Vaughan, 2009a, provide detailed explanations. Level 2 screening process is shown in Figure 8.

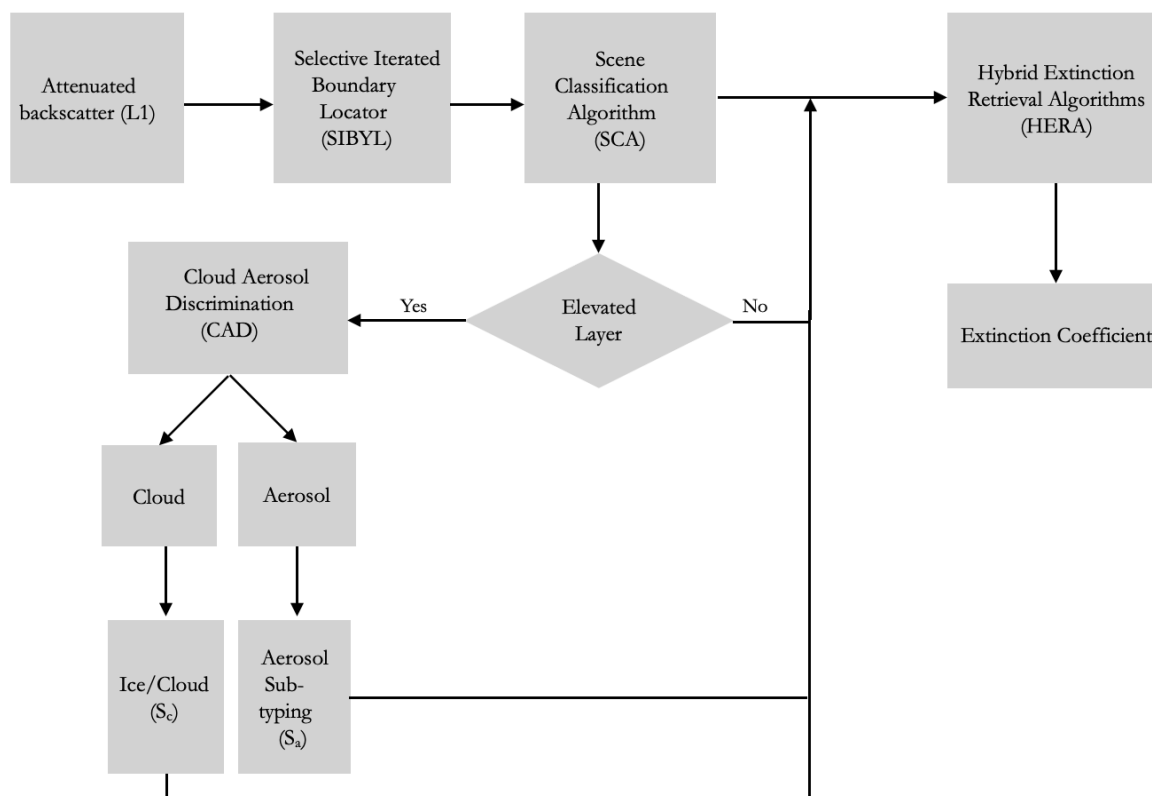


**Figure 8** Extinction retrieval process (Adapted from (M. H. Kim et al., 2018))

### Selective, iterated boundary location algorithm (SIBYL)

By monitoring and improvement of a backscattered scattered molecules signal and by utilizing a parameter called an attenuated scatter signal, SIBYL identifies features that correspond to the ratio of volume backscattered to molecular backscattered attenuated signals. SIBYL then uses a cut-off technique to determine the threshold of the aerosol profile. A ‘feature’ represents a large area with an increased backscatter signal that substantially exceeds Rayleigh's predicted molecular value (M. A. Vaughan et al., 2009). At high speeds, with low shot frequencies, a considerable number of profiles cannot be obtained due to air inhomogeneity. Signals should be averaged to improve SNR without loss of atmospheric inhomogeneity. The SIBYL algorithm is therefore careful to obtain an average signal from a spatially homogeneous atmosphere with comparable optical characteristics. In CALIOP lidar analysis SIBYL plays a crucial role finding extinction coefficient profiles since profiles of different features with varying optical properties are averaged and may result in erroneous findings that do not represent the real atmosphere.

### Scene Classifying Algorithms (SCA)

A collection of algorithms named SCA identify and categorize SIBYL-detected features and allocate lidar ratio. The data is then fed to Hybrid Extinction Retrieval Algorithm (HERA). SCA calculates a lidar ratio of a detected feature using two techniques to estimate the lidar ratio. One with high characteristics and another for non-high characteristics. SCA then estimate the lidar ratio of elevated features by estimating layer transmittance of clear air above and below the feature using the transmittance constrained technique (Fernald et al., 1972). The lidar ratio is calculated for non-detected feature types using the aerosol model and CAD algorithm to discriminated between the cloud and aerosol (Liu et al., 2009a). SCA determines the aerosol or cloud model based on the backscattered intensity, depolarization, and geophysical location of the measurement if the feature is not elevated. SCA calculates the volume depolarization ratio profile in the cloud layer and combined with auxiliary temperature data, the cloud phase (ice/ water clouds) when clouds are identified (Hu et al., 2009) (Hu et al., 2009). Whereas when an aerosol layer is found, the aerosol type is

determined by depolarization rate, backscattered intensity, and geophysical measurement site. The SCA classifies both the type of characteristics for elevated and non-elevated layers and provides a lidar ratio for the extinction recovery function in HERA.

Another algorithm that works as an intermediary to distinguish between cloud and aerosol using a 5-dimensional probability density function based on optical properties of the retrieved signal is Cloud-Aerosol Discrimination (CAD). The parameters used in Probability Density Function (PDF) are attenuated backscatter ( $\beta^*$ ), colour ratio( $\chi^*$ ) and volume depolarization ratio ( $\delta^*$ ), geolocation information (altitude ( $z$ ) and latitude).

The lidar ratio is also fixed depending on surface type, aerosol size distribution, 6-bit and composition in addition to the aforementioned parameters. However, for some types of aerosols, the colour ratio and attenuated backscatters are substantially overlapping because the colour ratio for aerosols is not used. The accuracy of aerosol extinction coefficient recovery depends heavily on the proper identification of the kind of aerosol. Clean marine, dusty marine, dust, polluted dust, clean continental (background aerosols), polluted continental, and elevated smoke are identified by CALIOP comparable to AERONET lidar ratio (Ackermann, 1998; Anderson et al., 2000; Franke et al., 2001; Holz et al., 2009; Müller et al., 2007; A. Young, 1995). Table 4 describes the lidar ratio for aerosols subtypes and aerosol subtyping is illustrated in Figure 9.

**Table 4** Lidar Ratio for aerosol types (V4.10) (Adapted from Kim et. al, 2018)

Aerosol subtype	Version 3	Version 4	Version 3	Version 4
	S <sub>a</sub> at 532 nm (sr)		S <sub>a</sub> at 1064 nm (sr)	
<b>Clean marine</b>	20 ± 6	23 ± 5	45 ± 23	23 ± 5
<b>Dust</b>	40 ± 20	44 ± 9	55 ± 17	44 ± 13
<b>Polluted continental/smoke</b>	70 ± 25	70 ± 25	30 ± 14	30 ± 14
<b>Clean continental</b>	35 ± 16	53 ± 24	30 ± 17	30 ± 17
<b>Polluted dust</b>	55 ± 22	55 ± 22	48 ± 24	48 ± 24
<b>Elevated smoke</b>	70 ± 28	70 ± 16	40 ± 24	30±18
<b>Dusty marine</b>	N/A	37 ± 15	N/A	37 ± 15

### Hybrid Extinction Retrieval Algorithm (HERA)

HERA mainly extracts the particle backscatter and extinction profiles from the blocks using fine (5 km) resolution input profiles and the description of the layer data provided by SIBYL at 532 nm and 1064 nm. HERA consists of two main elements. First is an algorithm at the highest level that picks an analytical path and analyses parameters. The analysis depends on atmospheric conditions in spatial extent. The second is called an extinction engine. It recovers extinction coefficient and backscattering profiles from the area of interest within the airspace over the spatial extent defined by the first element of HERA. In complex features where there are more unknown features, the method determines the optical depth by calculating the mean value determined across the complex feature by reducing the clear-air signals (S. A. Young & Vaughan, 2009a).



For the present work, version 4 data is used. In CALIPSO V4 products, there have been significant improvisations over earlier releases, particularly in regard to tropospheric aerosol types (Kar et al., 2018; M. H. Kim et al., 2018; M. Vaughan et al., 2019). Lidar ratio revisions might be the major cause for AOD alterations under Cloud-free circumstances, as (M. H. Kim et al., 2018) revealed in the study. In the early validation of the AOD (version 4) with respect to AERONET/MODIS, they found improvements compared with prior versions. Significant improvements were also reported in the oceanic regions.

**Table 5** Total number of files in each season and region

	MAM		JJA		SON		DJF	
	Day	Night	Day	Night	Day	Night	Day	Night
Indian Region	1616	1653	1671	1683	1658	1663	1638	1613
Desert Region	272	254	285	264	285	256	280	256
IGP	280	220	282	225	278	229	278	215
South India	276	240	281	248	279	247	282	235
Arabian Sea	207	274	221	281	214	270	214	269
Bay of Bengal	285	293	293	290	289	290	285	280

#### 4.1.1.2. Vertical Feature Mask

The product Vertical Feature Mask (VFM) (S. A. Young & Vaughan, 2009b), a level 2 CALIOP product, classifies aerosols and clouds via the procedures outlined in the preceding sections. However, in some situations, the intrinsic scattering characteristics of dust are comparable to those of clouds. The thick aerosols may be misclassified as clouds in the VFM product. (Liu et al., 2009b) reported this form of misclassification, however, less than 1% of instances are of such misclassification.

Although CALIPSO provides data up to the height of 30.1 km, but in the current work data up to the height of 4 km from the ground-surface will be used. The spatial resolution is shown in the Table 6.

**Table 6** VFM data resolution

Altitude Region		Vertical Resolution (meters)	Horizontal Resolution (meters)	Profiles per 5 km	Samples per Profile
Base (km)	Top (km)				
-0.5	8.2	30	333	15	290
8.2	20.2	60	1000	5	200
20.2	30.1	180	1667	3	55
<b>Total</b>					545

The aerosols/clouds are screened based on the flag. Each bin has a classification flag which is a 16-bit integer. The bits are interpreted as in Table no below.

**Table 7** VFM quality checks (CALIPSO, 2006)

Bits	Field Description	Bit Interpretation
1-3	Feature Type	0 = invalid (bad or missing data) 1 = "clear air" 2 = cloud 3 = aerosol 4 = stratospheric feature 5 = surface 6 = subsurface 7 = no signal (totally attenuated)
4-5	Feature Type QA	0 = none 1 = low 2 = medium 3 = high
10-12	If feature type = aerosol, bits 10-12 will specify the aerosol type	0 = not determined 1 = clean marine 2 = dust 3 = polluted continental 4 = clean continental 5 = polluted dust 6 = smoke 7 = Dusty Marine
13	Cloud / Aerosol /PSC Type QA	0 = not confident 1 = confident

**4.1.1.3. Aerosol Profile Data:**

The APro data product primarily provides particle extinction and backscatter as well as additional profile information (e.g., particulate depolarization ratios) derived from these fundamental products.

Spatial resolution: Ground - 5 Km

Vertical - 60 m

Total number of vertical bin: 145

Total number of horizontal profiles: 1

From the Aerosol Profile data, parameters like Latitude, Longitude, Day Night Flag, Profile UTC, Aerosol Layer Fraction, CAD Score, Atmospheric Volume Description, Extinction QC Flag 532, Extinction Coefficient 532, Extinction Coefficient Uncertainty 532 are used for the research work.

- Aerosol Layer Fraction (ALF): Since the atmospheric composition in each range bin is not homogeneous and due to non-homogeneity, each range bin is provided with the feature fraction in the aerosol profile products. The ALF describes the fraction of aerosols in spatial resolution.
- CAD Score: The cloud-aerosol discrimination score is the confidence value to discriminate between the cloud and aerosol based on the algorithm. The CAD score is derived by a 5-dimensional

probability density function (PDF) namely layer mean attenuated backscatter at 532 nm, layer-integrated volume depolarization ratio, the layer-integrated attenuated backscatter colour ratio, altitude, feature geolocation. The CAD range is between -100 to 100. The positive value signifies the confidence level of clouds and the negative value signifies the confidence level of aerosols. The larger the magnitude, the higher is the confidence level of the feature type i.e. cloud or aerosol (Liu et al., 2009b)

- Atmospheric Volume Description (AVD): AVD is a profile descriptive flag similar to the feature classification flag in VFM.
- Extinction QC Flag 532: The extinction QC flag is also a 16-bit integer that describes if the retrieval is constrained or unconstrained.
- Extinction Coefficient Uncertainty 532: This is absolute uncertainty in the extinction coefficient detected for particles in each bin.
- Extinction Coefficient 532: This represents the actual particle loading in each bin.

#### 4.1.2. Reanalysis Dataset

##### 4.1.2.1. MERRA 2

As part of validation work, MERRA 2 reanalysis data is used. The reanalysis data is available from 1980. MERRA-2 incorporates the assimilation of aerosol data and provides multi-decadal reanalysis for the assimilation of aerosols and meteorological measurements within a global data assimilation system. (Randles et al., 2017) and (Buchar, Randles, Silva, et al., 2017) have provided a thorough description and evaluation of the MERRA-2 aerosol analysis system. The MERRA-2 incorporates improvements to the Global Statistical Interpolation (GSI) analytical system (A. Molod et al., 2015; Andrea Molod et al., 2012). The great bulk of AOD measurements integrated into MERRA-2, particularly after 2002, is provided by MODIS when data are available from both the Terra and Aqua satellites. AOD measurements may only limit the total extinction of aerosols and vertically integrated extinctions, by assuming a set of optical characteristics that may be linked to the column aerosol mass. It should be noted that due to the coarse resolution of 0.5 x 0.625 degrees, there could be bias in the results.

**4.2. Workflow**

In the work, a conservative approach is used to extract the extinction profiles at the altitudes. The quality screened profiles are extracted to find the maximum mean extinction that has been there at different altitude levels. Since air is homogeneous i.e. many aerosols are present in satellite spatial resolution and lidar counts total extinction for a profile in the spatial resolution. If the feature is detected the spatial area in total is counted as an aerosol but in a real scenario, the air is well mixed in with the aerosols. So, clean air counts are also required to be added while averaging the total extinctions.

The mean extinction is calculated by the vertical integral of extinction coefficients after quality retrieval. However, a slightly different approach is used in CALIPSO. The clean air samples are also used during the calculation of mean. This is primarily done to reduce the bias in the data. A similar procedure is adopted while calculating the mean extinction value for aerosol type where the number of samples of other aerosols is taken into consideration however the extinction is assumed to be zero. Mean AOD in CALIPSO is also calculated uses the average-then-integrate approach. The mean extinction at each altitude is calculated and then the extinctions profiles are vertically integrated.

The frequency of occurrence is calculated using the count of aerosol type divided by the total aerosol count.

The flowchart of the work is shown in Figure No. 11 The screening procedure of the extinction coefficient is shown in Figure No. 10 (b) while for frequency of occurrence is shown in Figure No. 10 (a).

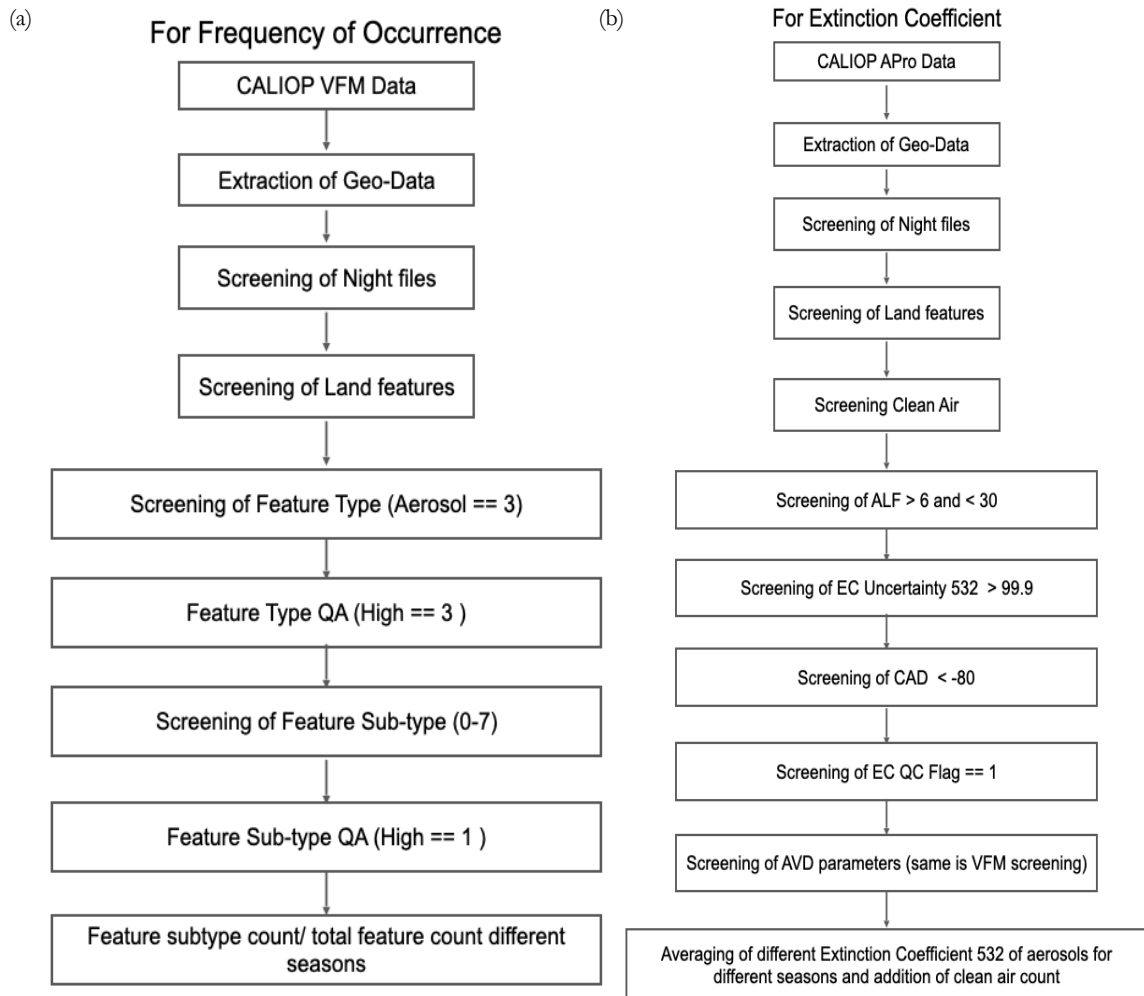


**Figure 10** Screening checks used in (a) frequency of occurrence (b) extinction coefficient retrieval

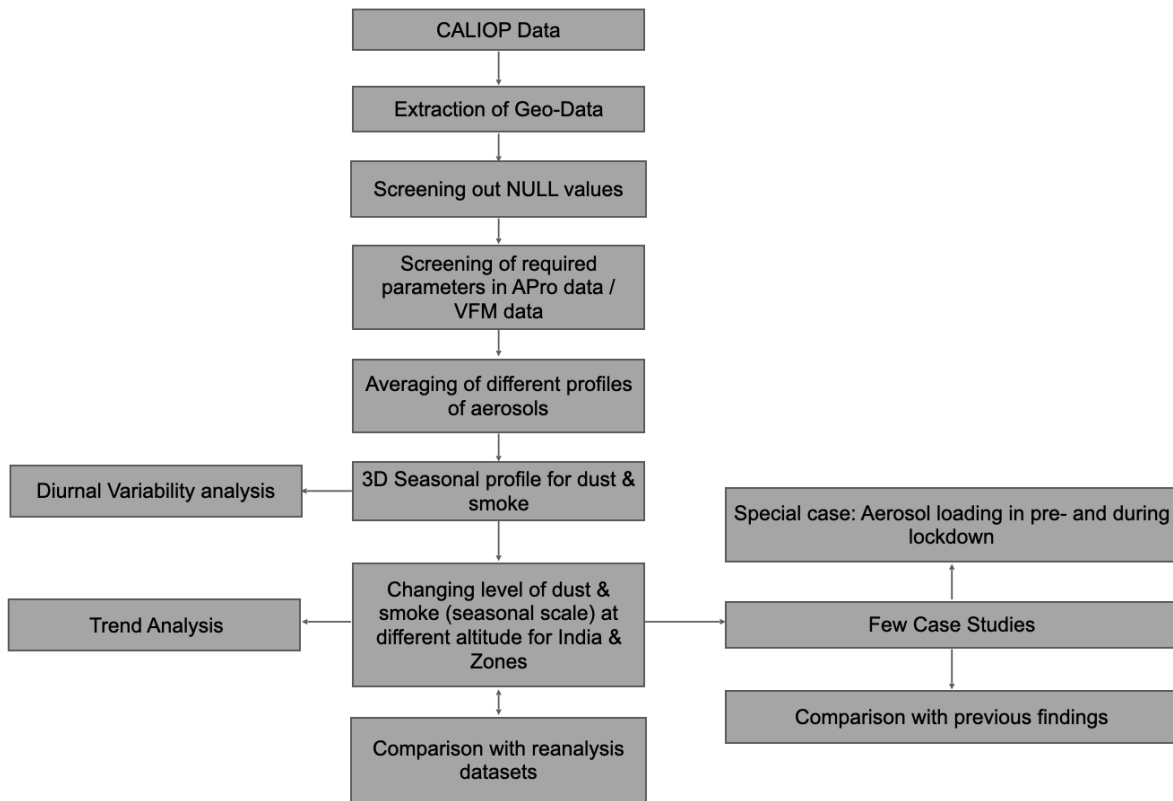


**Figure 11** Methodology

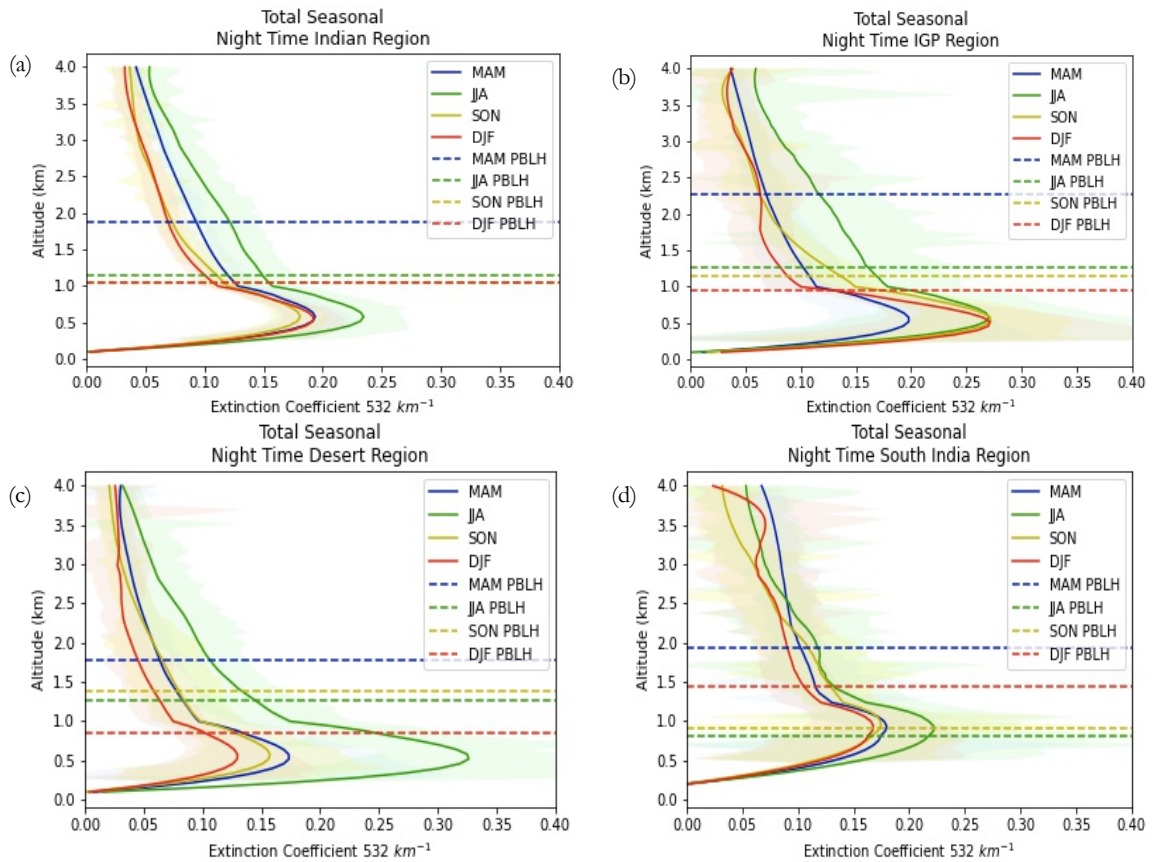
The CALIPSO dataset is first sub-setted for the desired region. In the following stage, individual diurnal monthly profiles for each aerosol type VFM and Aerosol Profile data are extracted using the screening parameters shown in Figure 10 (a) and (b), respectively. Following that, the retrieved profiles are averaged using the scheme stated earlier in the section. The daily variations in the relative distribution of aerosols in the atmosphere is depicted. Mann Kendall test was employed for trend analysis. The monthly mean AOD of the MERRA 2 dataset is utilized for dataset validation.

## 5. RESULTS AND DISCUSSION

### 5.1. Vertical distribution of aerosols over Indian land surface

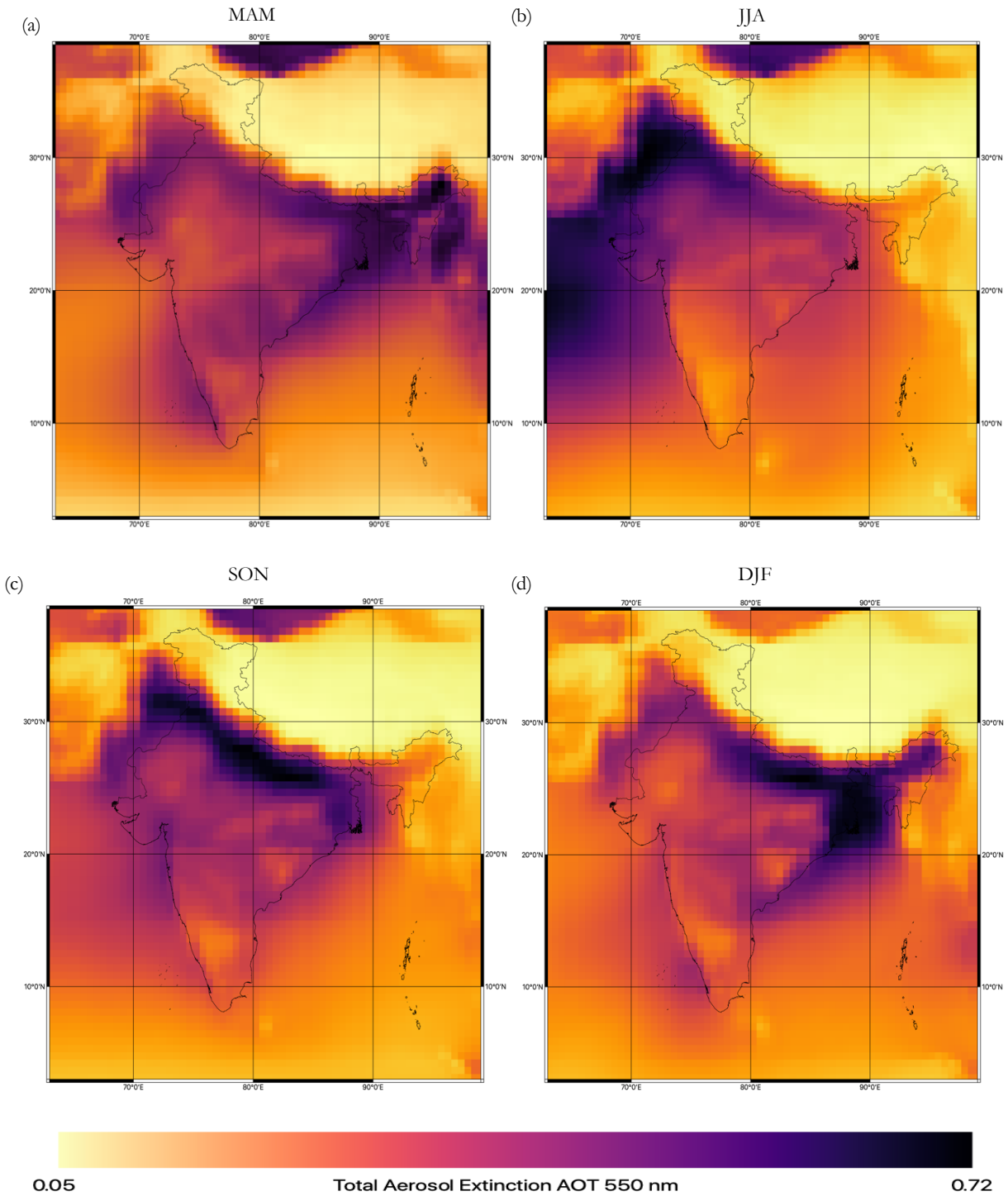
#### 5.1.1. Total Extinction

Larger extinction has been found below the PBLH in the Indian region in zones demarcated in Table 3. Seasonal difference in extinction profiles is found in all zones, with more visible contrast below the PBLH. The seasonal variation in extinction profiles is related to the seasonal dominance of distinct aerosol types in the area (Figure 12). Seasonal variation over PBLH might be due to varying concentrations of dust, polluted dust, and elevated smoke. In general Indian region is dominated by dust during MAM and JJA while in winters variation is due to the varying concentration of smoke (Ritesh Gautam et al., 2010; Kaskaoutis et al., 2011; KS et al., 2020; Mehta et al., 2016a; Mehta, Khushboo, et al., 2021; Ramachandran & Cherian, 2008; A. K. Srivastava et al., 2011). In all seasons, the bulk of aerosol loading is localized within 1 km of the ground surface. Vertical mixing is also found during MAM and JJA, in addition to seasonal contrast (Mehta et al., 2016b). The extinction coefficients in the JJA season are of higher magnitude in the Indian area and distinct zones when compared to other seasons. Distinct varieties of aerosols induce higher extinctions, which are largely driven by moisture-induced hygroscopic growth of hydrophilic aerosol particles (Altartaz et al., 2013). During the JJA the extinction profile in all zones is varied at all altitudes. Large seasonal variation is seen in different zones demarcated in chapter 3. Seasonal contrast is seen in IGP region as well. The seasonal variation in the IGP region is again related to dust and smoke variations, as observed in the Indian region. Seasonal variations in South India, on the other hand, are related to changing amounts of polluted dust and Smoke. The following sections provide a brief description of the individual aerosol contribution.



**Figure 12** Seasonal nighttime extinction coefficient 532 retrievals and frequency of occurrence plots (a-b) Indian region (c-d) IGP region (e-f) Desert region (g-h) South India region

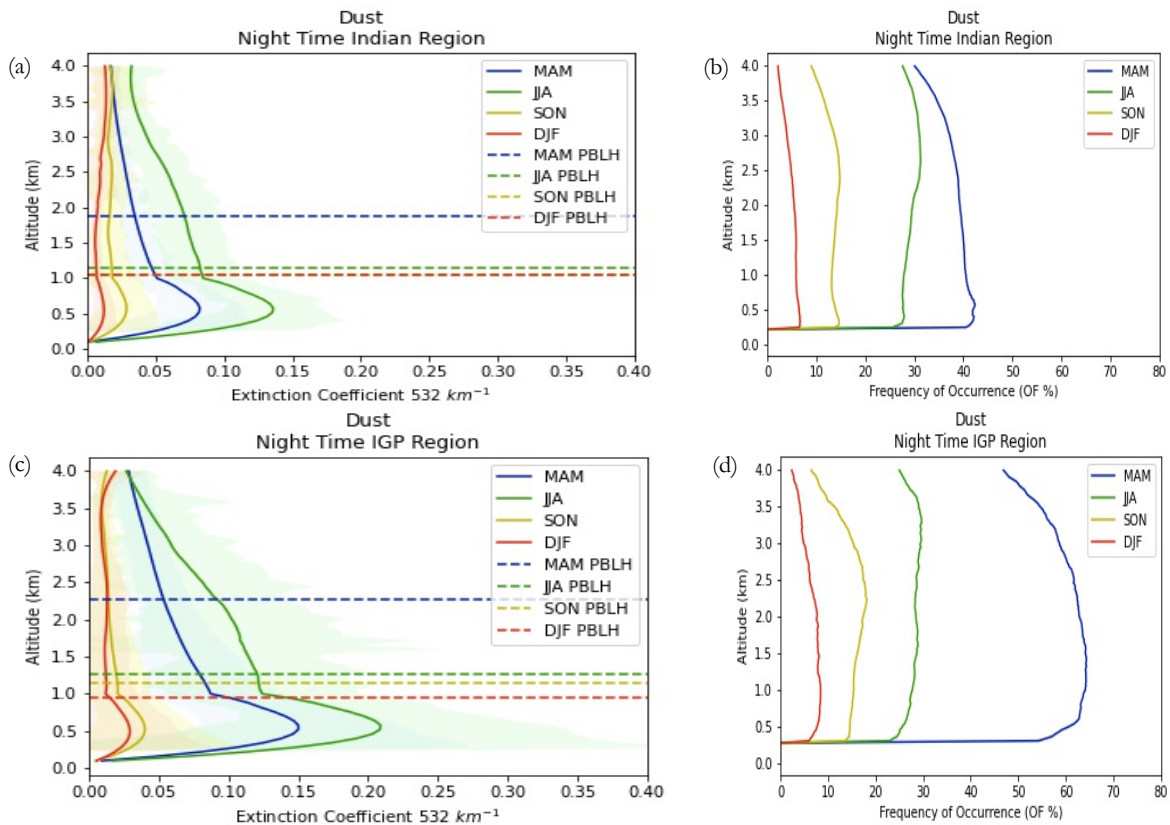
In terms of spatial variation of aerosols, there is a visible difference in AOD in the Indian region as well as distinct zones (Figure 7, 13). In the northern Indian region, high AOD is observed in JJA, which is comparable to higher extinction profiles. Higher optical depth is recorded during SON due to widespread stubble burning in the IGP region. AOD varied in distinct zones in different seasons, similar to the seasonal vertical distribution of extinction profiles in respective zones.

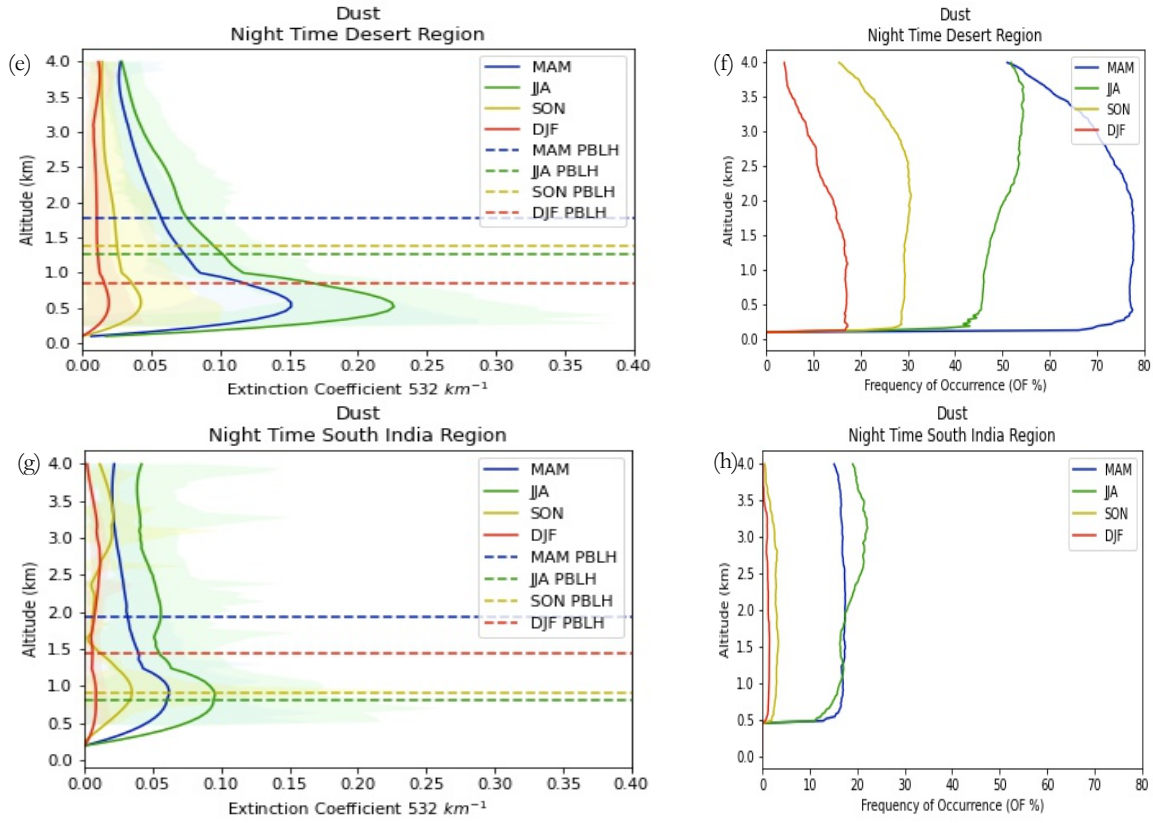


**Figure 13** Seasonal Total Aerosol Extinction (MERRA-2)

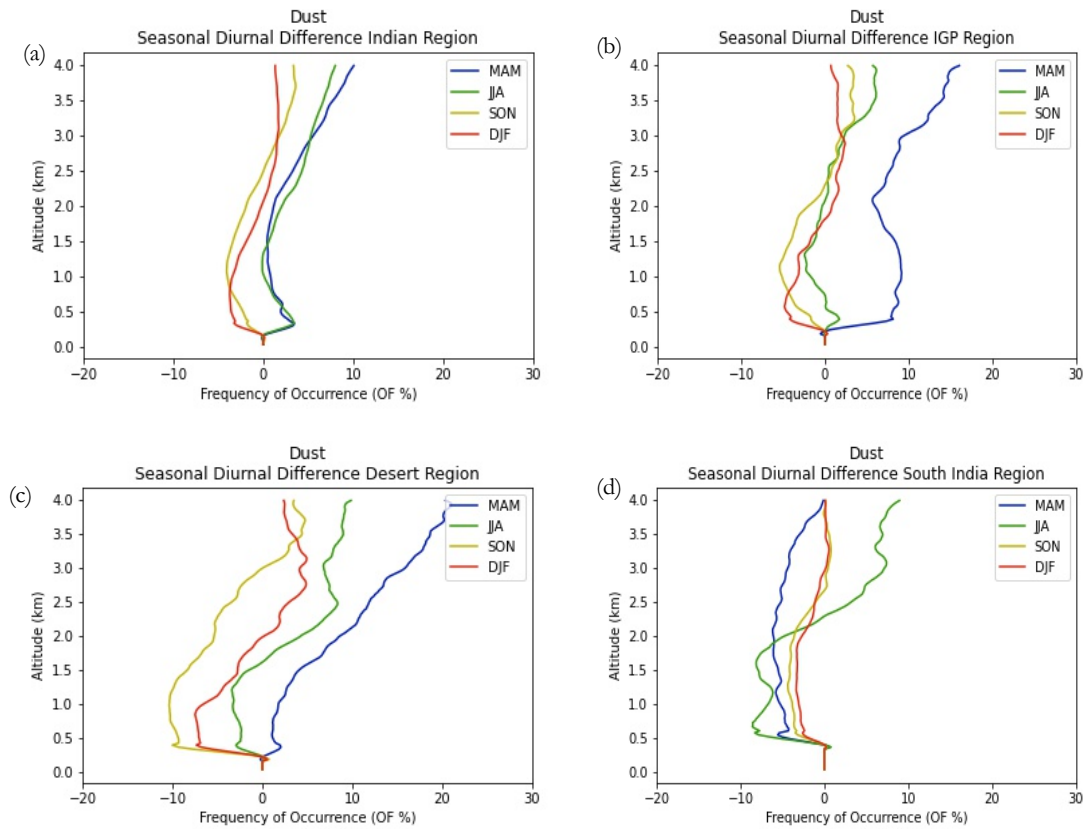
5.1.2. Dust

Seasonal differences in extinction coefficient and frequency of occurrence of dust is seen in both the Indian region and distinct zones of study area. Dust is seen to be the major aerosol during the MAM and JJA seasons. The high frequency of occurrence during MAM season indicates there more dust activity in the month of April and May. The extinction coefficient is higher during the JJA because of high extinction profile retrieval throughout the season due to high relative humidity and particle size as previously discussed in chapter 2. However in terms of frequency dust is will distributed in MAM (Figure 14 (b), (d), (f)). The desert region has the largest extinction and frequency of occurrence of dust, which is due to both local sources and dust carried from the Arab region (Figure 14 (f)). On contrary, the frequency of dust does not exceed 25% at specific elevations in the South Indian area (Figure 14 (h)). The dust has also had been observed to have a substantial diurnal variation (Figure 15). Dust settles at night due to gravity pull, and the extinction coefficient for dust is lower at night when compared to daylight. However, the increased frequency of occurrence is noticed at night in the IGP region and desert region. This is due to a the greater occurrence of the dust storm in the evening or night. The diurnal fluctuation in Figure No. 15 also confirms a greater frequency of occurrence below the PBLH. The dust loading in the IGP and Desert region is substantial during MAM, both during the day and at night (Figure 15 (b), (c)). Dust transport occurs mostly during the daytime after MAM. A similar observation of a higher frequency of occurrence during the daytime in other seasons (Figure 15). It is worth noting that there is a diurnal fluctuation of dust below PBLH during the winter seasons (SON and DJF), but not at higher altitudes (Figure 15). Throughout the summer, the diurnal difference at lower elevations varies in different zones, depending on wind direction and dust transport capacity. An exception is South India region where dust mostly dominated during the daytime in all season. This is primarily due to the wind direction from the source. The region seems to be converging zone of winds from two different directions. One from the dust regions and another from the south peninsular region. The concentration levels could also be lined with the dust flux, that describes the dust emissions, transportability and directions. (Appendix -III).



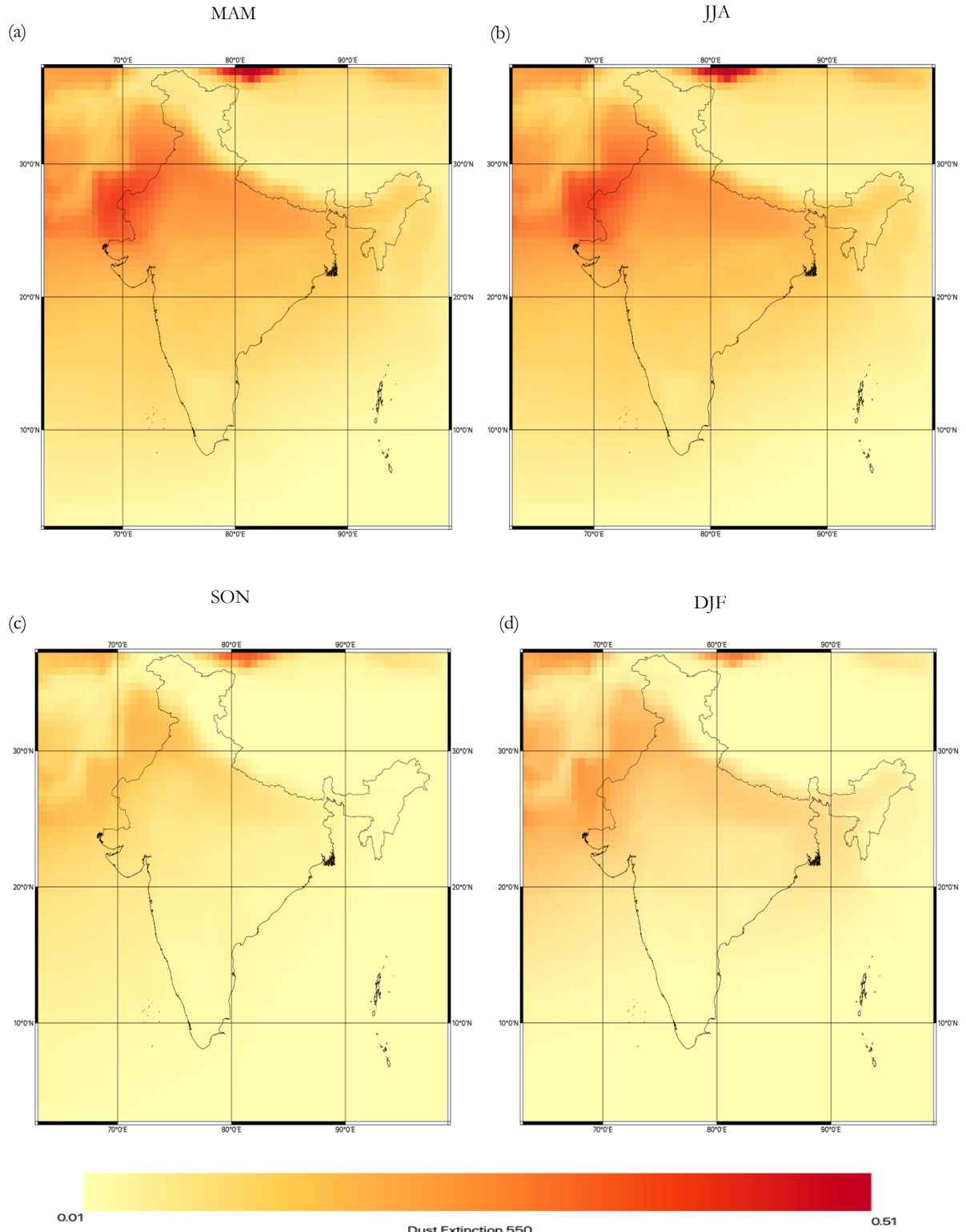


**Figure 14** Dust seasonal nighttime extinction coefficient 532 retrievals and frequency of occurrence plots (a-b) Indian region (c-d) IGP region (e-f) Desert region (g-h) South India region



**Figure 15** Dust diurnal difference of frequency of occurrence plots (a) Indian region (b) IGP region (c) Desert region (d) South India region

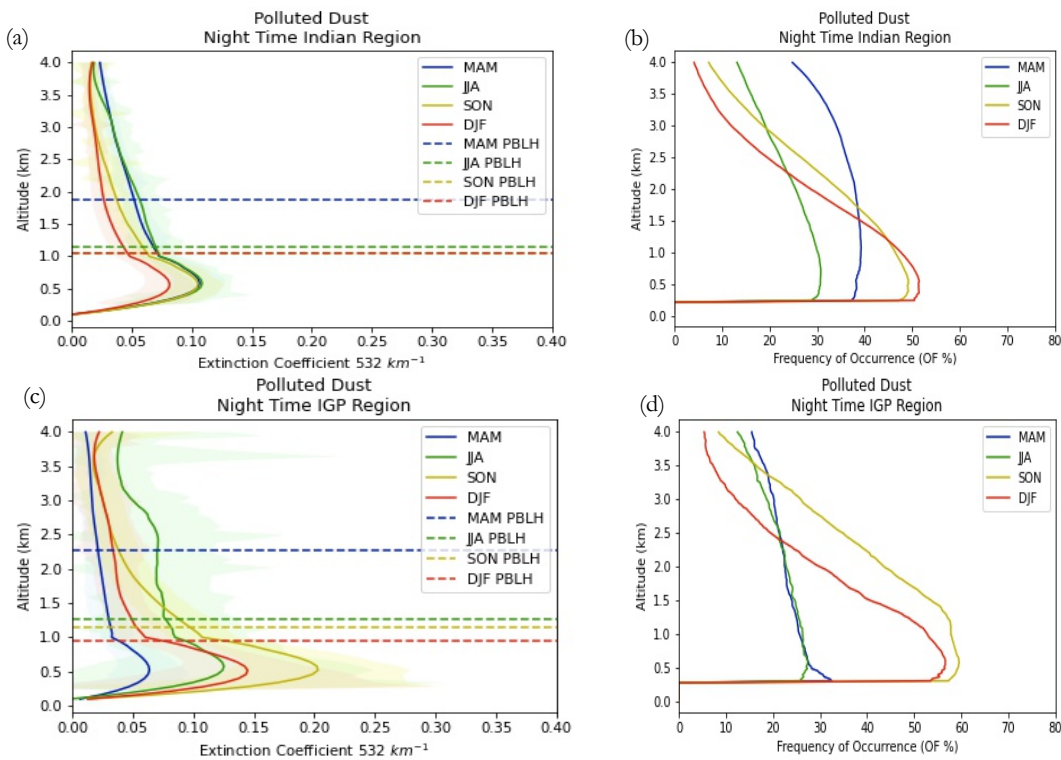
In Figure 16 the seasonal spatial distribution of dust in the Indian region is shown. Higher loading is seen in the north-western part of India, i.e., the desert region. In comparison to MAM season, higher extinction is JJA season, a similar observation was also seen in extinction profiles Figure 14. The seasonal contrast of extinction profiles and frequency of occurrence is in line with the seasonal spatial distribution.

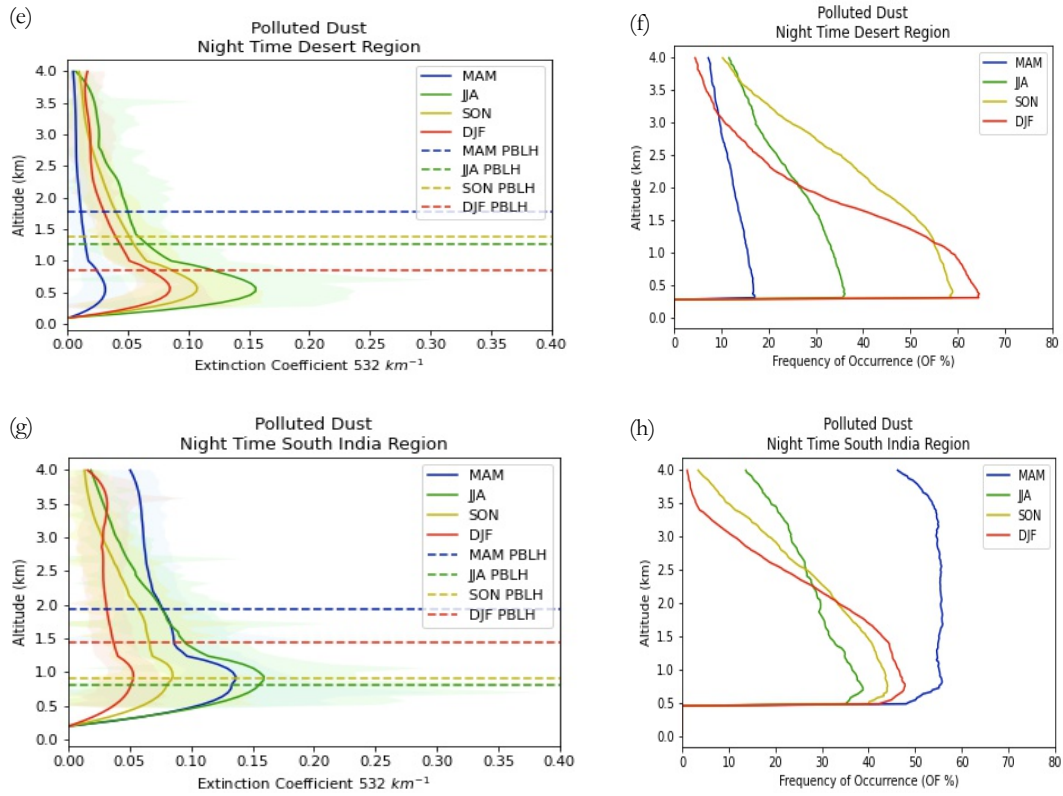


**Figure 16** Seasonal dust extinction at 550 nm (a) MAM (b) JJA (c) SON (d) DJF

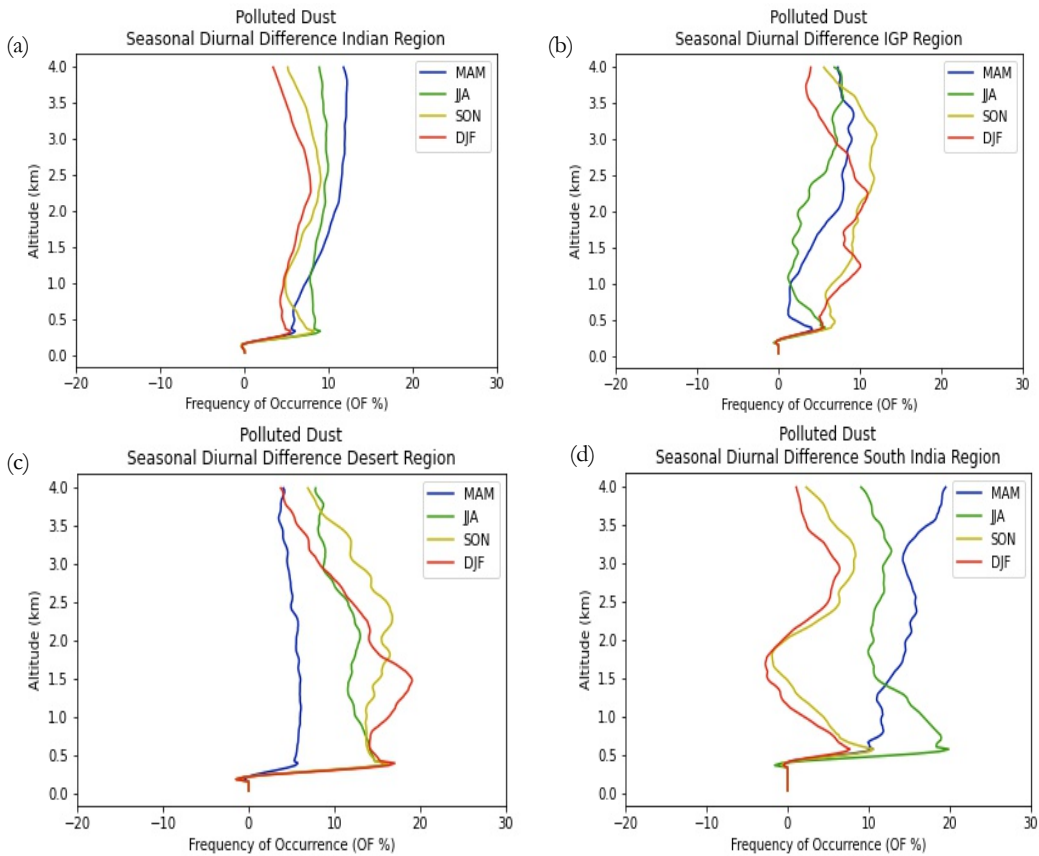
### 5.1.3. Polluted dust

The majority of polluted dust concentrations is confined to a height of one kilometre. This is seen in the extinction coefficient as well as the frequency of occurrence. Polluted dust distribution changes seasonally in different parts of India. The most important factors for dust-smoke intermixing are relative humidity, wind speed, and dust particle size, all of which influence the magnitude of the extinction coefficient. During SON and DJF, polluted dust continues to prevail, with a frequency of occurrence around 50% below 1 km height in all zones. South India region is an exception, where polluted dust loading is high during the pre-monsoon season (Figure 17 (h)). Relatively high concentration of smoke is found in the South India region, frequency of occurrence of polluted dust are heavily dependent on dust supply from the Arab region or the Indian Desert region or loose soil within the region. Because the South India area receives early rains and has a late monsoon retreat, polluted dust loading is more intense during MAM and DJF (Figure 4 and 5). During MAM, anthropogenic smoke particles combine with dust transported by winds at 950 hPa and 850 hPa that arrives from desert regions before the monsoon. The SON season has the highest extinction coefficient in the IGP region due to the significant intermixing of dust with smoke particles generated by stubble burning, which is supported by relative humidity. Seasonal diurnal variability is also seen in several zones of the research region (Figure 18). However, the concentration remains greater at night than during the day due to increased relative humidity and a better signal-to-noise ratio. The seasonal contrast for SON and DJF in the IGP region remains visible in terms of frequency of occurrence and extension patterns (Figure 18). The fraction distribution of the extinction coefficient in Section 5.2 further validates the frequency distribution and diurnal difference to the extinction coefficient.





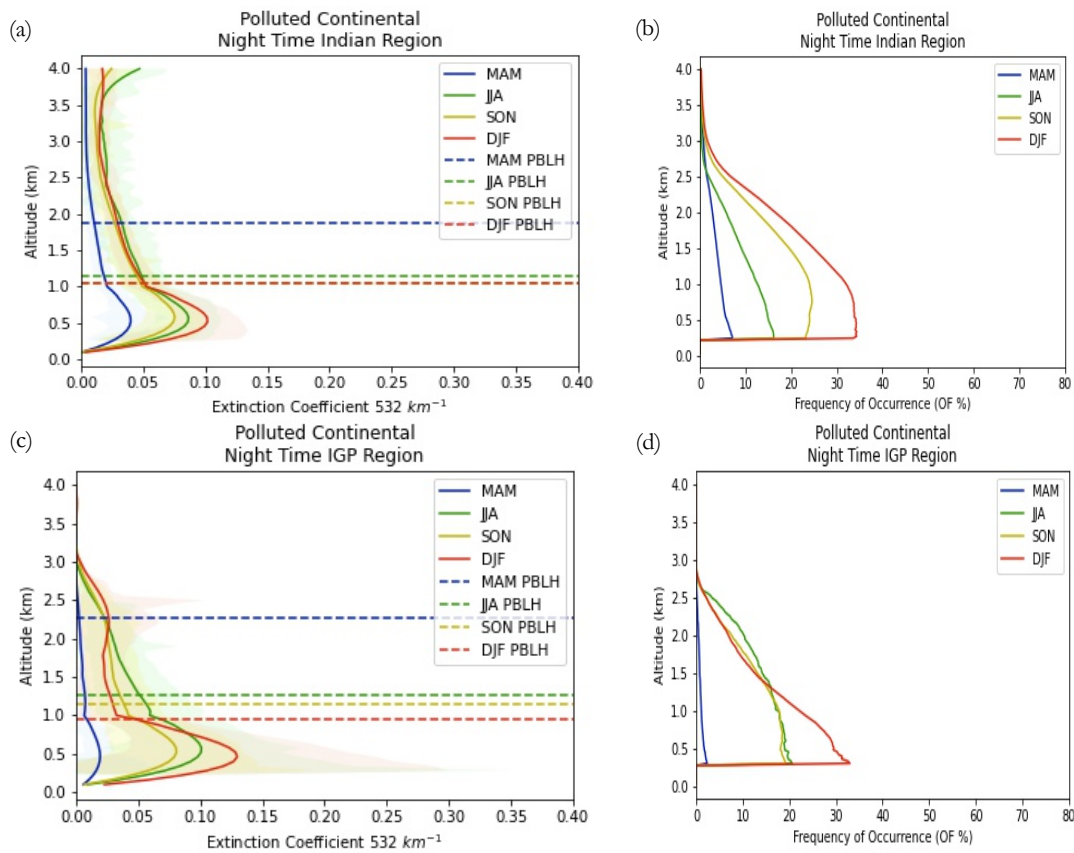
**Figure 17** Polluted dust seasonal nighttime extinction coefficient 532 retrievals and frequency of occurrence plots (a-b) Indian region (c-d) IGP region (e-f) Desert region (g-h) South India region



**Figure 18** Polluted dust diurnal difference of frequency of occurrence plots (a) Indian region (b) IGP region (c) Desert region (d) South India region

5.1.4. Polluted continental

Polluted continental is one of the predominant aerosols type throughout the winter, particularly in DJF. Seasonal variability of extinction coefficient and frequency distribution may be seen in the different regions, as shown in Figure No. 19. The maximum concentration is confined within 1 km of the ground surface in all zones, beyond which the frequency and extinction decrease rapidly. The polluted continental particles reached a maximum up to the height of 3 km. However, there is a slight difference in the concentration of polluted continental during JJA in the South India region due to monsoon influence and rainfall washout. Because of increased PBLH, convective activities, and greater concentrations of dust or polluted dust during the MAM season, the polluted continental contributes the least in terms of extinction coefficient and frequency in all areas. When it comes to geographical distribution, when compared to the rest of India, the South India area is still heavily dominated by polluted continental throughout the winters. While JJA and SON are in the IGP area, their occurrence is almost equal up to PBLH. In terms of diurnal variation, it can be noted that the frequency of occurrence of polluted continental in JJA at night is higher in the IGP region and during SON in the South Indian region (Figure 19). Interestingly, during MAM season, polluted continental is found in higher concentrations than during the day in all locations. High irregularities are found in frequency distribution in the South India region. The bell-shaped curve is an observed diurnal difference during the JJA season in South India, owing to differences in wind speed and direction. Strong winds of 850 hPa blow from the Arabian Sea bring clear air, while moderate winds of 500 hPa blow from the Arabian Sea and the Gujarat area polluted air into the region (Figure 3 (c), (d)). During winter rains, winds from the north exit to the Arabian Sea, bringing pollutants from various places to South India during the SON season. The percentage fraction distribution of extinction profile further validates the diurnal variability and frequency of occurrence (refer to section 5.2).



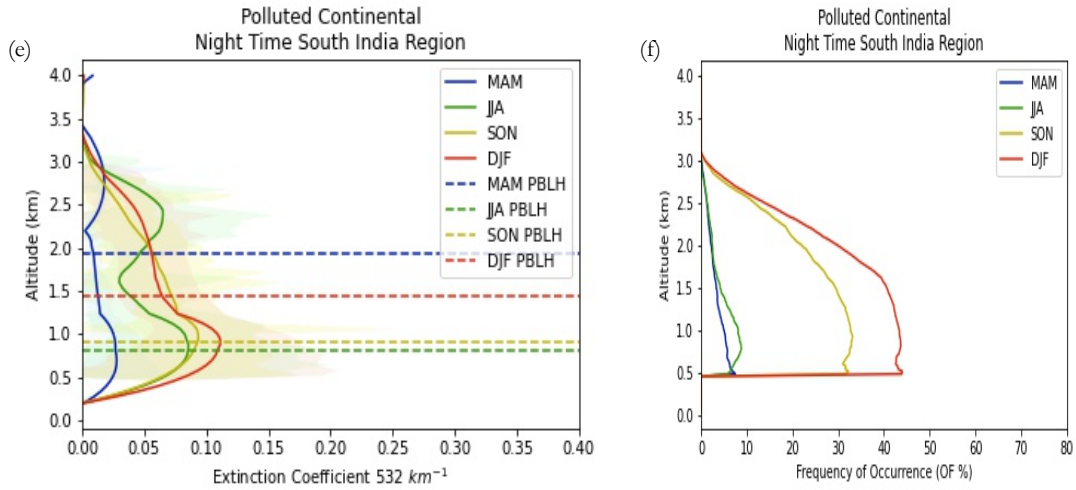


**Figure 19** Polluted continental seasonal nighttime extinction coefficient 532 retrievals and frequency of occurrence plots (a-b) Indian region (c-d) IGP region (e-f) South India region

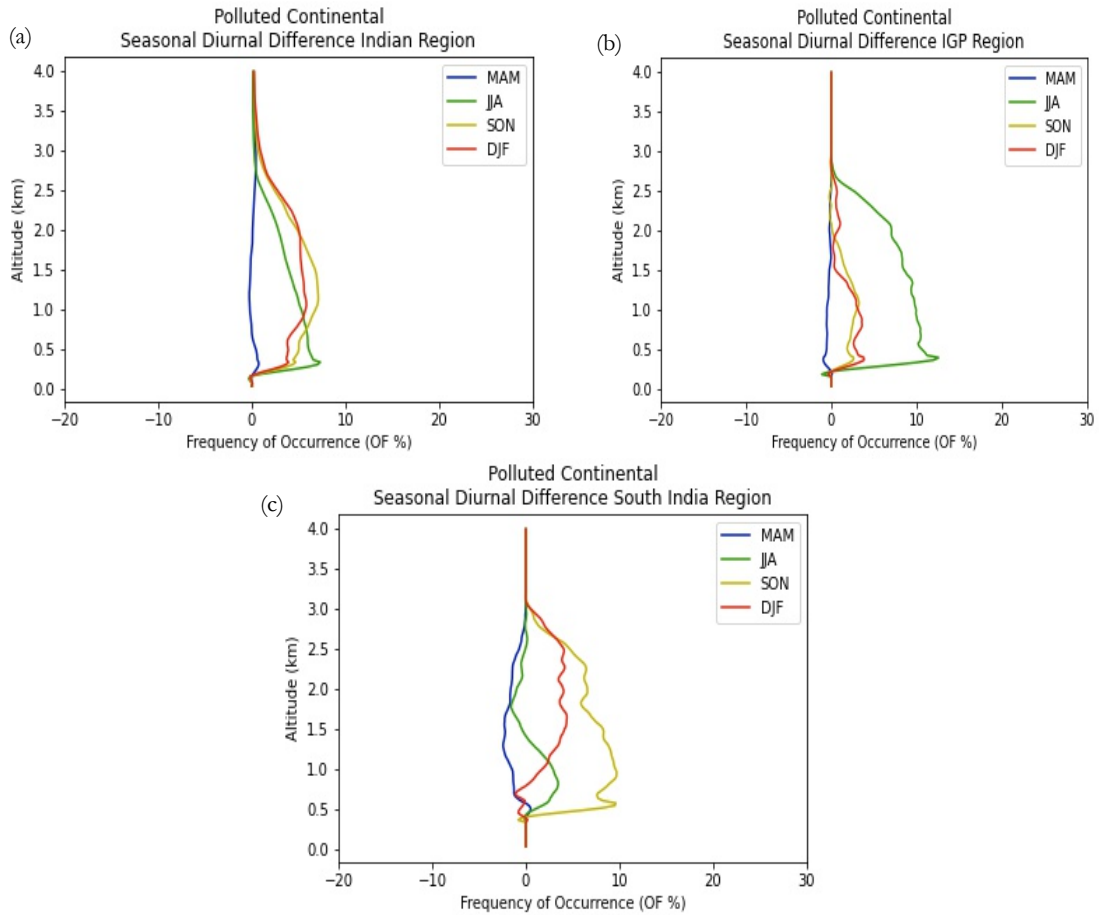


**Figure 20** Dust diurnal difference of frequency of occurrence plots (a) Indian region (b) IGP region (c) South India region

5.1.5. Smoke

Elevated smoke has high seasonal contrast in the Indian region as well as demarcated zones. Summer forest fires/wildfires, agricultural residue burning, and substantial stubble burning during SON, all contribute to the seasonal variance. It must be noted that the smoke concentrations are highly variable in space and time, they cause the highest uncertainties in aerosol estimation. The seasonal contrast in terms of extinction coefficient and frequency is apparent in the Indian region. The increased frequency of rising smoke during SON is caused by widespread stubble burning in the IGP region. It is important to mention that the frequency of occurrence is greater during JJA in IGP, which requires more research. However, this may be related to bagasse burning in June. The demarcated region also found to be the converging zone of winds from different parts of the country (Figure 3 (c), (d)). Winds at 500 hPa carries smoke from sugar mills in the IGP belt to such elevations. From fig. no, it is evident that nighttime concentration is higher. The MAM season in both the IGP region and the Indian region has the least diurnal fluctuation.

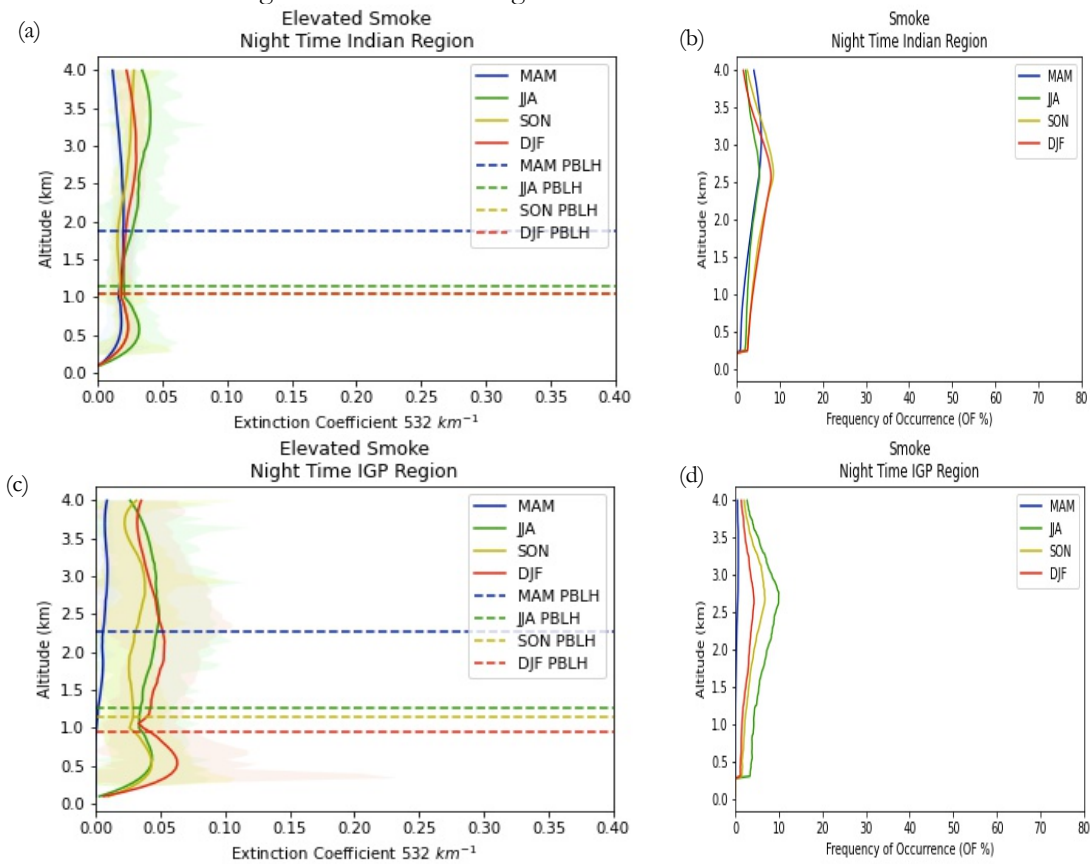


Figure 21 Smoke seasonal nighttime extinction coefficient 532 retrievals and frequency of occurrence plots (a-b) Indian region (c-d) IGP region (e-f) Desert region

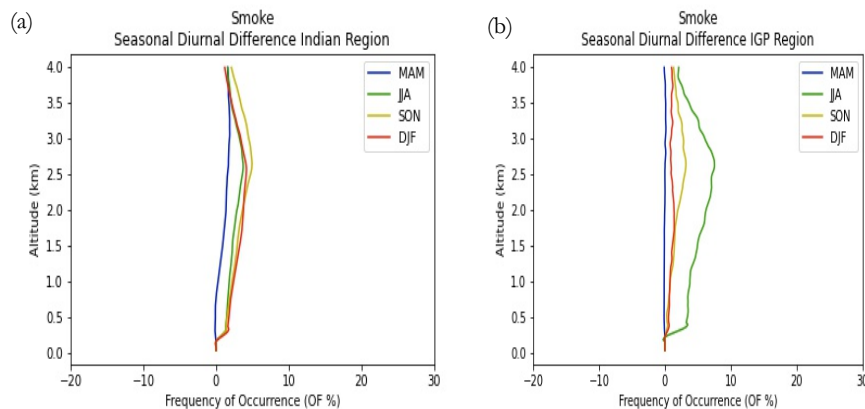
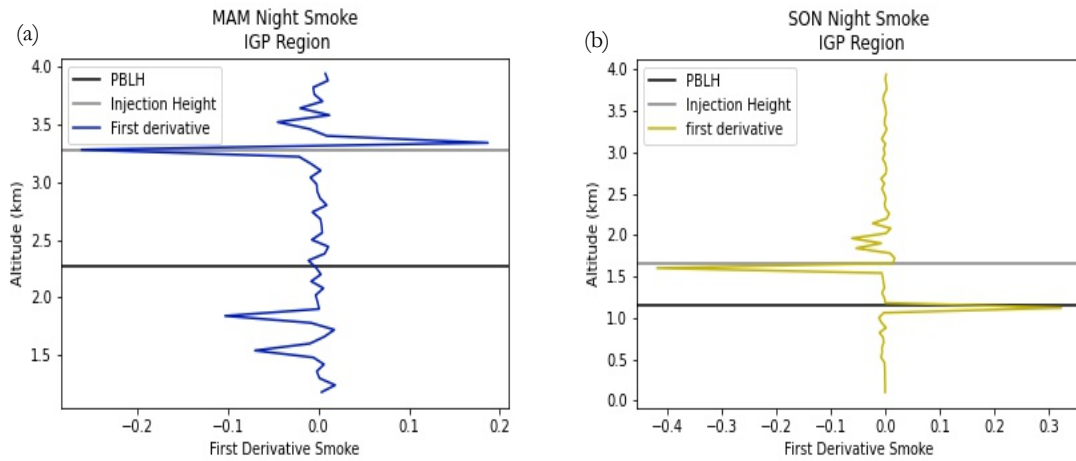


Figure 22 Dust diurnal difference of frequency of occurrence plots (a) Indian region (b) IGP region

The smoke injection height:

The two seasons are carefully selected to compare the smoke injection height of two different residue burning seasons (Figure 23). During the MAM wheat residue is burnt while in SON rice residue is burnt. Apart from the stubble bring, the PBLH in the two seasons found to be significantly different. To calculate the injection height, the minima are calculated using the first-order derivative. The minimum slope in MAM was determined to be at 3.2 km and is substantially higher than the season's mean PBLH ( $2.275 \pm 0.176$  km). While in SON, the smoke injection height was found at 1.67 km, near the seasonal mean PBLH ( $1.15 \pm 0.178$  km). The lower injection height during SON is due to lower thermal convection. While for mean injection height, further derivatives are required to be calculated in the tropospheric column. A similar observation was reported by (KS et al., 2020).



**Figure 23** Smoke Injection Height in IGP region (a) MAM season (b) SON season

## 5.2. Percentage fraction of aerosols over land surface

The extinction coefficient fractional distribution in altitude bin of 0-2 km and 2-4 km is shown in Figures 24, 25. The fractional distribution which is the concentration contribution of aerosol type can be compared to the frequency of occurrence of respective aerosol subtype, which describes the relative distribution of aerosol type in the atmosphere.

### 5.2.1.1. MAM Lower bin (0-2 km):

In lower altitudes, i.e. 0-2 km, polluted dust, and dust are present in about equal proportions during the day and night in the Indian region. This is similar to frequency distribution in Figure No. 14 (a), 17 (a). The near similar proportion is due to dominance of polluted dust in the South Indian region while in Northern India the dust is more prevalent. In terms of regional variability during the season, the South Indian region is dominated by polluted dust, and the percentage portion increases considerably at night which is well captured in the diurnal difference of MAM polluted dust Figure No. 17(d). Smoke aerosols show a significant reduction of 10% among other aerosols in the South India region. The IGP and Desert area is dominated by dust, with the desert region having the greatest loading of dust among all regions. The diurnal variability of dust aerosol in the IGP region is considerable, but low variation is reported in the desert zone in lower altitudes. Similar observation was noted in Figure No. 14 (d), 14 (f).

### 5.2.1.2. MAM Upper bin (2-4 km):

Polluted dust is the major aerosol in the Indian region in the upper bin, with higher concentrations at night. Like 0-2 km bin dust is major aerosol in 2-4 km bin, with similar diurnal variability, however, the extinction retrieval are of lower magnitude than the 0-2 km bin. The near-equal distribution of dust is previously noticed for the Indian region in Figure 14(b), 17(b). Dust again dominated the IGP and Desert region, with the desert region having the largest proportion of dust. The diurnal fluctuation is comparable to the 0-2 km bin. An important observation here is that the frequency of occurrence of dust increased in upper altitudes in the desert region during the nighttime (Figure No. 16 (c)). This might be possibly due to the higher frequency of dust events starting late in the evening or ongoing long range transport of dust. Polluted dust still dominates the South Indian region both during daytime and nighttime, it does in 0-2 km bin.

### 5.2.1.3. JJA Lower bin (0-2 km):

According to the schedule of monsoon outlined in Chapter 3, when the monsoon arrives, the aerosols type in the 0-2 km bin varies. The monsoon act as a wet deposit for dust and smoke also reduces during the season. In the Indian region, clean continental (background aerosols), are also present in comparatively higher percentages during JJA, although the percentage fraction falls during the night. Besides clean continental aerosols, oceanic aerosols rose in the Indian coastal area, with no diurnal fluctuation. The dust becomes a dominant aerosol in the Indian region both during daytime and nighttime. The increase could be because of the washout of polluted dust due to rain across a significant part of the country. In terms of the zonal variation of aerosols types in the 0-2 km bin of the JJA, dust is the predominant aerosol both during the day and at night in the IGP region and the Desert region. During the day, there is no substantial seasonal drop in dust percentage in the IGP region and desert region, while there is a considerable reduction at night in the same bin. This is because of the decrease in dust activities during the nighttime and the change in wind directions. It is noteworthy that a considerable seasonal decrease in dust aerosols in the desert region is found both at night and during the day. Dust, polluted dust, and polluted continental are in considerable proportions during daytime in the south India region. Although polluted dust levels were reduced in the JJA compared to the MAM, it remained the dominating aerosol in the night at lower elevations in the South India region.

### 5.2.1.4. JJA Upper bin (2-4 km):

Dust again in JJA is the most prevalent aerosol in the 2-4 km bin in the Indian region, just as it is in the 0-2 km bin. In the Indian region, there is a substantial seasonal drop in polluted dust concentration during the season. During the day and at night, the seasonal reduction is 10% and 20%, respectively. Smoke levels also vary in the Indian region, there is 10 percent more smoke loading at night. In the top bin compared to the lower bin of the Indian region, the concentration of clean continental, dusty marine, and marine is found to be higher, especially during the day.

Now, in terms of zonal variability, dust is the main aerosol in the IGP and Desert region. Like the Indian region, daytime dust loading is higher in the upper bin during the season. In both IGP and the Desert areas, there is a significant seasonal drop in the dust at night is noted. Polluted dust has a substantial contribution at higher elevations, but it is lower than dust. It was also found that smoke concentrations rise during the night, similar to the Indian region. During the JJA season in South India, dust is the most prevalent aerosol during the day, while dust, polluted dust, and smoke are present in about equal amounts at night. Among all aerosols, significant seasonal decrease in polluted dust concentrations in South India, 30% and 20% during the daytime and nighttime, respectively.

#### **5.2.1.5. SON Lower bin (0-2 km):**

An upsurge in human activity occurs following the monsoon season. Polluted dust is the dominating aerosol in the Indian region, IGP, and Desert region both during the day and at night with no substantial diurnal variability. During the night, however, the total proportion of smoke and polluted continental equals polluted dust. This is because of large-scale stubble burning in the IGP. Also, due to lower the PBLH, the dispersion space for the pollutants decreases. There is a considerable seasonal drop in dust concentration in the Indian region and other zones, both during the day and at night. However, in terms of diurnal variability, the daytime concentration during SON is higher than at nighttime. The diurnal fluctuation in the frequency of occurrence is reflected in (Figure 15). Similar findings may be noted in the IGP and the Desert region. While polluted continental is the main aerosol in south India. Polluted dust is also present in nearly equal to the polluted continental percentage, both during nighttime. In terms of diurnal variability, polluted dust and polluted continental loading in the atmosphere during SON are higher at night than during the day in the Indian region and the demarcated zones (Figure 18, 20).

#### **5.2.1.6. SON Upper bin (2-4 km):**

During the season, as previously stated in the previous subsection, massive stubble burning and industrial pollution occur in the north Indian region. However, compared to lower bin during the season, elevated smoke is a dominant aerosol during the night in the Indian region, IGP, and South India region. While during the day, polluted dust, smoke, and polluted continental aerosols are present in about equal proportions in the 2-4 km bin. However, it is to be noted here that due to long-distance dust movement throughout the season, the dust is present in a comparable portion of polluted dust throughout the daylight. However, the dust fraction reduces during the nighttime (Figure 15).

#### **5.2.1.7. DJF Lower bin (0-2 km):**

During the winter, polluted continental is the major aerosol at night, whereas polluted dust is the dominating aerosol during the daytime in the Indian region, IGP region. However, both day and nighttime in the regions, the total proportion of smoke and polluted continental is greater than polluted dust. While in the South India region, polluted continental alone dominant aerosol both during daytime and at nighttime with negligible diurnal variability. Seasonal increase in polluted continental aerosol observed in all regions. However, in terms of diurnal variability, the concentration of polluted continental is more during daytime when compared to nighttime. The smoke aerosols experience a seasonal decrease during the day when compared to the night. In terms of diurnal variability of smoke within the season, nighttime smoke concentration in DJF is higher than in the daytime. The diurnal fluctuation of polluted continental is negligible.

#### **5.2.1.8. DJF Upper bin (2-4 km):**

As previously noted, some aerosols have height restrictions. Elevated smoke is an important characteristic of higher altitudes. During the night, smoke is the major aerosol in the Indian region, whereas polluted continental aerosol was the dominating aerosol during the day at higher altitudes. Compared to nighttime, smoke loading is 7% less than during the day. Smoke again is the dominating aerosol in the IGP region, both during the day and at night. The nighttime concentration is slightly higher than in the daytime. Compared to the SON, polluted dust concentrations dropped during DJF, but smoke concentrations rose both at night and during the day. Smoke remained prevalent in the South India region, both at night and during the day. The daytime concentration of smoke is lower than at nighttime levels.

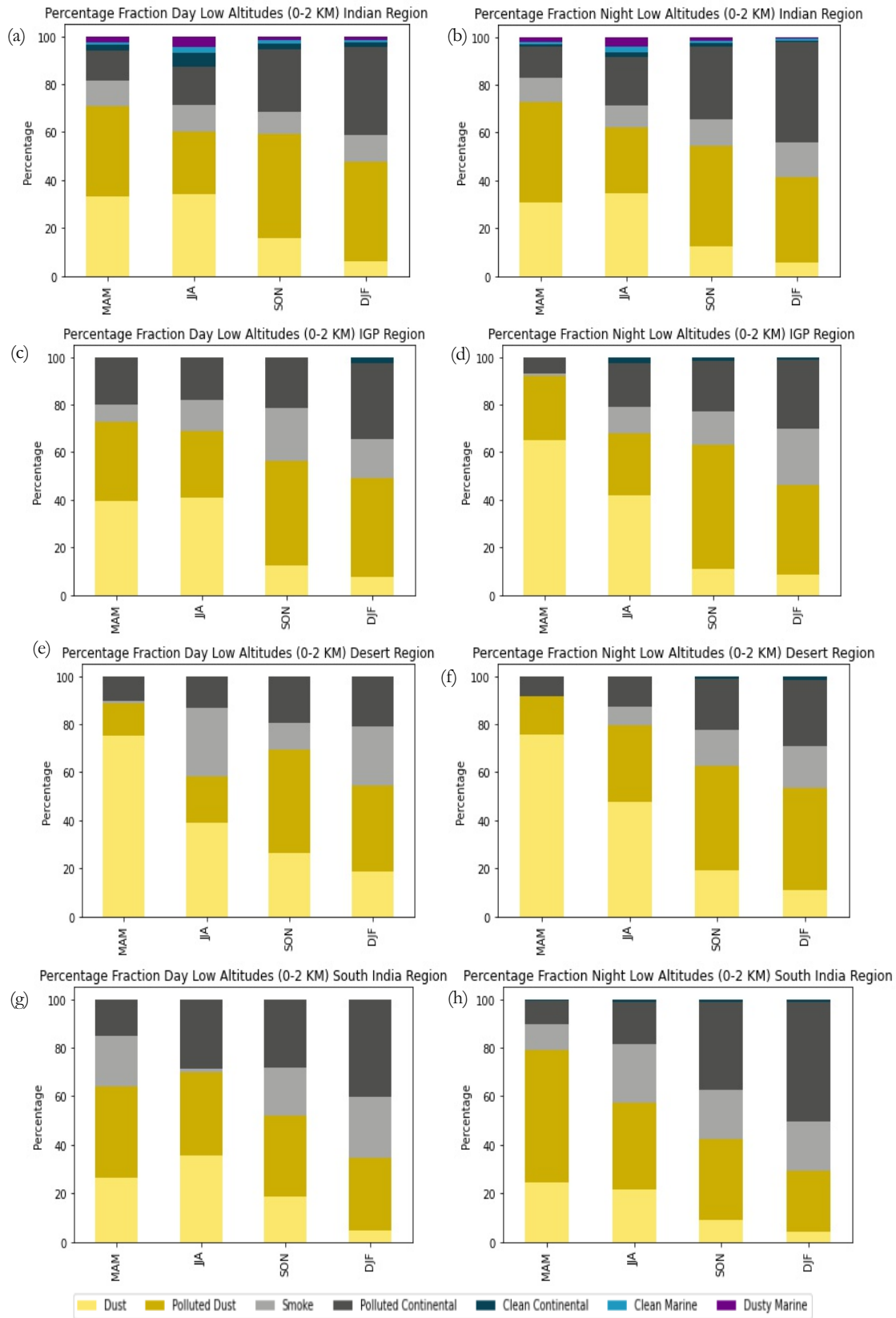


Figure 24 0-2 km seasonal diurnal percentage fraction of aerosols (a-b) Indian region (c-d) IGP region (e-f) Desert region (g-h) South India region

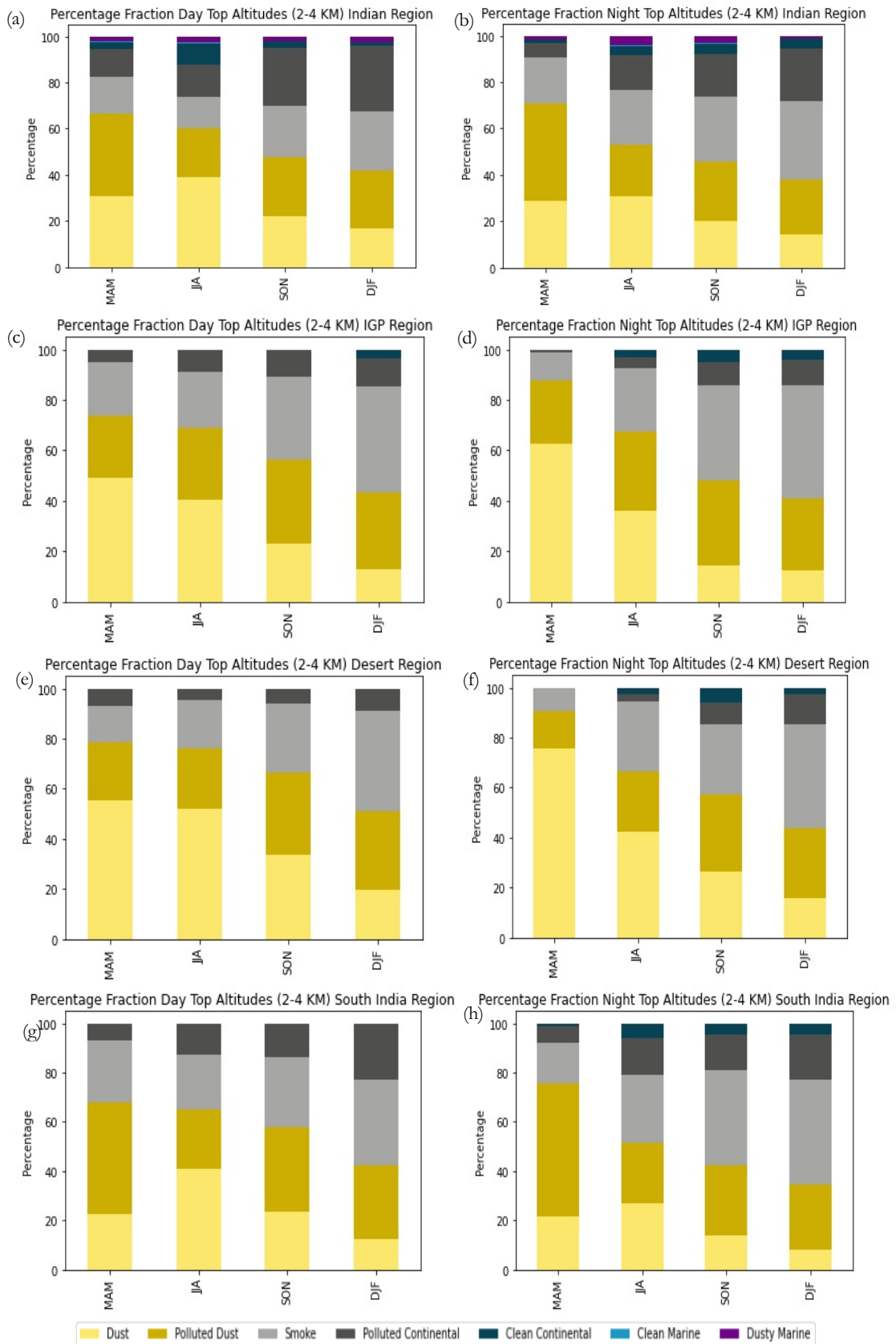
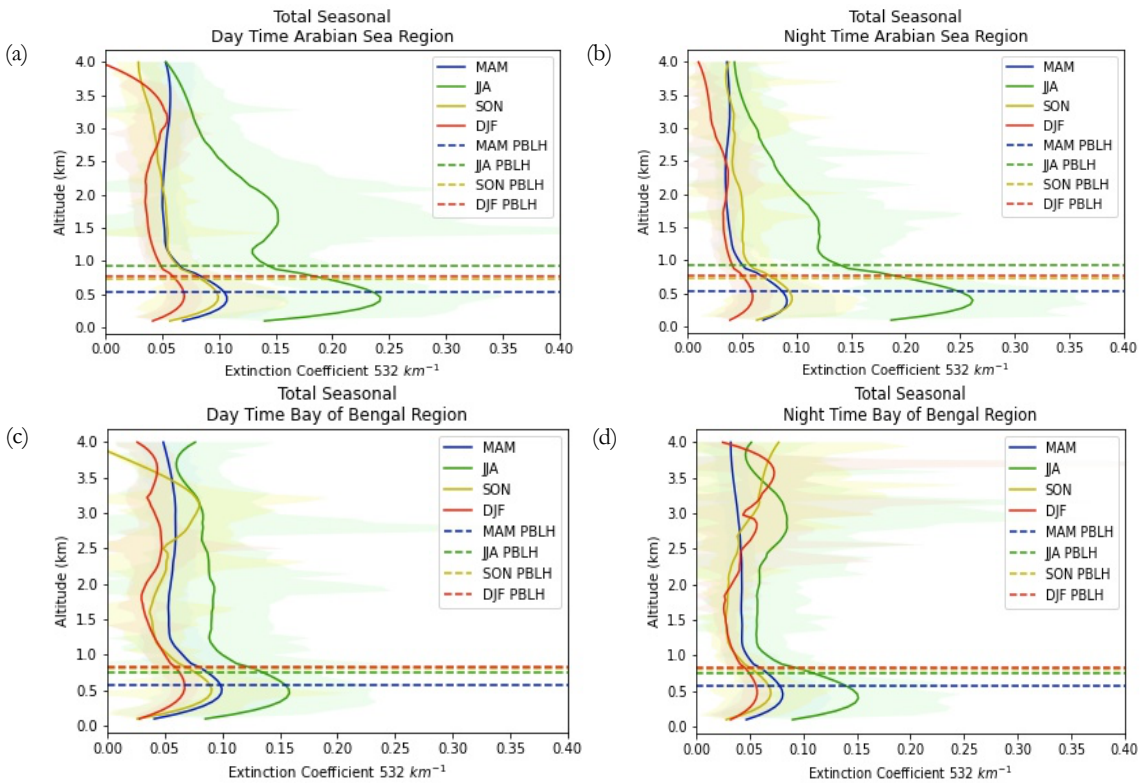


Figure 25 2-4 km seasonal diurnal percentage fraction of aerosols (a-b) Indian region (c-d) IGP region (e-f) Desert region (g-h) South India region

### 5.3. Vertical distribution of Aerosols over Oceanic Region

#### 5.3.1. Total Extinction

During JJA, high extinction profiles are observed during the daytime and nighttime in the Arabian Sea and the Bay of Bengal. The dusty marine aerosol may be responsible for such increase in extinction profiles. Lower altitudes show comparable pre- and post-monsoon extinction patterns, whereas higher altitudes show a small increase during SON. This is due to stubble burning in the IGP region, with smoke particles dispersing to the Bay of Bengal region due to wind conditions. It may also be noted that both the oceanic regions are near the Indian mainland coast. Because of the proximity, the influence of aerosols over the landmass can also be seen on the oceanic surface. A peak is also visible at 3 km height in JJA, which is caused by winds of 500 ha that flow from the desert region to the Bay of Bengal. In the Arabian Sea during DJF, a comparable peak is observed, which is primarily caused by prevailing winds. Some studies have also shown that strong winds at 850 hPa can transport dust-like particles from Somalia to the northern Arabian Ocean and the Gulf of Oman. This is one of the four dust transfer routes in the Arabian Sea. However, dust transportation in the Bay of Bengal is mostly due to dust transported by winds from the Thar Desert. In the next sections, the altitude-wise distribution is further discussed.



**Figure 26** Diurnal seasonal extinction coefficient 532 retrievals and frequency of occurrence plots (a-b) Arabian Sea (c-d) Bay of Bengal

**5.3.2. Marine**

Marine is frequently linked with sea salt, which is generated in two ways: first, through a fundamental process involving winds, and second, through a gas-to-particle conversion process. These particles contribute to cloud formation and are considered to have a substantial impact on the energy budget associated with ocean surfaces. Sea salt was identified up to a height of 2.5 km (Figure No. 27). Seasonal differences exist in both the Arabian Sea and the Bay of Bengal. In both locations, however, the prevalence is lowest during MAM season. During the JJA season, there is a high concentration of marine in terms of extinction profiles. The diurnal difference in both water surfaces is different. While marine in the Bay of Bengal is more prevalent during nighttime in all seasons, in the Arabian Sea marine is more prevalent during day-time pre-monsoon and monsoon.

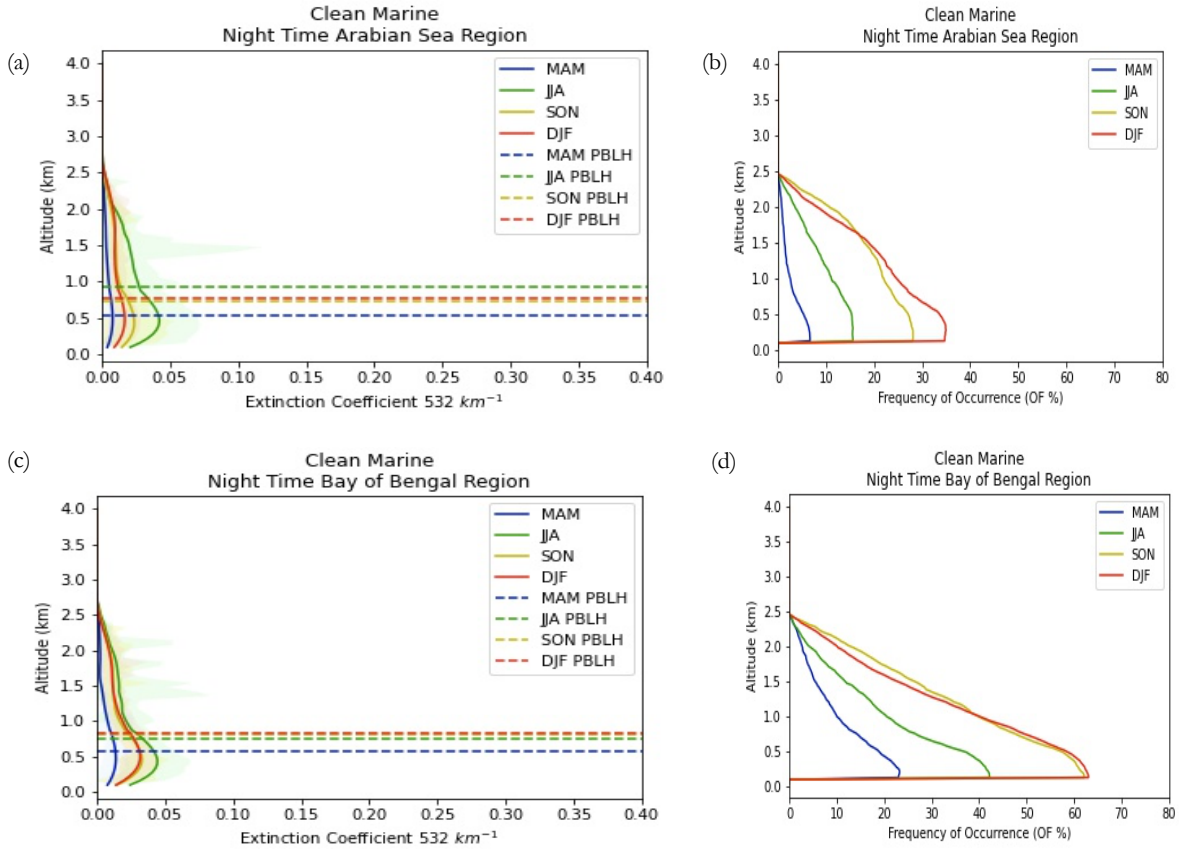


**Figure 27** Marine seasonal nighttime extinction coefficient 532 retrievals and frequency of occurrence plots (a-b) Arabian Sea (c-d) Bay of Bengal

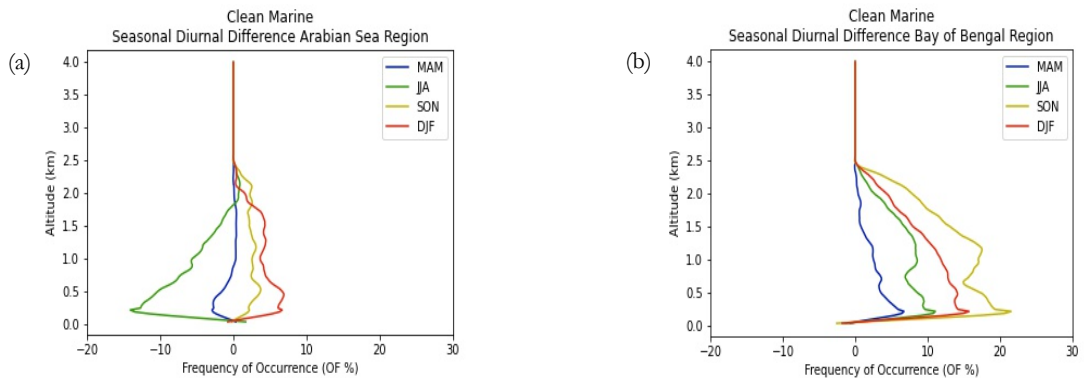


**Figure 28** Marine diurnal difference of frequency of occurrence plots (a) Arabian Sea (b) Bay of Bengal

5.3.2.1. Dusty marine

Dusty marine is an amalgamation of sea spray and dust particles. Dusty marine in the Arabian Sea occurs with about similar frequency in all seasons up to a height of 500 m, with a minor fluctuation in the MAM season. However, there is a seasonal change in dusty marine in the Bay of Bengal, which is largely due to the region's supply of dust. It is noteworthy that the nighttime concentration of dusty marine is more than the daytime. Dusty marine is more visible during the day because the concentration of dust is higher during the daytime than at nighttime owing to gravity attraction. Also, seasonal contrast is visible in terms of diurnal variability, which is also in line with dust distribution over the landmass.

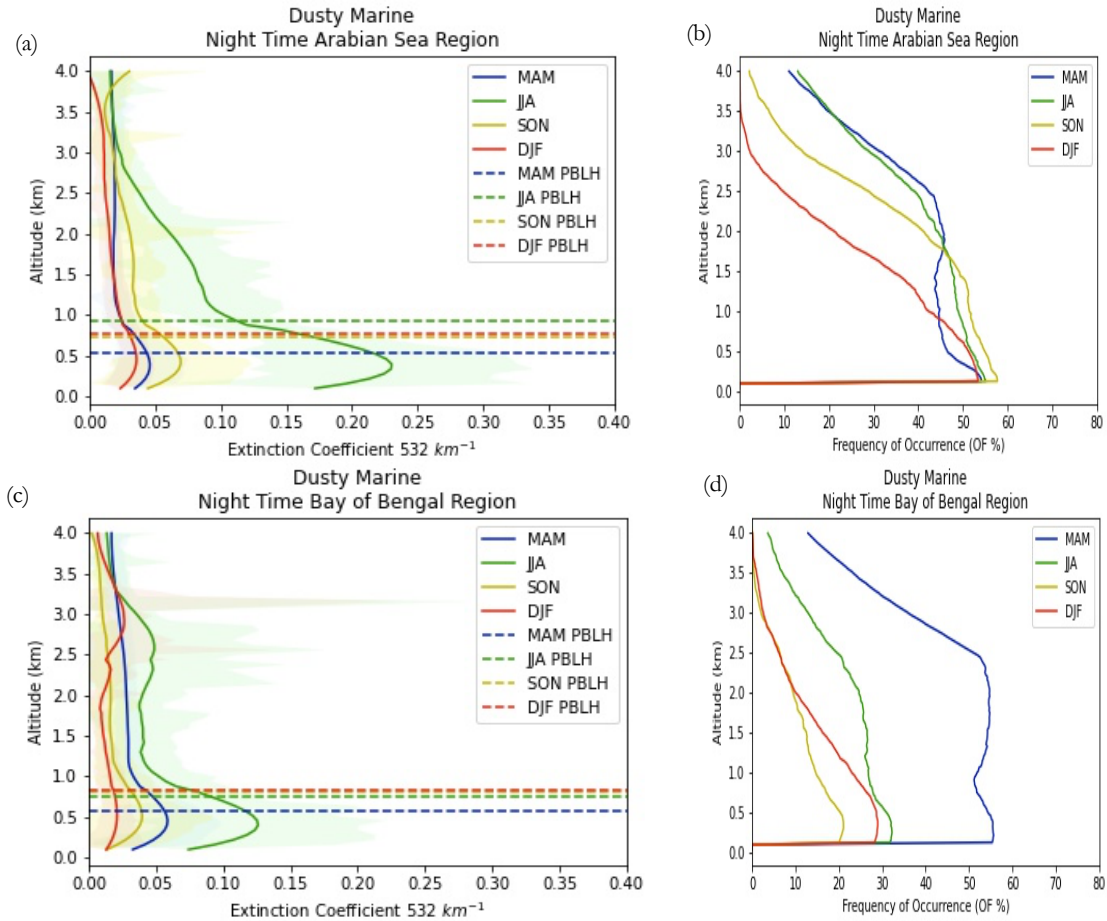


Figure 29 Dusty marine seasonal nighttime extinction coefficient 532 retrievals and frequency of occurrence plots (a-b) Arabian Sea (c-d) Bay of Bengal

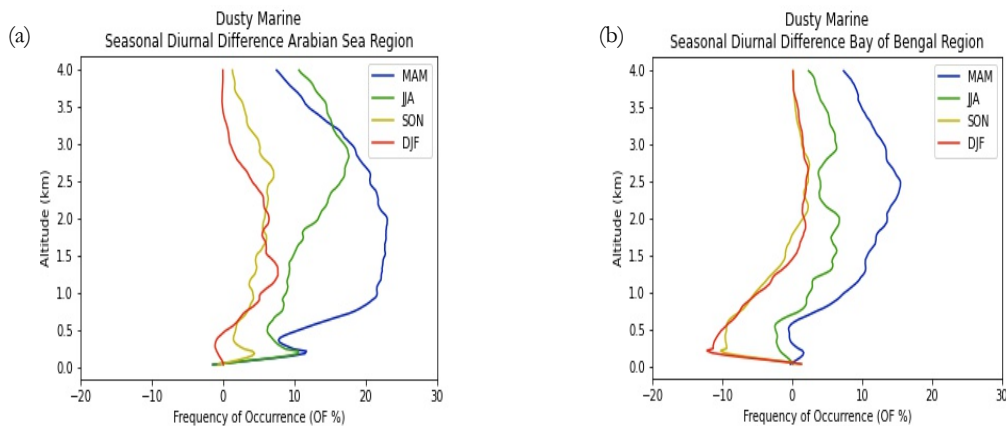
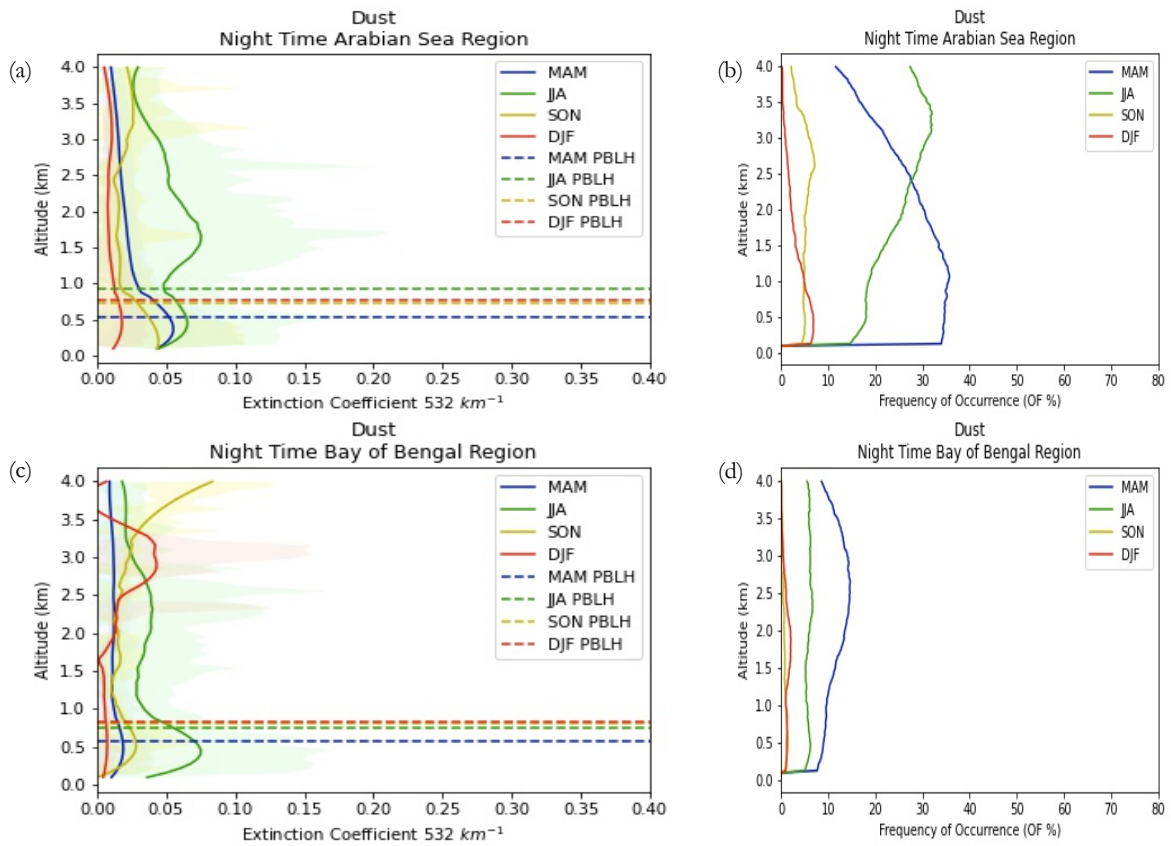


Figure 30 Dusty marine diurnal difference of frequency of occurrence plots (a) Arabian Sea (b) Bay of Bengal

**5.3.3. Dust**

The wind speed and direction from the source influence dust transport in the oceanic regions. Seasonal differences in dust may be noticed in both the Arabian Sea and the Bay of Bengal, with dust being more noticeable during the MAM and JJA seasons. During the MAM season, winds blow from the Arab region to the Indian subcontinent at all elevations, but the concentration is modest and dust loses height during its trajectory. During JJA, winds of 500 hPa blow from the Indian desert surface, bringing dust into the Arabian Sea (Figure 3). During the day, dust is more noticeable at lower altitudes in MAM, SON, DJF while at higher altitudes, the diurnal variation is insignificant. The seasonal contrast is greater in the Bay of Bengal due to the region's dust movement capability via wind. During MAM, high winds move dust from the desert region to other regions. Dust transportation is reduced during the JJA season due to a shift in wind direction, and this drop is exacerbated during the SON and DJF when polluted dust and smoke are carried. The dust in the Bay of Bengal is not simply mineral dust, but also dust from exposed agricultural regions during crop rotation. Higher elevations exhibit diurnal variations during MAM and JJA in the Bay of Bengal region.



**Figure 31** Dusty seasonal nighttime extinction coefficient 532 retrievals and frequency of occurrence plots (a-b) Arabian Sea (c-d) Bay of Bengal

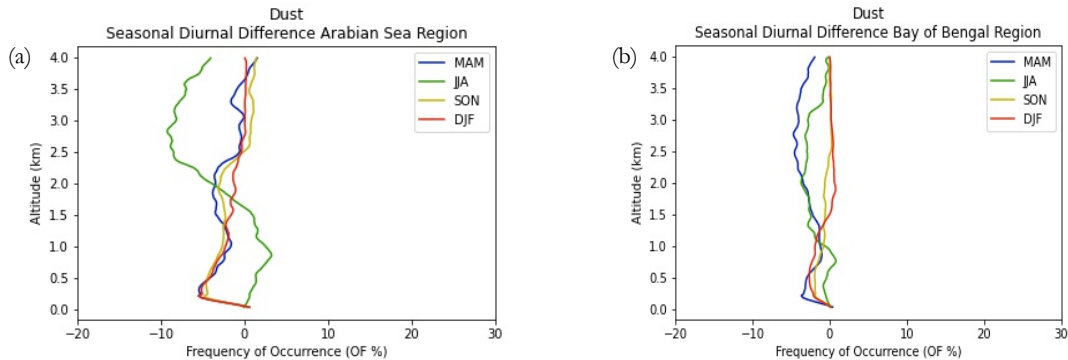


**Figure 32** Dust diurnal difference of frequency of occurrence plots (a) Arabian Sea (b) Bay of Bengal

## 5.4. Percentage fraction of aerosols over ocean surface

The extinction coefficient fractional distribution in altitude bin of 0-2 km and 2-4 km is shown in Figures 33, 34. The fractional distribution which is the concentration contribution of aerosol type can be compared to the frequency of occurrence of respective aerosol subtype, which describes the relative distribution of aerosol type in the atmosphere.

### 5.4.1. MAM Lower bin (0-2 km):

In terms of aerosol contribution, the lower bin of MAM is heterogeneous. Dust is the major aerosol type in the Arabian Sea both during the day and at night, with a greater concentration during the day. Smoke is present because of the region's closeness to the Indian landmass. Dusty marine is likewise one of the primary aerosols at night, with a considerable concentration nevertheless, the concentration of dusty marine is substantially less during the day. A similar observation was noted in the diurnal variability of dusty marine (Figure No. 30). Dusty marine is the dominating aerosol in the Bay of Bengal, both during the day and at night. However, smoke is present in about similar proportions during the daytime, owing to wind outflow from the IGP region. Marine is also found in the Bay of Bengal, although the concentration at night is somewhat higher than during the day. It is noteworthy that dusty marine concentration is much greater in the Bay of Bengal than in the Arabian Sea. A higher concentration of anthropogenic aerosols near the ground surface was also reported by (Nair et al., 2010).

### 5.4.2. MAM Upper bin (2-4 km):

During the MAM season, polluted dust is the major aerosol at higher altitudes in the Arabian Sea during the day, and dusty marine is the major aerosol at night, although smoke is also prevalent in a comparable range. While in the Bay of Bengal, dust, polluted dust, and smoke are present in about similar proportions during the day. Dusty marine is the dominating aerosol at night in the Bay of Bengal. Dusty marine dust has a significant diurnal fluctuation in both the Arabian Sea and the Bay of Bengal. The nighttime concentration in the Bay of Bengal is 18% more than the daytime concentration, while the dusty marine concentration in the Arabian Sea is 15% higher at night. The diurnal fluctuation of dust in the Arabian Sea is negligible at higher altitudes. There is 5% higher dust loading in the Bay of Bengal throughout the day than nighttime. Compared to the lower bin, the top bin has a higher concentration of dust, particularly during daytime in the Bay of Bengal.

### 5.4.3. JJA Lower bin (0-2 km):

The proportion of dusty marine in the atmosphere increases substantially during the day and night in the Arabian Sea in comparison to MAM. However, the concentration of dusty marine in the Bay of Bengal decreases (seasonal decrease) at night. It is worth mentioning that the concentration of dust in the Arabian Sea increased substantially as compared to the MAM season lower bin. During the night, the concentration of dusty marine is higher than daytime in both locations in Figure No. 30. Along with a seasonal increase in dusty marine, marine rose in both zones during JJA. The concentration of marine in the Arabian Sea is somewhat greater during the day, whereas it is higher at night in the Bay of Bengal. This had been previously reported in the frequency distribution plot. There is also a seasonal rise in the concentration of dust in the Bay of Bengal.

### 5.4.4. JJA Upper bin (2-4 km):

The concentration and diurnal variability of dusty marine in the upper bin remained consistent with the upper bin of MAM in the Arabian Sea during the day and night. Considerable seasonal increase in the dust fraction in the Arabian Sea during the daytime and nighttime. The dust is the dominating aerosol in the Arabian Sea, both during the day and at night. The percentage fraction of dust is greater during the day than at night. During the night, smoke is the most prevalent aerosol in the Bay of Bengal; conversely, dust is the most prevalent aerosol during the day due to the persistent supply of dust from the desert region (Figure 3). The percentage fractions of dusty marine and dust in the upper bin are about identical. Compared to MAM, dust rose during the day in the upper bin. The top bin experienced a seasonal reduction in the concentration of dusty marine during the nighttime in the Bay of Bengal. Dusty marine has negligible diurnal variability.

**5.4.5. SON Lower bin (0-2 km):**

Dusty marine is the dominating aerosol in the Arabian Sea both during the day and at night, with the daytime proportion being greater than the nighttime proportion. The seasonal decrease in dusty marine concentration is also observed during the night, but a minor seasonal rise during the day. Marine is also present in the bottom bin. The seasonal decline in marine is greater during the day and negligible at night.

In the Bay of Bengal region, dusty marine and dust are present in about similar proportions during the day, accounting for 28 percent each. During the night, dusty marine is the dominating aerosol, although smoke, marine, and dust are all present in comparable concentrations. The smoke increased seasonally as a result of intensive stubble burning in IGP, which is transported by the wind into the Bay of Bengal. Similar to smoke, marine nighttime concentrations are higher than daytime concentrations and have undergone seasonal increases in the respective bin.

**5.4.6. SON Upper bin (2-4 km):**

During SON, there is a decrease in dust, but a rise in smoke concentration in the Arabian Sea is observed. A significant increase in smoke was seen both during the day and at night, resulting in smoke being the dominating aerosol in the upper bin both during the day and at night. In terms of diurnal variability, the concentration of smoke at night is higher than during the day. Seasonal reduction of dust during the daytime was more significant (25%) while at night was (12-13%). The Arabian Sea has a modest seasonal rise in dusty marine during the day, while the nighttime seasonal fluctuation in the upper bin is negligible. However, the percentage of dusty marine is higher at night than during the day.

In the Bay of Bengal region, like the Arabian Sea, a substantial seasonal increase in smoke concentration is observed and smoke is found to be dominating aerosol both during the day and at night. Nighttime concentration is greater than daytime concentration. During the night, there is a significant seasonal drop in dusty marine, but during the day, the seasonal concentration is the same as JJA in 2-4 km.

**5.4.7. DJF Lower bin (0-2 km):**

In the Arabian Sea, dusty marine and smoke have comparable percentage fractions of 33 percent during the day, but smoke is the dominant aerosol at night. There is a modest seasonal drop in dust fraction. The concentration of marine aerosol changes is insignificant both diurnally and seasonally. The seasonal concentration of dusty marine decreases slightly, although the nighttime concentration in DJF exceeds the daytime concentration. During the day, dusty marine is the main aerosol in the Bay of Bengal region, while at night, marine is the dominating aerosol. There is a seasonal rise in marine and smoke aerosol concentrations, but a seasonal reduction in dusty marine concentrations at night. The concentrations of marine and smoke are lower during the day than at night and are in comparable proportions. It is also noted that the dusty marine concentration in the lower bin is highest during MAM and decreases till DJF season in the Bay of Bengal. While marine increases in each season. A similar observation was seen for marine in the Arabian Sea, and no such trend was seen in the case of dusty marine.

**5.4.8. DJF Upper bin (2-4 km):**

Both during the day and at night, smoke is the dominant aerosol in the Arabian Sea and the Bay of Bengal. The diurnal fluctuation of smoke aerosol in the Bay of Bengal region is negligible, and there is a seasonal rise in smoke concentration in the region. However, in the Arabian Sea region, the seasonal rise and concentration of smoke are greater at night. Conversely, in the Bay of Bengal region, dusty marine, there is a seasonal rise at night.

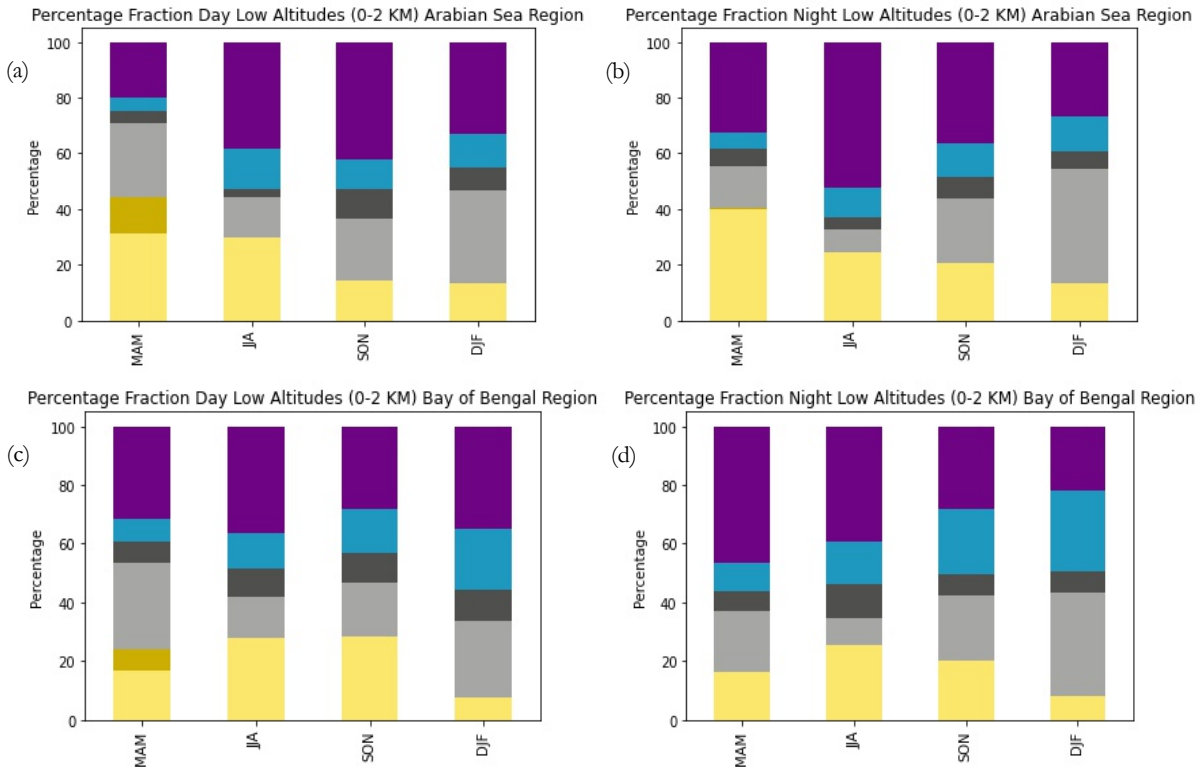


Figure 33 0-2 km seasonal diurnal percentage fraction of aerosols (a-b) Arabian Sea (c-d) Bay of Bengal

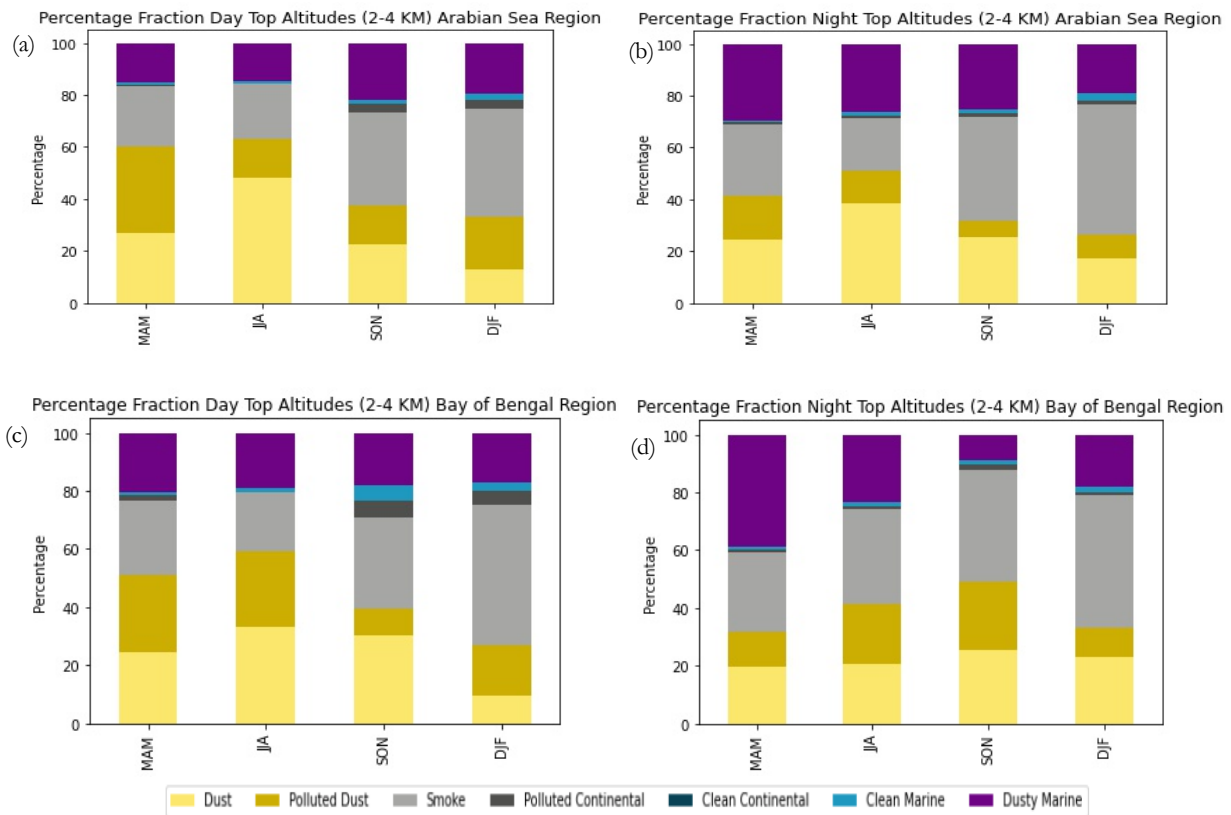


Figure 34 2-4 km seasonal diurnal percentage fraction of aerosols (a-b) Arabian Sea (c-d) Bay of Bengal

### 5.5. AOD and MERRA2 comparison

As part of the validation of CALIPSO derived column integrated mean is compared with the monthly mean MERRA 2 AOD. It must be noted that MERRA 2 data is at a coarser resolution and is an assimilated data and the observation is taken on cloud-free conditions. The CALIPSO derived extinction profiles are subject to uncertainties due to retrieval algorithm, Lidar ratio for surface types and cloud conditions. The systematic bias of CALIPSO AOD with AERONET has been previously reported by (H. Kim & Paulson, 2013; A. H. Omar et al., 2013; Schuster et al., 2012; Solanki & Singh, 2014). Comparison of CALIPSO dataset with ground-based sensors has been discussed in chapter 2 however improved retrieval are improved in V4 CALIPSO data (Kar et al., 2018; M. H. Kim et al., 2018; M. Vaughan et al., 2019). It must be noted that proper AOD estimation by CALIOP sensor is highly dependent on CALIPSO orbital pass at the time of the event. In the current work, V4 data is used.

MERRA 2 estimated slightly lower AOD compared to CALIPSO column integrated AOD on land surfaces. The underestimation has already been reported by (Buchard, Randles, da Silva, et al., 2017). However, except JJA CALIPSO column integrated mean AOD of CALIPSO is lower than that of MERRA 2 in the Desert region, which needs further verification. Since MERRA 2 assimilates MISR data over bright surfaces, a negative bias is reported by (Mangla et al., 2020). A similar observation is noted for AOD and Dust optical depth in the JJA season in the Indian region. A large variation is seen during dust during JJA, this is primarily due to the washout of dust particles during the season. Another reason is that in the current work, extinction profiles are also retrieved during the cloudy conditions while in MERRA 2 only cloud-free conditions are considered. Dust AOD in the South India region in Figure No. 35 is the best manifestation of the variation where monsoon arrives comparatively earlier than other zones in the study area. In the current research, polluted continental and elevated smoke is combined from the CALIPSO dataset, while in MERRA 2 Organic Carbon and Black Carbon is combined. Since smoke concentrations are highly variable in comparison to dust, this adds uncertainty in MERRA 2 estimates (Buchard, Randles, da Silva, et al., 2017; E. Sun et al., 2019).

#### 5.5.1. Total

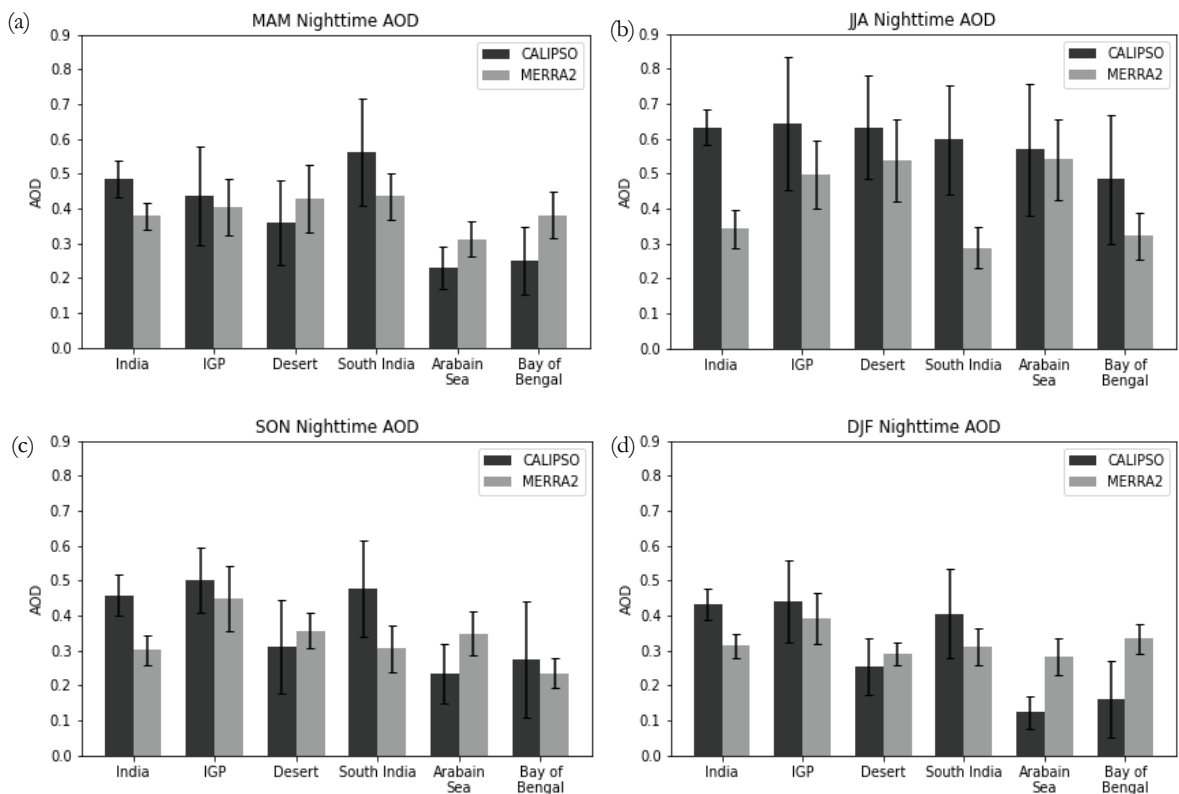


Figure 35 CALIPSO and MERRA 2 seasonal nighttime AOD

5.5.1.1. Dust

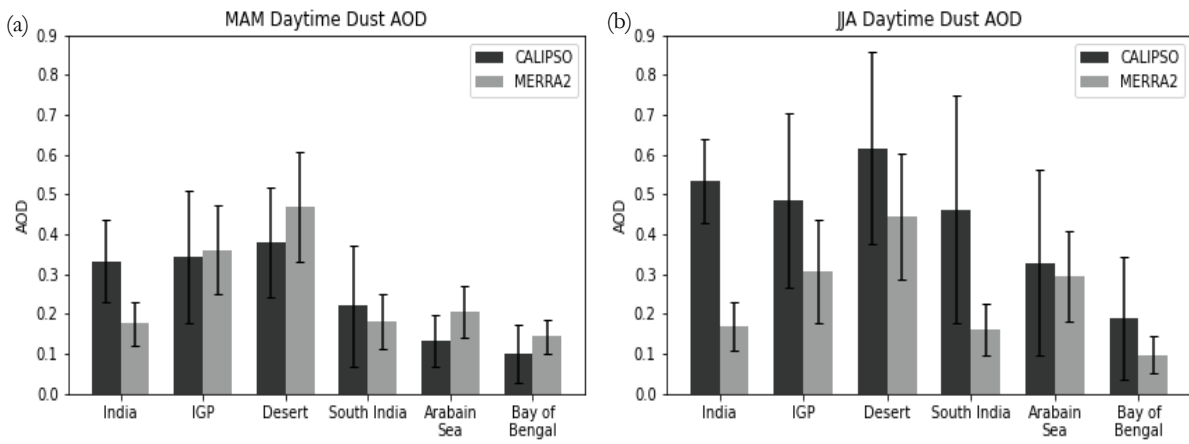


Figure 36 CALIPSO and MERRA 2 seasonal nighttime dust AOD

5.5.1.2. Polluted dust

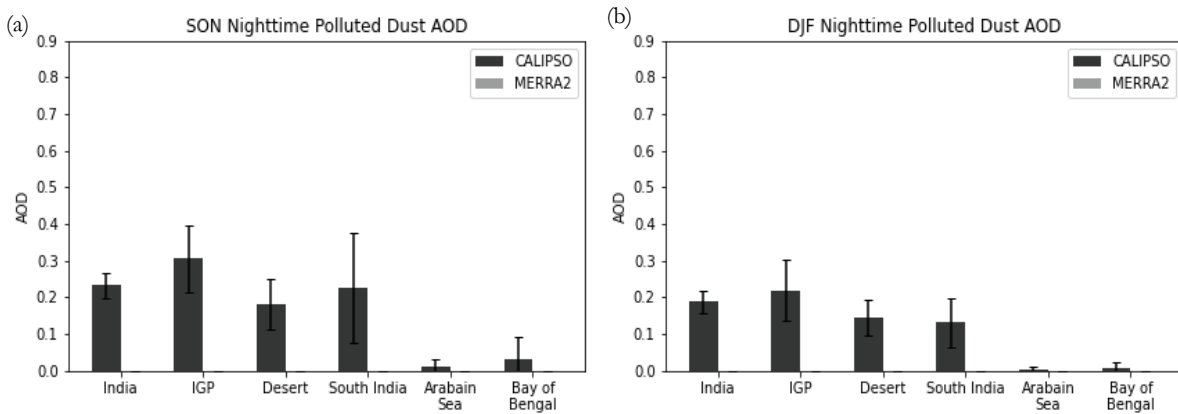


Figure 37 CALIPSO and MERRA 2 seasonal nighttime polluted dust AOD

5.5.1.3. Smoke

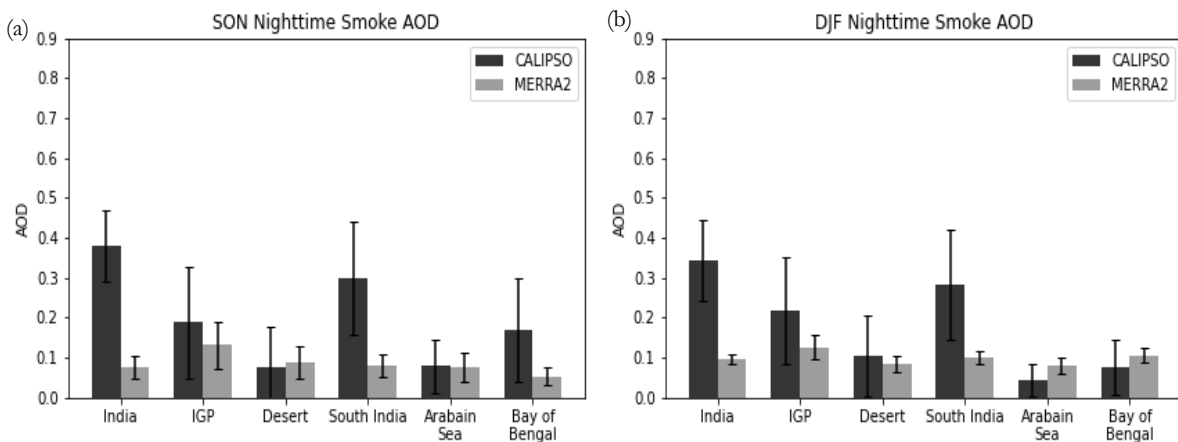


Figure 38 CALIPSO and MERRA 2 seasonal nighttime smoke AOD

**5.6. Trend analysis**

**5.6.1. Total AOD trend analysis**

The seasonal trend analysis was performed for the Indian region and the zones within the study area, the changing nature of aerosol loading in the region. The non-parametric Mann-Kendall test is used to check the significance test. It may be noted that due to the disagreement between the two data as explained in section 5.5 the trend between the two datasets may not agree with each other. Also, during the analysis, it was found that on the longer temporal range some trends between the two datasets did not agree due to which the temporal range was further divided into 2007-2013 and 2014-2020.

Dissimilarity in AOD between the two datasets was seen mostly in the MAM season in comparison to another season. An increasing trend (0.00146) during MAM was seen for the Indian region, while MERRA-2 showed a weakly decreasing trend (-0.00051). However, the two datasets showed similar trends during (2007-13 and 2014-20). A decreasing trend was seen in the IGP region, which may be attributed to the decreasing trend in the dust. South India region needs further validation with other sources as MERRA 2 showed a significantly decreasing trend (0.0673) while CALIPSO showed a non-significant increasing trend (0.00036). It may be possible due to the increasing polluted dust trend in the zone, which MERRA 2 does not characterize. In the JJA season, decreasing trend is seen in the Indian region as well as different demarcated zones. An exception again is the South India region was during daytime slope values of both datasets were significant however during, nighttime the two datasets showed near similar decreasing trend values. This might be ascribed to the region's cloud cover as a result of the region's early beginning of monsoon (Figure No. 4). During post-monsoon seasons, the trends from both datasets are similar and showed an increasing trend. Significantly increasing trends are seen during the DJF over the land surface.

Daytime	Nighttime	↑ - Increasing trend	↓ - Decreasing trend	*/* - Significantly decreasing/ increasing
---------	-----------	----------------------	----------------------	--

**Table 8 MAM AOD trend**

	2007-2020		2007-2013		2014-2020	
	CALIPSO	MERRA 2	CALIPSO	MERRA 2	CALIPSO	MERRA 2
Indian Region	↑	↓	↑	↑	↓	↓
IGP Region	↓	↓	↑	↓	↑	↑
Desert Region	↑	↑	↓	↑	↓	↑
South India	↑	↓*	↓	↑	↑	↓
Arabian Sea	↓	↓	↑	↓	↑	↓
Bay of Bengal	↓	↑	↑	↑	↑	↑

**Table 9 JJA AOD trend**

	2007-2020		2007-2013		2014-2020	
	CALIPSO	MERRA 2	CALIPSO	MERRA 2	CALIPSO	MERRA 2
Indian Region	↓	↓	↑	↓	↓	↓
IGP Region	↓	↓	↓	↓	↓	↓
Desert Region	↓	↓	↓	↓	↓	↓
South India	↑	↓	↓	↓	↓	↓
Arabian Sea	↓	↓	↓	↓	↓	↑
Bay of Bengal	↓	↓	↑	↓	↑	↑

**Table 10** SON AOD trend

	2007-2020		2007-2013		2014-2020	
	CALIPSO	MERRA 2	CALIPSO	MERRA 2	CALIPSO	MERRA 2
Indian Region	↑	↑	↑	↑	↓	↓
IGP Region	↑	↑	↑	↑	↑	↑
Desert Region	↑	↑	↓	↓	↑	↑
South India	↑	↑	↑	↑	↓	↓
Arabian Sea	↓	↑	↓	↑	↓	↑
Bay of Bengal	↑	↑	↑	↑	↓	↓

**Table 11** DJF AOD trend

	2007-2020		2007-2013		2014-2020	
	CALIPSO	MERRA 2	CALIPSO	MERRA 2	CALIPSO	MERRA 2
Indian Region	↑*	↑*	↑	↑	↑	↑
IGP Region	↑*	↑	↑	↑	↓	↓
Desert Region	↑*	↑*	↑	↓	↑	↓
South India	↑*	↑	↑	↑	↑	↑
Arabian Sea	↓	↑	↑	↓	↑	↑
Bay of Bengal	↑	↑	↓	↓	↑	↑

**5.6.2. Dust AOD trend analysis**

The decreasing trend is seen in CALIPSO data set in both seasons, with a Desert region. CALIPSO during the MAM season showed a decreasing trend of (-0.00040) whereas MERRA showed an increasing trend of (0.00254). Similar variation was observed in the Desert region between 2007-13 and 2014-20. The variation between the two could be linked to the explanation in section 5.5. A significantly decreasing trend is seen in oceanic regions in the study area.

**Table 12** MAM Dust AOD trend

	2007-2020		2007-2013		2014-2020	
	CALIPSO	MERRA 2	CALIPSO	MERRA 2	CALIPSO	MERRA 2
Indian Region	↓	↓	↑	↑	↓	↑
IGP Region	↓	↓	↓	↑	↑	↑
Desert Region	↓	↑	↓	↑	↓	↑
South India	↓	↑	↑	↑	↑	↑
Arabian Sea	↓	↓	↑	↑	↑	↑
Bay of Bengal	↓	↑	↓	↑	↑	↑

**Table 13** JJA Dust AOD trend

	2007-2020		2007-2013		2014-2020	
	CALIPSO	MERRA 2	CALIPSO	MERRA 2	CALIPSO	MERRA 2
Indian Region	↓	↓	↑	↓	↓	↓
IGP Region	↓	↓	↓	↓	↓	↓
Desert Region	↓	↓	↑	↓	↓	↓
South India	↓	↓	↓	↓	↓	↓
Arabian Sea	↓*	↓	↓	↓	↓	↑
Bay of Bengal	↓*	↓	↓	↑	↓	↑

**5.6.3. Polluted dust AOD trend analysis**

During pre-monsoon and monsoon, an increasing trend is seen in polluted dust, significantly increasing in the Indian region during MAM. This may be because of the high dust loading/emissions during and wind speed in the season. During the season, due to the change of crop, the loose soil dust is also carried away by the high winds. Post-monsoon decreasing polluted dust trend is seen in the Indian region and the zones due to change in wind direction, however, this may need proper characterization. This is primarily because apart from desert dust, soil dust also contribute of in the formation of and the polluted dust particle. Again, during DJF the winds blow from the desert region, which further intermixes with continental pollution particles. It is to be noted that polluted dust is also formed due to intermixing of soil dust.

**Table 14** Polluted dust AOD trend (MAM and JJA)

	MAM			JJA		
	2007-2020	2007-2013	2014-2020	2007-2020	2007-2013	2014-2020
Indian Region	↑*	↓	↑	↑	↑	↑
IGP Region	↑	↑	↑	↑	↑	↑
Desert Region	↑	↑	↑	↑	↑	↓
South India	↑	↓	↑	↑	↓	↓

**Table 15** Polluted dust AOD trend (SON and DJF)

	SON			DJF		
	2007-2020	2007-2013	2014-2020	2007-2020	2007-2013	2014-2020
Indian Region	↓	↓	↓	↓	↑	↓
IGP Region	↓	↓	↓	↑	↑	↑
Desert Region	↓	↓	↓	↑	↑	↓
South India	↓	↓	↓	↑	↓	↑

#### 5.6.4. Smoke

Indian region post-monsoon is dominated by anthropogenic aerosols like smoke, polluted continental etc. Unlike dust, smoke emissions are highly variable in space and time, however the concentration of smoke in the IGP region remains near consistent. The low underestimation of smoke in MERRA 2 has been previously been reported by (Randles et al., 2017) due to the integration of data from multiple platforms. An increasing trend for smoke is observed in both datasets in the Indian region. But it may be noted that decreasing trends are seen in both datasets during 2014-2020 in the Indian region as well as in South India. Smoke emissions continue to rise in the IGP region, which is mostly due to stubble burning in the region. A significantly increasing trend during 2007-2020 is reported by CALIOP in the IGP region.

**Table 16** SON Smoke AOD trend

	2007-2020		2007-2013		2014-2020	
	CALIPSO	MERRA 2	CALIPSO	MERRA 2	CALIPSO	MERRA 2
Indian Region	↑	↑	↓	↑	↓	↓
IGP Region	↑*	↑	↑	↑	↑	↑
South India	↑	↑	↑	↑	↓	↓

**Table 17** DJF Smoke AOD trend

	2007-2020		2007-2013		2014-2020	
	CALIPSO	MERRA 2	CALIPSO	MERRA 2	CALIPSO	MERRA 2
Indian Region	↑	↑	↓	↓	↓	↑
IGP Region	↑*	↓	↑	↓	↓	↓
South India	↑*	↑	↑	↓	↑	↑

#### 5.6.5. Oceanic aerosols trend analysis

Oceanic aerosols here is the combination of sea-salt and dusty marine aerosols. In near all seasons, there is good agreement between the trends of the two datasets. It is largely noticed that there is an increasing trend in oceanic aerosols both during nighttime, similar observations are noted during daytime. An important observation here is that decreasing trend in oceanic aerosols is seen in the SON season. A few studies have reported the weakening of winter monsoon due to which the wind over the Bay of Bengal and Arabian Sea has decreased (Natesan & Subramanian, 1991; Parvathi et al., 2017; HuiJun Wang & He, 2012). As discussed earlier wind is the primary parameter of oceanic aerosol formation, due to decreased wind speeds in the region, a decreasing trend is seen. It should be noted that a few studies have already reported no direct correlation between increasing oceanic aerosol and increasing cyclones in the region during the season (Luo et al., 2019). The studies have reported an increase in cloud cover and convective activities due to oceanic aerosols.

**Table 18** MAM Oceanic Aerosol AOD trend

	2007-2020		2007-2013		2014-2020	
	CALIPSO	MERRA 2	CALIPSO	MERRA 2	CALIPSO	MERRA 2
Arabian Sea	↑	↑	↓	↑	↑	↑
Bay of Bengal	↑	↑	↑	↑	↑	↑

**Table 19** JJA Oceanic Aerosol AOD trend

	2007-2020		2007-2013		2014-2020	
	CALIPSO	MERRA 2	CALIPSO	MERRA 2	CALIPSO	MERRA 2
Arabian Sea	↑	↑	↑	↓	↑	↑
Bay of Bengal	↓	↑	↑	↑	↓	↑

**Table 20** SON Oceanic Aerosol AOD trend

	2007-2020		2007-2013		2014-2020	
	CALIPSO	MERRA 2	CALIPSO	MERRA 2	CALIPSO	MERRA 2
Arabian Sea	↓	↓	↓	↓	↓	↑
Bay of Bengal	↓	↓	↑	↑	↓	↓

**Table 21** DJF Oceanic Aerosol AOD trend

	2007-2020		2007-2013		2014-2020	
	CALIPSO	MERRA 2	CALIPSO	MERRA 2	CALIPSO	MERRA 2
Arabian Sea	↑	↑	↓	↓	↑	↓
Bay of Bengal	↑	↑	-	-	↓	↓

### 5.7. Trend analysis in altitude bins

Indian region is majorly dominated by dust and polluted dust during MAM, however, due to variability in dominance in various zones as discussed earlier. The trend in each bin for total extinction is majorly decided by the dominant aerosol. An increasing trend in the Indian region is due to the significantly increasing trend of polluted dust in 0-2 km in the Indian region. A similar observation is seen in the 2-4 km bin as well. The decreasing trend in 0-2 km of IGP and desert region goes in line with decreasing trend of dust in the corresponding bin. However, the upper bin of the IGP region and desert region have a weakly decreasing trend, which is also in line with the weakly decreasing slope of dust in the corresponding bin.

The increasing trend in the upper bin of the IGP and desert region may be attributed to the relatively higher increasing trend in extinction profiles of other aerosols in the corresponding bin. Similar observations were noted for the South Indian region.

During monsoon, dust is a major aerosol type on both lower and upper bins in the Indian region and demarcated zones. The decreasing trend in extinction profiles is seen in the Indian region and zones due to the decreasing trend in dust extinction profiles. Similar observations were noted during nighttime for the Indian region and zones.

Post monsoon, as the anthropogenic activities increases, smoke is the dominant aerosol in the region. Post monsoon increasing trend is seen in both SON and DJF in total extinction profiles and extinction profiles of smoke. Increasing in smoke is noted both during daytime and nighttime in all regions in both bins.

**Table 22** Seasonal AOD (Total) trend

	MAM		JJA		SON		DJF	
	0-2 km	2-4 km						
Indian Region	↑	↑	↓	↓	↑	↑	↑*	↑
IGP Region	↓	↑	↓	↓	↑	↑	↑	↑
Desert Region	↓	↑	↓	↓	↑	↑	↑	↑
South India	↑	↑	↓	↑	↑	↑	↑	↑
Arabian Sea	↑	↑	↓	↑	↑	-	↑	↑
Bay of Bengal	↓	↑	↓	↓	↓	↑	↑	↑

**Table 23** Dust AOD trend

	MAM		JJA		SON		DJF	
	0-2 km	2-4 km						
Indian Region	↓	↓	↓	↓	↓	↓	↑	↓
IGP Region	↓	↓	↓	↓	↓	↑	↑	↑
Desert Region	↓	↓	↓	↓	↓	↑	↑	↓
South India	↑	↓	↓	↑	↓	↓	↓	↓

**Table 24** Polluted dust AOD trend

	MAM		JJA		SON		DJF	
	0-2 km	2-4 km						
Indian Region	↑*	↑*	↑	↑	↓	↓	↑	↓
IGP Region	↓	↑	↑	↓	↓	↑	↑	↑
Desert Region	↑	↑	↓	↑	↓	↑	↑	↑
South India	↑	↓	↑	↑	↓	↓	↑	↓

**Table 25** Smoke AOD trend

	MAM		JJA		SON		DJF	
	0-2 km	2-4 km						
Indian Region	↑	↑	↑	↑	↑	↑	↑	↑
IGP Region	↑	↑	↑	↓	↑	↑	↑	↑
South India	↑	↑	↑	↓	↑	↑	↑	↑

**Table 26** Oceanic aerosol AOD trend

	MAM		JJA		SON		DJF	
	0-2 km	2-4 km						
Arabian Sea	↑	↑	↑	↑	↓	↓	↑	-
Bay of Bengal	↑	↑	↓	↓	↓	↓	↑	-

**5.8. Special Case: April-May 2020 COVID-19 lockdown case study**

**5.8.1. Vertical profiles to total aerosol**

During the lockdown, researchers from all across the world investigated changes in air quality in their respective regions. Many people sought to study based on AOD in the Indian region (Madineni et al., 2021; M. K. Mishra & Rathore, 2021b; S. K. Pandey & Vinoj, 2021; Pathakoti et al., 2020b). Only a few research has looked at the vertical distribution of aerosols during the period (Mehta, Hooda, et al., 2021; S S Prijith et al., 2021). Significant changes in air quality have also been documented in the Indian region, according to the some researchers. Within India, (S. Gautam, 2020) discovered geographical variation in AOD. In similar a context, vertical distribution is examined in the current case study. The extinction profiles of several aerosol types during April-May 2020 are compared to the averaged extinction profiles for April-May 2015-19 (Figure 39). Total aerosol loading was reduced by approximately 10% during the day and 12.59% during the night in the Indian region. A similar observation was made by (Mehta, Hooda, et al., 2021; Pathakoti et al., 2020a). The decreased anthropogenic activity was predicted to result in lower aerosol loading, however much of the reduction was ascribed to a substantial drop in dust aerosols. A few studies have also reported an increase in certain aerosols in various regions, which is investigated further in this section. Significant reduction in extinction profiles was observed in the IGP region in terms of regional variability of total aerosol loading reduction in different zones described in Chapter 3. In the South India region, insignificant changes in total AOD has been noted however significant variability in extinction profiles is observed.

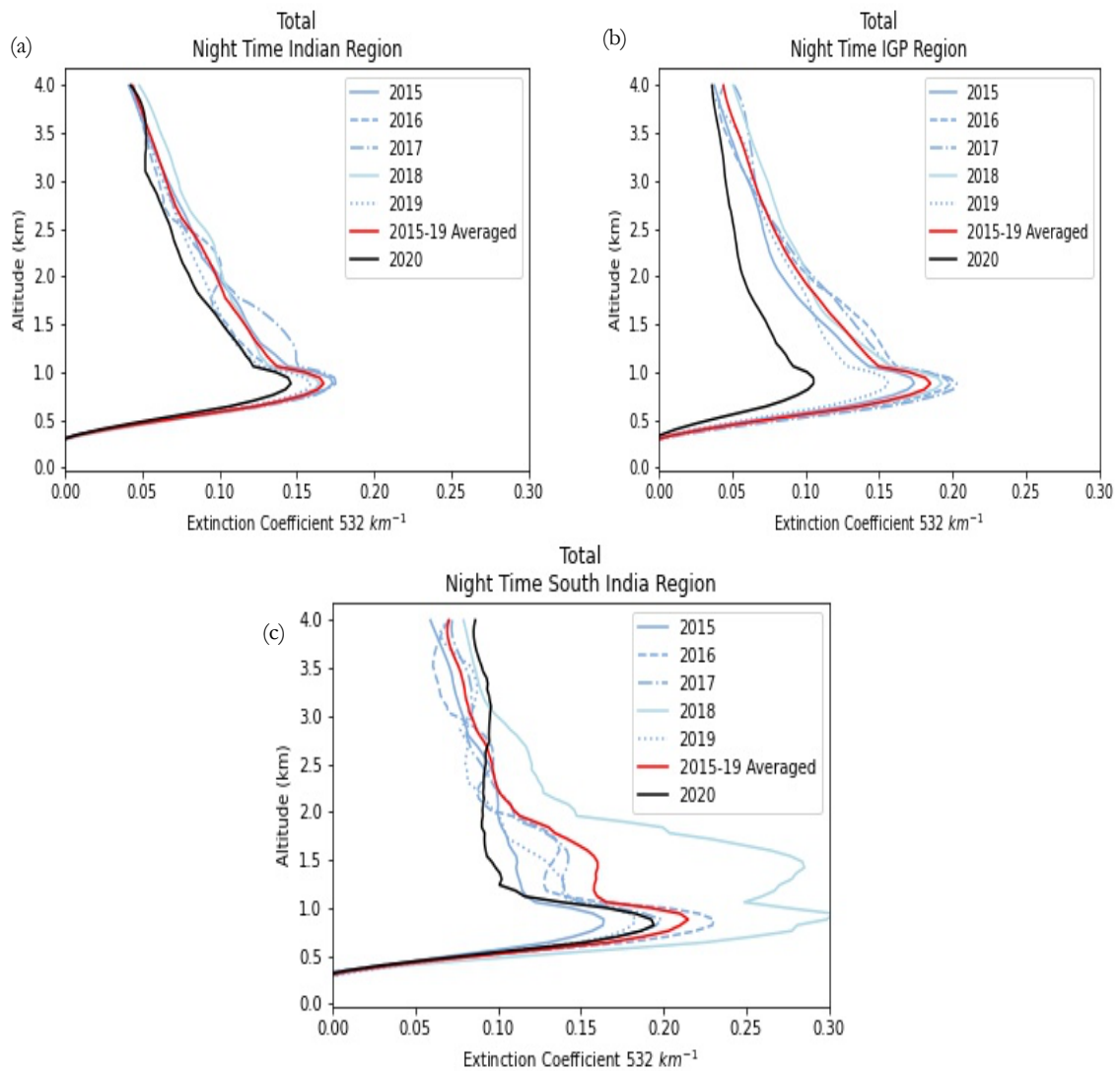


**Figure 39** Extinction coefficient nighttime during lockdown and before lockdown in (a) Indian region (b) IGP region (c) South India region

**5.8.2. Dust vertical profiles**

Among different aerosol types, a major reduction is noted in dust aerosol significantly in the IGP region. Similarly, a reduction in the frequency of occurrence is also noted in Figure 40. Nighttime reduction is higher when compared to daytime in India and zones. Near about 40% reduction is observed in dust loading in the Indian region during nighttime. The reduction is near consistent in both 0-2 km and 2-4 km altitudes bin. The nighttime reduction was more than daytime. The desert region is not considered, avoiding bias in comparison because of the unavailability of data of May 2020 for the region. It is noted that the year 2018 extinction profile for dust in Indian region is higher than the 2015-19 mean extinction profiles, which are because of the dust storm in Northern India. The sources of particles are during on 7 May 2018, 8 May 2019, 8 May 2020 are checked using HYSPLIT model (Figure 42). It is found that the majority of the particles were from the local sources compared to the distinct dust sources in previous years.

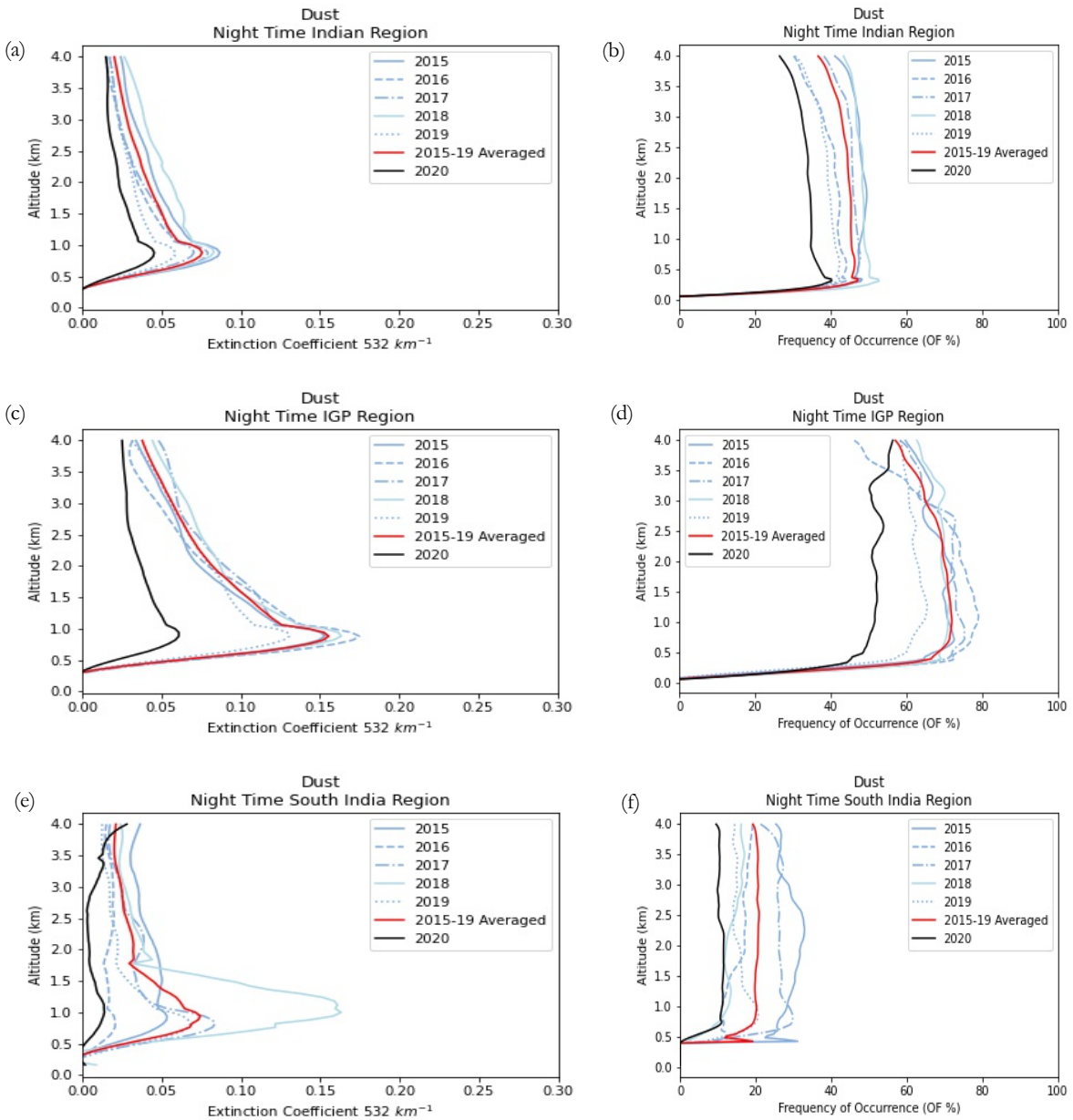


**Figure 40** Dust extinction coefficient and frequency of occurrence during nighttime during lockdown and before lockdown in (a) Indian region (b) IGP region (c) South India region

**5.8.3. Polluted dust vertical profiles**

A few studies reported slightly increase in AOD in certain areas, especially in the state of Maharashtra, Central India, North East. The cause of such an increase is linked with the active fires in the region during the period (S S Prijith et al., 2021). High variability is seen in extinction profiles is noted in the South India region. Lower altitudes up to 1 km and higher altitudes above 2.5 km saw an increase in extinction coefficients. Among the several zones of the research area, the IGP region had a significant rise (32 per cent) in polluted dust during the nighttime (Figure 41 (b)). On the contrary, during the daytime, a decrease in extinction profiles was observed in the IGP region. The percentage increase of polluted dust in the region however is less than the decrease of dust and other anthropogenic aerosols.

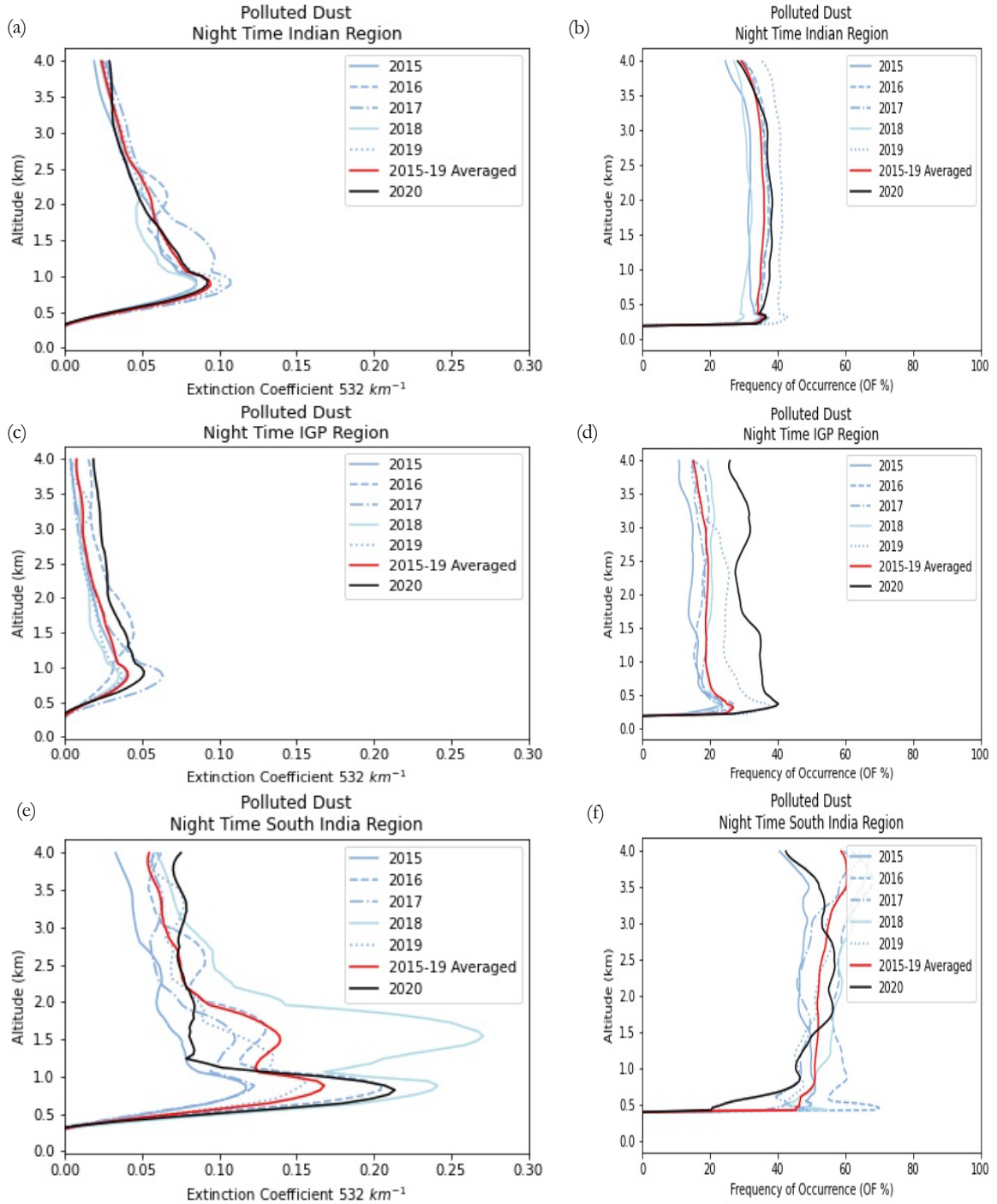


**Figure 41** Polluted dust extinction coefficient and frequency of occurrence during nighttime during lockdown and before lockdown in (a) Indian region (b) IGP region (c) South India region

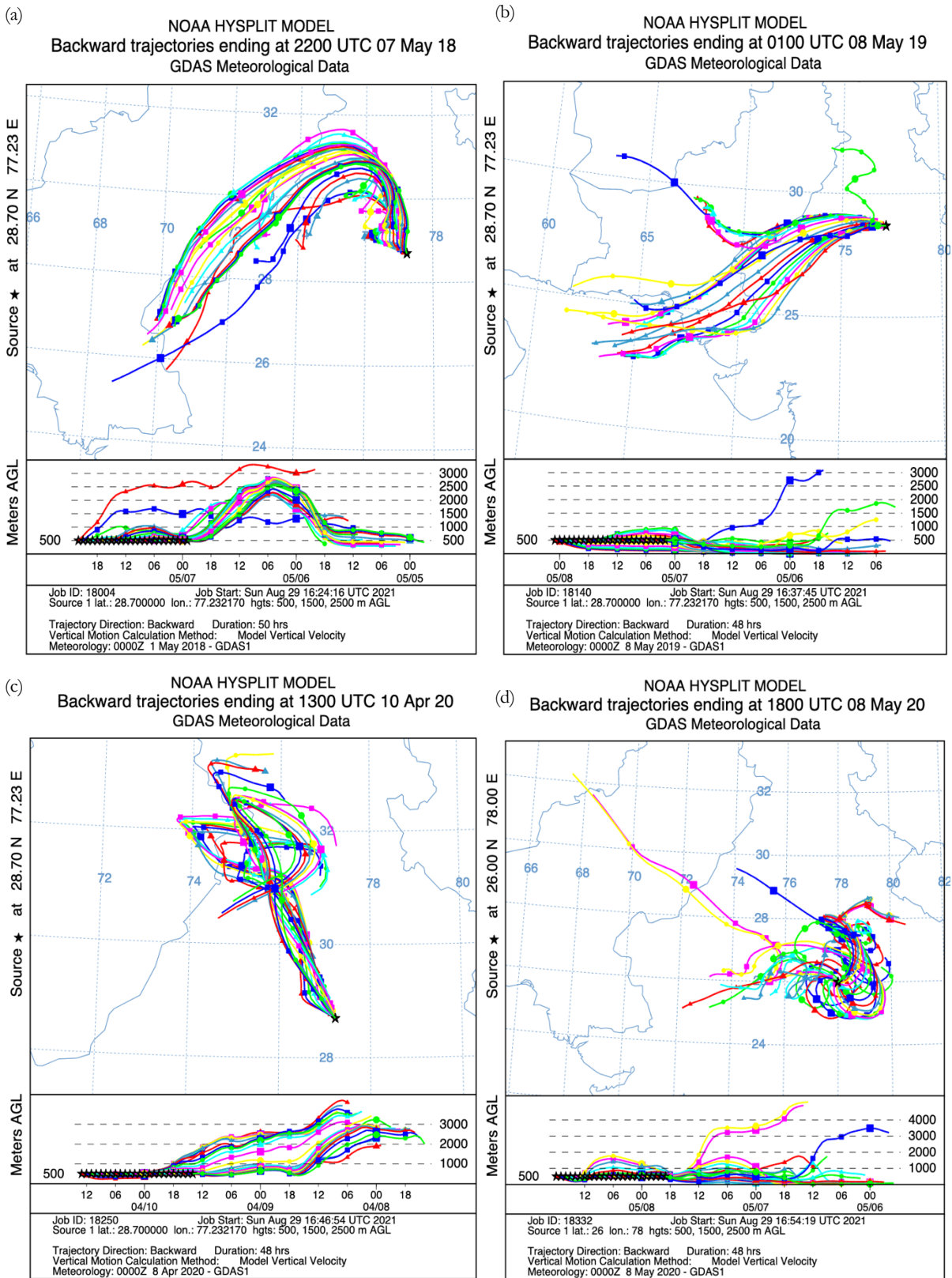
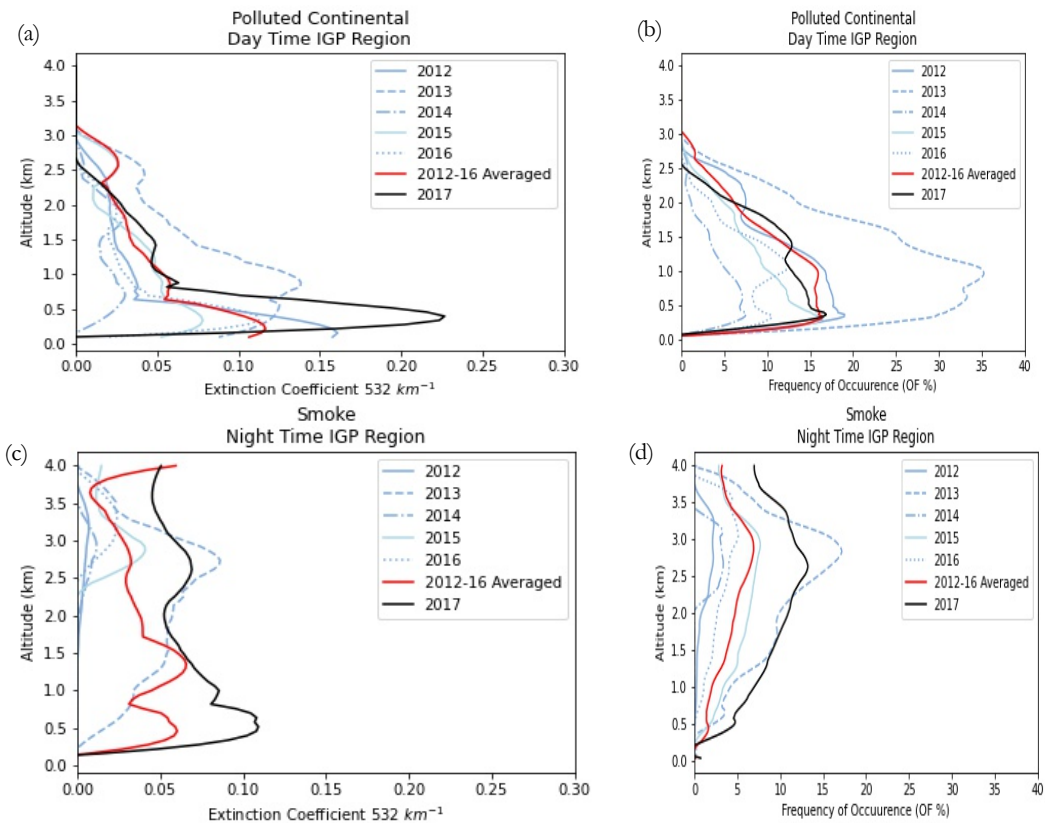


Figure 42 HYSPLIT back trajectory analysis for IGP region (a) 7 May 2018 (b) 8 May 2019 (c) 10 April 2020 (d) 8 May 2020

**5.9. Special Case: Smoke cases of India**

During winter, polluted continental and smoke are the dominant aerosols in the Indian region. As noted previously, stubble burning causes a rapid increase in smoke concentration in the area. It should be emphasized that the IGP designated zone does not encompass all stubble burning locations, particularly in the Punjab region. However, an increase is seen in the defined zone. The extinction profiles of different aerosol types during October-November 2017 are compared with October-November 2015-19 averaged extinction profiles. There is a rise in elevated smoke concentration in the region, both in terms of extinction coefficient and frequency of occurrence. There is also a significant increase in polluted continental extinction values, although the distribution in the atmosphere remains the same as in previous years. During the analysis, it was also found that the concentration, occurrence frequency of polluted continental were high in 2013 (Figure 43 (b)). It should be noted that there was only few CALIPSO orbital pass over the region during the peak time, the next orbital snapshot is shown in Figure 44. The latitude v/s altitude vertical feature mask is shown in the figure. It is visible that the major concentration of polluted continental aerosols is in Northern India. During trajectory analysis, it is found that there is a contrast between the trajectory of particles during 2013 and 2017. In 2013, the source of the particles was below 270 m, which depicts the dominance of polluted continental aerosols which travelled with the ground surface winds (Figure 45 (a)). During November 2017, however, particles in the area were also transported by distant sources at heights more than 1000 m (Figure 45 (b)). The smoke particles in the region were transported by smoke injected into the free troposphere, but smoke is also injected into the atmosphere from local sources. The smoke injection study has been previously studied in section 5.1.5.



**Figure 43** Extinction coefficient and frequency of occurrence for (a-b) Polluted continental (day-time) (c-d) Elevated Smoke (nighttime)

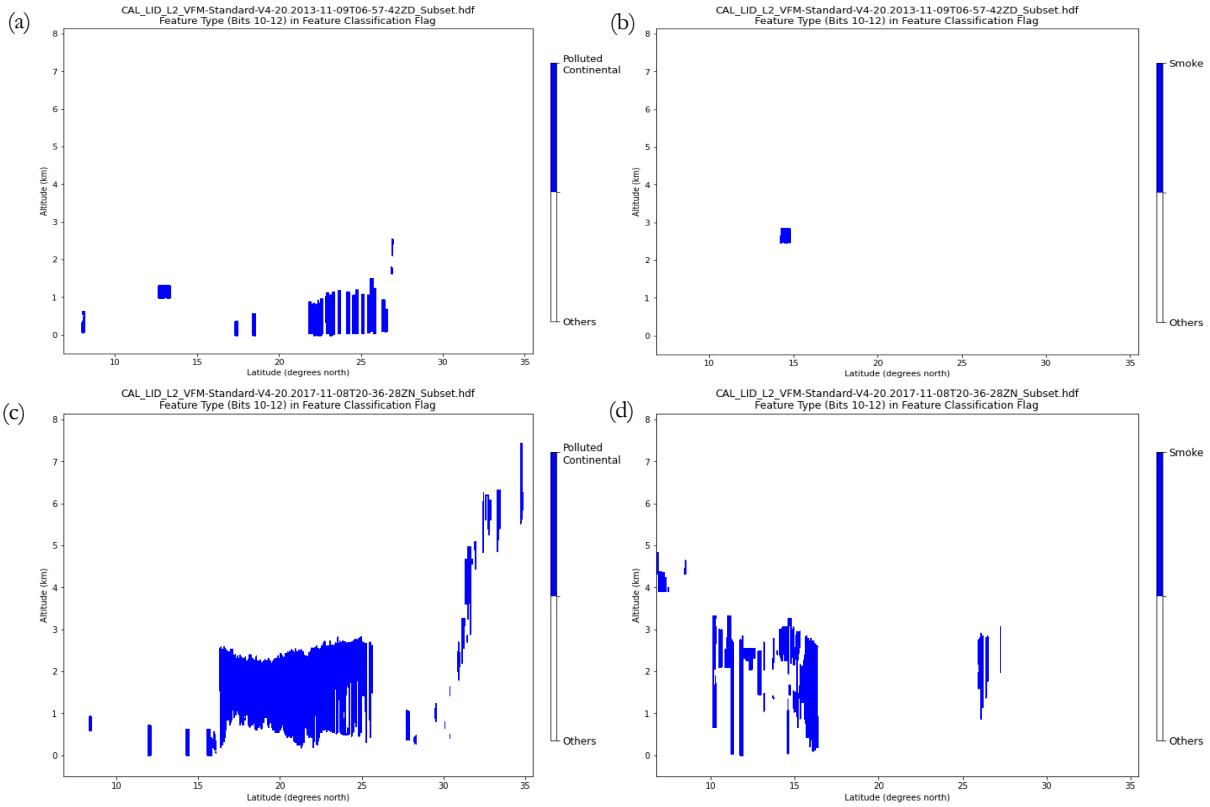


Figure 44 Latitudinal Cross-section view of Vertical feature Mask for (a-b) Polluted continental (c-d) Elevated Smoke

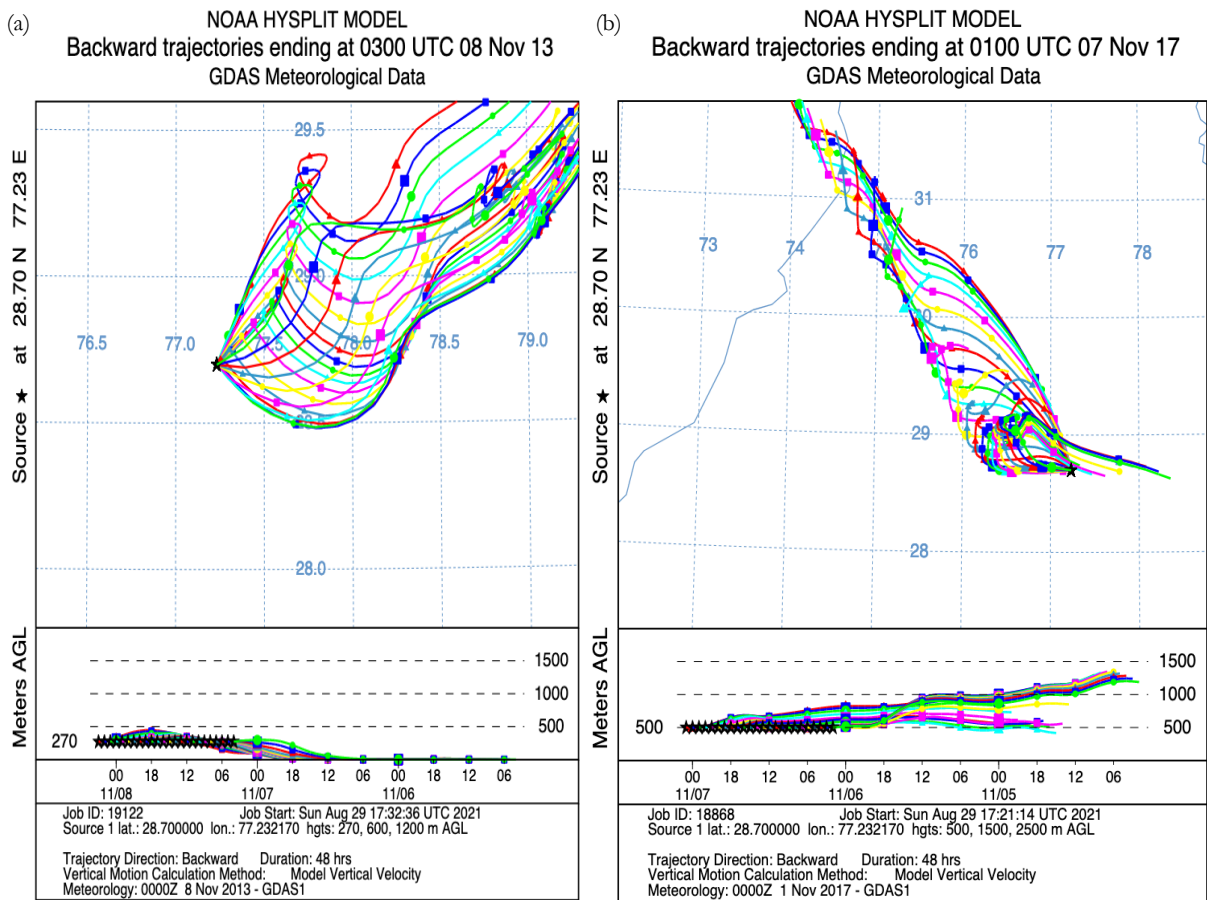
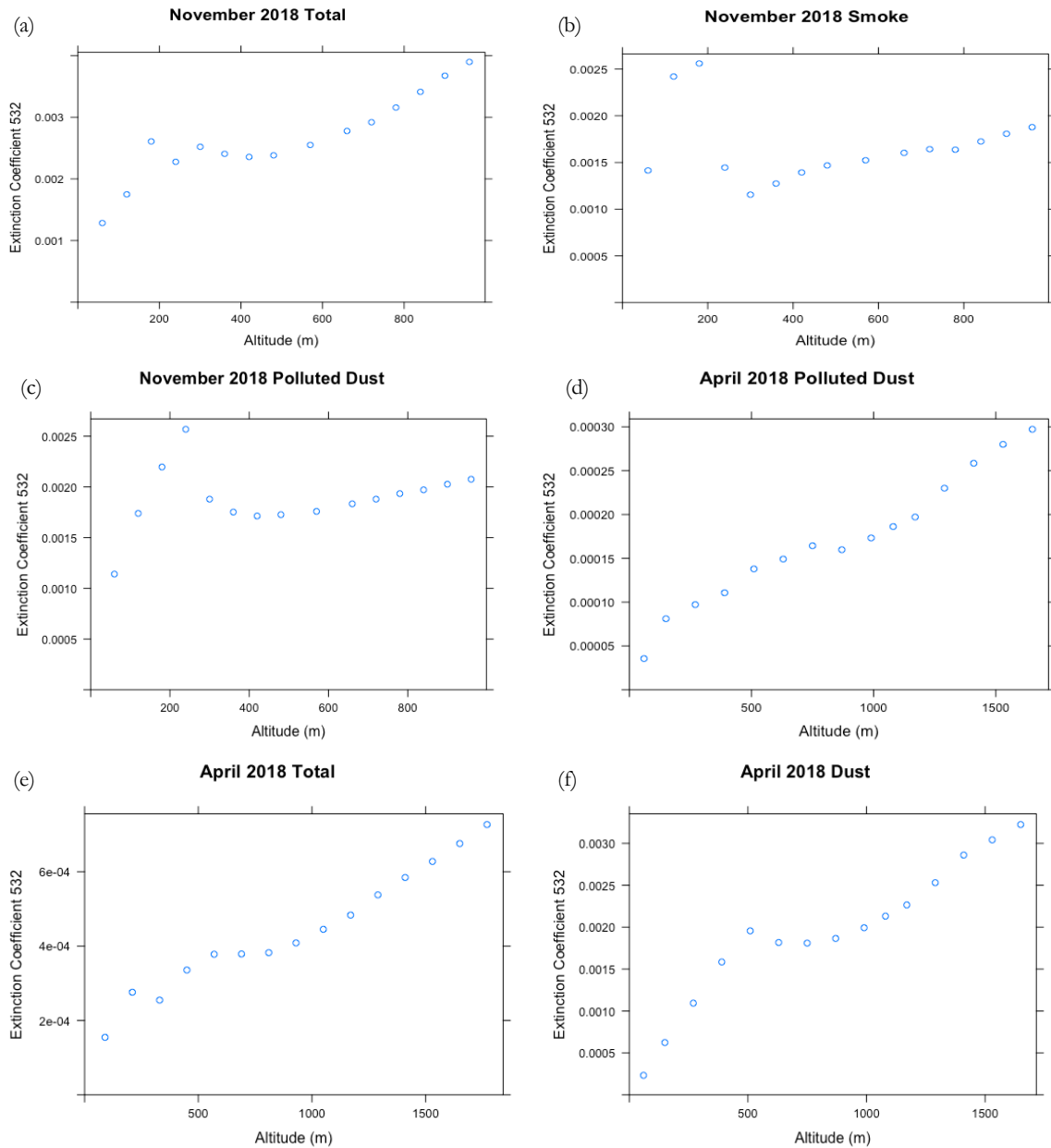


Figure 45 HYSPLIT back trajectory analysis for IGP region (a) 8 November 2013 (b) 7 November 2017

**5.10. Vertical spatial autocorrelation:**



**Figure 46** Variogram for seasonal extinction profiles

The vertical spatial autocorrelation of three main aerosols, Dust, Smoke, and polluted dust, was examined for the Indian area. The choice was made based on the prevalence of an aerosol type in a season. The nighttime semi-variance of total extinction, extinction due to smoke, and extinction due to polluted dust was checked in November 2018, whereas the daylight semi-variance of total extinction, extinction due to dust, and extinction due to polluted dust were checked in April 2018. For comparison, polluted dust was chosen during both seasons. Figure 46 shows that the total extinction range in the respective season was greater than the aerosol subtype. It may also be noted that the range of autocorrelation of total extinctions and aerosol types is lower than the respective PBLH. This is more visible in polluted dust, the April 2018 range is higher than the November 2018 range. Similar variability was also tested for other regions and the range were near similar. However, in the case of smoke, it varied on a yearly basis depending upon the emissions. It is also worth noting that the autocorrelation range of total extinctions and aerosol types is smaller than the corresponding PBLH. This is evident in polluted dust; the range in April 2018 is greater than the range in November 2018. Similar variability was examined in other regions, and the ranges were near identical. In the case of smoke, however, it changed annually based on emissions.

## 6. CONCLUSION

Indian region witnesses strong seasonal contrast in terms of aerosols dominance. During the pre-monsoon and monsoon seasons, the dust has a high dominance, whereas anthropogenic particles like smoke and polluted continental are prominent during the winter. Climatic circumstances and transport of dust from the Thar Desert or the Arab region heavily influenced natural aerosol dominance in the Indian area. The Asian area is experiencing a significant rise in anthropogenic aerosols because of fast economic growth. Both China and India had rapid economic growth over similar time periods. With regular regulations in place, China experienced solar brightening, whilst the Indian region continues to experience solar dimming. It is noteworthy that polluted dust varies throughout seasons and zones, and is also connected to solar dimming in the Indian subcontinent. Based on their height and diurnal fluctuation, these aerosols' feedback mechanisms in the climate are ascribed. The transport mechanism and radiative properties of the dust and smoke particles are based on their vertical distribution can be vital input to understand such climatic variations. During pre-monsoon and monsoon, the dust particles can impede the monsoon, whereas the smoke particles, depending upon their concentration and moisture levels, can cause sudden rainfalls. However, the feedback mechanism of polluted dust is complex to understand and requires a depth understanding of extinction profiles, AOD and trends at different altitude levels in correlation to other climate variables. The variability of these aerosols also causes uncertainty in the global models and regional models, as this distribution of aerosols is used in underlying trigger functions in GCM and RCM models. However, such feedback mechanism requires not only vertical distribution but also the temporal analysis of the distribution. The work in the thesis attempted a three-dimensional spatio-temporal analysis of aerosols that could be used in comparative assessment of such studies.

The dominant aerosol in the Indian region may not incorporate the regional variability, this purely depends on the meteorological condition and the aerosol source. Since the Indian region has heterogeneous topography and meteorological conditions, the study area is carefully further divided into different zones, namely Indo-Gangetic Plains (IGP), desert region, South India. A brief explanation of the Indian region and different zones are explained in chapter 3. Taking the simple case of MAM season, while there is a near equal percentage fraction of dust and polluted dust in the Indian region, dust is dominant in desert and IGP region while polluted dust is dominant in the South India region. Two different zones are also demarcated in the ocean region near the coastal region to understand the extent of influence of aerosols in the oceanic region.

Several studies have been conducted in the past to compare CALIOP observations with ground sensors and reanalysis datasets, such as MERRA2. Ground sensors have a strong correlation of extinction patterns, but MERRA 2 has a low bias. The MERRA 2 dataset is mostly derived from MODIS and ground-based sensors. It should be emphasized that the monthly mean of extinction profiles is derived based on the number of orbital passes in the delimited zones; as a result, CALIOP may miss severe occurrences such as the May 2018 dust storm, peak smoke extinction in November 2017, and so on (Appendix- II). As a result, when compared to MERRA 2, the CALIOP may underestimate the overall monthly mean extinction.

For each aerosol type, the seasonal extinction patterns and frequency of occurrence study regions are described. It should be emphasized that the frequency of occurrence is the relative distribution of occurrence of an aerosol type at an altitude compared to other aerosol types. The extinction coefficients represent the magnitude of the aerosol loading, whereas the frequency of occurrence represents a relative distribution in the atmosphere among other particles. The diurnal fluctuation is likewise shown in terms of occurrence, but the fractional distribution is shown in terms of extinction coefficients. For all delineated zones, the fractional

distribution is shown in both 0-2 km and 2-4 km bins during the day and night. For oceanic zones, the bin fraction is also shown. Later, a comparative trend analysis of the CALIPSO extinction coefficient and MERRA 2 was undertaken for major aerosol types in dominating seasons from 2007 to 2020. Trend analysis was also performed for the years 2007-2013, and the years 2014-2020 were also given for comparison. Sen's slope was used to determine the trends, and the Mann-Kendall test was used to check for monotonicity. However, there are chances of minor discrepancies in some trends between CALIPSO column integrated data and MERRA AOD. However, the patterns agreed in a considerable number of situations. Further trends are also reported for 0-2 km and 2-4 km for aerosol types for different seasons for a better understanding of vertical distribution.

Towards the end of the thesis, a special case of lockdown during April-May 2020 is compared with 2015-19 averaged extinction during the same season. The vertical distribution of aerosols with significant changes in the Indian region and different zones is presented. The trajectory analysis is also presented to identify the source of particles. Another special case of smog incidents in the IGP region is also presented. Wherein polluted continental and elevated smoke are focused for comparison. Again, to identify the source of particles, trajectory analysis is performed to identify the source of the particles. The vertical spatial autocorrelation was checked for the Indian region for three major aerosols: dust, smoke, polluted dust. The selection was first made based on the dominance of aerosol type in a particular season. During November 2018 nighttime semi-variance of total extinction, extinction due to smoke and extinction polluted dust checked while in April 2018 daytime semi-variance for total extinction, extinction due to dust, extinction due to polluted dust was a check. Polluted dust was a check for both seasons for comparative assessment. It may also be noted that the range of autocorrelation of total extinctions and aerosol types is lower than the respective PBLH. This is more visible in the case of polluted dust; April 2018 range is higher than the November 2018 range. Similar variability was also tested for other regions and the range were near similar. However, in the case of smoke, it varied on yearly basis depending upon the emissions.

The major findings related to AOD and for each aerosol type are mentioned below:

### 1. Extinction profiles and AOD:

- High extinction profiles and column integrated value is found in JJA in all zones.
- Extinction profiles of higher magnitude are confined within 1 km from the ground surface.
- High PBLH is found in MAM season and lowest PBLH is found in DJF.
- Increasing trend of AOD is observed in 2-4 km bin in MAM season in all regions.
- Decreasing trend of column integrated values of extinction profiles is reported during JJA in all zones. Except in the 2-4 km bin of the Arabian Sea and South India region, the decreasing trend is observed in both 0-2 km and 2-4 km bin of all regions. The increase could be primarily attributed to the increasing of dust and polluted dust in 2-4 km of both regions.
- Increasing trend of column integrated values of extinction profiles is noted post-monsoon (SON and DJF). An increasing trend is also observed in both 0-2 km bin and 2-4 km bin.
- A Monotonic increasing trend is also seen post-monsoon in the Arabian Sea during the day as well as the night.

### 2. Dust

- Pre-monsoon:
  - More prominent feature during the nighttime due to the high frequency of dust storms late evening.
  - Vertical mixing of dust is observed during the season.

- Majority of the dust particles are transported from the Thar Desert and the Arab region.
- Decreasing trend of dust is observed in India and all zones.
- Highest loading of dust among different zones is found in the Desert region with a decreasing trend.
- Considerable fraction is seen in the Indian region as well as the IGP region.
- Significant reduction is noted during the Lockdown period of April-May 2020, especially in the IGP region.
- Significant proportion of Dust among other aerosols is found in the Arabian Sea region during pre-monsoon.
- Monotonic increasing trend for dust is found in IGP region during daytime.
- Monsoon:
  - Dust is more prominent during daytime in JJA.
  - Higher extinctions and column integrated values were observed for dust during JJA compared to other seasons.
  - Decreasing trend is observed for dust in India and all zones, with a monotonic decreasing trend during nighttime in the Indian region.
  - Dust is found in a significant proportion of 2-4 km bin during daytime in the Arabian Sea.
- Post monsoon and Winter:
  - Dust is more prominent during the daytime in the winter.
  - Significant reduction in dust loading is seen post-monsoon in India and different zones during SON. However, an increasing trend is noted in the 2-4 km altitude bin during daytime which manifests the ongoing long-range transport of dust.
  - Monotonically increasing trend is noted for dust during DJF both during day and night in the Indian region. An increasing trend is seen in lower altitudes Indian region, especially IGP and desert region.

### 3. Polluted dust:

- The major concentration of polluted dust is within  $\sim 1$  km from land surface.
- Higher vertical mixing is observed in pre-monsoon and monsoon seasons however, the aerosol is more prominent in the winter.
- Pre-monsoon and Monsoon:
  - A significant proportion of polluted dust during pre-monsoon is observed in the Indian region, especially in the South India region.
  - Higher loading of polluted dust in MAM season is seen during the nighttime.
  - An increasing trend is noted both during daytime and nighttime however, the daytime trend was monotonically increasing in the Indian region.
  - An increasing trend of polluted dust is also seen in the monsoon period in the Indian region, IGP and South India.
  - An Increase in polluted dust loading was observed during the lockdown in the IGP region.
- Post Monsoon:
  - Dominant aerosol in the Indian region as well as in demarcated zones.
  - Higher loading is seen during the nighttime an exception is the South India region wherein high variability is seen at different altitudes.
  - The decreasing trend is seen post-monsoon in India as well as in different zones.
  - An increasing trend is seen in 2-4 km bin in the IGP region.

- Winter
    - Present in considerable proportion in India as well as different zones.
    - Polluted dust is more dominant during nighttime in the winter.
    - The decreasing trend is noted in the 0-2 km bin in all zones during nighttime in SON, however an increasing trend is seen in the same bin during DJF season.
- 4. Smoke:**
- Polluted continental is found up to the height of 2.5 km, however, majorly concentrated at ~1 km.
  - High loading of smoke is found during nighttime in all regions in all seasons due to relatively less turbulent environments and wildfires which are reported mostly late evening or stubble burning during the nighttime.
  - Pre-monsoon and monsoon:
    - Higher loading of smoke was seen in the IGP during JJA.
    - During pre-monsoon and monsoon season, a relatively lower concentration of polluted continental is found in the South India region when compared to other zones.
  - Post-Monsoon and Winter:
    - More than 40% of aerosol loading in India and different zones is due to polluted continental and smoke in both 0-2 km bin and 2-4 km bin during SON and the loading further increases in DJF season.
    - Major concentration of smoke is found in <1 km altitudes in both seasons.
    - Sudden spike is seen in smoke loading during SON. This is due to relatively lower PBLH and extensive stubble burning in the IGP region.
    - Increasing trend is seen for smoke aerosols in India as well as other zones post-monsoon. South India region showed a decreasing trend from 2014 during nighttime.
    - Smoke injection height during SON was significantly lower than MAM season.
- 5. Oceanic Aerosols:**
- Clean continental extinction coefficients are lower than that of dusty marine in both oceanic regions.
  - Marine is majorly concentrated up to a height of 2.5 km.
  - Higher loading of dusty marine among other aerosols is found in both Arabian Sea and Bay of Bengal in all seasons. Compared to the Arabian Sea extinction profiles, of dusty marine is higher in the Bay of Bengal.
  - Marine is predominantly found in higher concentrations during SON and DJF in both water surfaces.
  - Higher concentration of Marine is found during Nighttime in all seasons; however, an exception is of higher concentration during daytime in JJA in the Arabian Sea.
  - Increasing trend is seen in Oceanic aerosols in all seasons in both regions.

**Recommendations:**

In the Indian region, there is considerable seasonal variability in aerosol types; depending on the characteristics of the aerosol type, each of these aerosols has an essential role in influencing regional climate. A few cases have been investigated in the current work, but regional characterization in other locations is also required, particularly in hilly regions where long-range aerosol transport is exacerbating climate change at higher elevations. To properly comprehend the atmospheric dynamics, the vertical distribution and trends analysis performed in the thesis work must be studied with the other climate variables in 3-D space. However, due to the slightly larger uncertainty in airborne sensors, thorough validation with ground-based sensors is essential for reliable estimates. Furthermore, rising levels of polluted dust and rising AOD in the winter because of anthropogenic aerosol require additional attention.

## LIST OF REFERENCES

---

- Ackermann, J. (1998). The Extinction-to-Backscatter Ratio of Tropospheric Aerosol: A Numerical Study. *Journal of Atmospheric and Oceanic Technology*, 15(4), 1043–1050.  
[https://doi.org/https://doi.org/10.1175/1520-0426\(1998\)015<1043:TETBRO>2.0.CO;2](https://doi.org/https://doi.org/10.1175/1520-0426(1998)015<1043:TETBRO>2.0.CO;2)
- Al-Saadi, J., Szykman, J., Pierce, R. B., Kittaka, C., Neil, D., Chu, D. A., Remer, L., Gumley, L., Prins, E., Weinstock, L., MacDonald, C., Wayland, R., Dimmick, F., & Fishman, J. (2005). Improving National Air Quality Forecasts with Satellite Aerosol Observations. *Bulletin of the American Meteorological Society*, 86(9), 1249–1262. <https://doi.org/10.1175/BAMS-86-9-1249>
- Albrecht, B. A. (1989). Aerosols, cloud microphysics, and fractional cloudiness. *Science*, 245(4923), 1227–1230. <https://doi.org/10.1126/SCIENCE.245.4923.1227>
- Aloysius, M., Mohan, M., Parameswaran, K., George, S. K., & Nair, P. R. (2008). Aerosol transport over the Gangetic basin during ISRO-GBP land campaign-II. *Annales Geophysicae*, 26(3), 431–440. <https://doi.org/10.5194/ANGE0-26-431-2008>
- Alpert, P., Kaufman, Y. J., Shay-El, Y., Tanre, D., da Silva, A., Schubert, S., & Joseph, J. H. (1998). Quantification of dust-forced heating of the lower troposphere. *Nature* 1998 395:6700, 395(6700), 367–370. <https://doi.org/10.1038/26456>
- Altartaz, O., Bar-Or, R. Z., Wollner, U., & Koren, I. (2013). Relative humidity and its effect on aerosol optical depth in the vicinity of convective clouds. *Environmental Research Letters*, 8(3), 034025. <https://doi.org/10.1088/1748-9326/8/3/034025>
- Anderson, T. L., Masonis, S. J., Covert, D. S., Charlson, R. J., & Rood, M. J. (2000). In situ measurement of the aerosol extinction-to-backscatter ratio at a polluted continental site. *Journal of Geophysical Research: Atmospheres*, 105(D22), 26907–26915. <https://doi.org/10.1029/2000JD900400>
- Andreae, M. O., & Rosenfeld, D. (2008). Aerosol–cloud–precipitation interactions. Part 1. The nature and sources of cloud-active aerosols. *Earth-Science Reviews*, 89(1–2), 13–41. <https://doi.org/10.1016/J.EARSCIREV.2008.03.001>
- Aswini, M. A., Kumar, A., & Das, S. K. (2020). Quantification of long-range transported aeolian dust towards the Indian peninsular region using satellite and ground-based data - A case study during a dust storm over the Arabian Sea. *Atmospheric Research*, 239, 104910. <https://doi.org/10.1016/J.ATMOSRES.2020.104910>
- Babu, S. S., Manoj, M. R., Moorthy, K. K., Gogoi, M. M., Nair, V. S., Kompalli, S. K., Satheesh, S. K., Niranjana, K., Ramagopal, K., Bhuyan, P. K., & Singh, D. (2013). Trends in aerosol optical depth over Indian region: Potential causes and impact indicators. *Journal of Geophysical Research: Atmospheres*, 118(20), 11,794–11,806. <https://doi.org/10.1002/2013JD020507>
- Badarinath, K. V. S., Kharol, S. K., Sharma, A. R., & Krishna Prasad, V. (2009). Analysis of aerosol and carbon monoxide characteristics over Arabian Sea during crop residue burning period in the Indo-Gangetic Plains using multi-satellite remote sensing datasets. *Journal of Atmospheric and Solar-Terrestrial Physics*, 71(12), 1267–1276. <https://doi.org/10.1016/J.JASTP.2009.04.004>
- Badarinath, K. V. S., Kumar Kharol, S., & Rani Sharma, A. (2009). Long-range transport of aerosols from agriculture crop residue burning in Indo-Gangetic Plains—A study using LIDAR, ground measurements and satellite data. *Journal of Atmospheric and Solar-Terrestrial Physics*, 71(1), 112–120. <https://doi.org/10.1016/J.JASTP.2008.09.035>
- Banerjee, P., & Kumar, S. P. (2014). Dust-induced episodic phytoplankton blooms in the Arabian Sea during winter monsoon. *Journal of Geophysical Research: Oceans*, 119(10), 7123–7138. <https://doi.org/10.1002/2014JC010304>
- Barber, R. T., Marra, J., Bidigare, R. C., Codispoti, L. A., Halpern, D., Johnson, Z., Latasa, M., Goericke, R., & Smith, S. L. (2001). Primary productivity and its regulation in the Arabian Sea during 1995. *Deep Sea Research Part II: Topical Studies in Oceanography*, 48(6–7), 1127–1172.

[https://doi.org/10.1016/S0967-0645\(00\)00134-X](https://doi.org/10.1016/S0967-0645(00)00134-X)

- Beck, H. E., Zimmermann, N. E., McVicar, T. R., Vergopolan, N., Berg, A., & Wood, E. F. (2018). Present and future Köppen-Geiger climate classification maps at 1-km resolution. *Scientific Data* 2018 5:1, 5(1), 1–12. <https://doi.org/10.1038/sdata.2018.214>
- Bollasina, M., Nigam, S., & Lau, K.-M. (2008). Absorbing Aerosols and Summer Monsoon Evolution over South Asia: An Observational Portrayal. *Journal of Climate*, 21(13), 3221–3239. <https://doi.org/10.1175/2007JCLI2094.1>
- Boucher, O., & Haywood, J. (2001). On summing the components of radiative forcing of climate change. *Climate Dynamics* 2001 18:3, 18(3), 297–302. <https://doi.org/10.1007/S003820100185>
- Boucher, O., Randall, D., Artaxo, P., Bretherton, C., Feingold, G., Forster, P., Kerminen, V.-M., Kondo, Y., Liao, H., Lohmann, U., Rasch, P., Satheesh, S. K., Sherwood, S., Stevens, B., & Zhang, X. Y. (2013). *Clouds and aerosols in Climate Change 2013: The Physical Science Basis. Contribution of Working Group I to the Fifth Assessment Report of the Intergovernmental Panel on Climate Change* (T. F. Stocker, D. Qin, G.-K. Plattner, M. Tignor, A. S. K., J. Doschung, A. Nauels, Y. Xia, V. Bex, & P. M. Midgley (Eds.)). Cambridge University Press. <https://doi.org/10.1017/CBO9781107415324.016>
- Boucher, O., & Tanré, D. (2000). Estimation of the aerosol perturbation to the Earth's Radiative Budget over oceans using POLDER satellite aerosol retrievals. *Geophysical Research Letters*, 27(8), 1103–1106. <https://doi.org/10.1029/1999GL010963>
- Boucher, Olivier. (2015). Atmospheric Aerosols. *Atmospheric Aerosols*, 9–24. [https://doi.org/10.1007/978-94-017-9649-1\\_2](https://doi.org/10.1007/978-94-017-9649-1_2)
- Buchard, V., Randles, C. A., da Silva, A. M., Darmenov, A., Colarco, P. R., Govindaraju, R., Ferrare, R., Hair, J., Beyersdorf, A. J., Ziemba, L. D., & Yu, H. (2017). The MERRA-2 aerosol reanalysis, 1980 onward. Part II: Evaluation and case studies. *Journal of Climate*, 30(17), 6851–6872. <https://doi.org/10.1175/JCLI-D-16-0613.1>
- Buchard, V., Randles, C. A., Silva, A. M. da, Darmenov, A., Colarco, P. R., Govindaraju, R., Ferrare, R., Hair, J., Beyersdorf, A. J., Ziemba, L. D., & Yu, H. (2017). The MERRA-2 Aerosol Reanalysis, 1980 Onward. Part II: Evaluation and Case Studies. *Journal of Climate*, 30(17), 6851–6872. <https://doi.org/10.1175/JCLI-D-16-0613.1>
- CALIPSO. (2006). *CALIPSO Quality Statements : Lidar Level 2 Vertical Feature Mask CALIPSO Data Read Software CALIPSO Lidar Level 2 Vertical Feature Mask*.
- CALIPSO - Data File Ordering Web Tool - By Data Month*. (n.d.). Retrieved September 8, 2021, from [https://www-calipso.larc.nasa.gov/resources/calipso\\_users\\_guide/order\\_data.php](https://www-calipso.larc.nasa.gov/resources/calipso_users_guide/order_data.php)
- Carmichael, G. R., Adhikary, B., Kulkarni, S., D'Allura, A., Tang, Y., Streets, D., Zhang, Q., Bond, T. C., Ramanathan, V., Jamroensan, A., & Marrapu, P. (2009). Asian Aerosols: Current and Year 2030 Distributions and Implications to Human Health and Regional Climate Change. *Environmental Science and Technology*, 43(15), 5811–5817. <https://doi.org/10.1021/ES8036803>
- Carslaw, K. S., Lee, L. A., Reddington, C. L., Pringle, K. J., Rap, A., Forster, P. M., Mann, G. W., Spracklen, D. V., Woodhouse, M. T., Regayre, L. A., & Pierce, J. R. (2013). Large contribution of natural aerosols to uncertainty in indirect forcing. *Nature* 2013 503:7474, 503(7474), 67–71. <https://doi.org/10.1038/nature12674>
- Cavaliere, O., Cairo, F., Fierli, F., Di Donfrancesco, G., Snels, M., Viterbini, M., Cardillo, F., Chatenet, B., Formenti, P., Marticorena, B., & Rajot, J. L. (2010). Variability of aerosol vertical distribution in the Sahel. *Atmospheric Chemistry and Physics*, 10(24), 12005–12023. <https://doi.org/10.5194/ACP-10-12005-2010>
- Charlson, R. J., Schwartz, S. E., Hales, J. M., Cess, R. D., Coakley, J. A., Hansen, J. E., & Hofmann, D. J. (1992). Climate forcing by anthropogenic aerosols. *Science*, 255(5043), 423–430. <https://doi.org/10.1126/SCIENCE.255.5043.423>
- Cheng, Y. F., Wiedensohler, A., Eichler, H., Su, H., Gnauk, T., Brüggemann, E., Herrmann, H.,

- Heintzenberg, J., Slanina, J., Tuch, T., Hu, M., & Zhang, Y. H. (2008). Aerosol optical properties and related chemical apportionment at Xinken in Pearl River Delta of China. *Atmospheric Environment*, 42(25), 6351–6372. <https://doi.org/10.1016/J.ATMOSENV.2008.02.034>
- CLAQUIN, T., SCHULZ, M., BALKANSKI, Y., & BOUCHER, O. (1998). Uncertainties in assessing radiative forcing by mineral dust. *Tellus B*, 50(5), 491–505. <https://doi.org/10.1034/J.1600-0889.1998.T01-2-00007.X>
- Cohen, J. B., Ng, D. H. L., Lim, A. W. L., & Chua, X. R. (2018). Vertical distribution of aerosols over the Maritime Continent during El Niño. *Atmospheric Chemistry and Physics*, 18(10), 7095–7108. <https://doi.org/10.5194/ACP-18-7095-2018>
- Das, S., Dey, S., Dash, S. K., & Basil, G. (2013). Examining mineral dust transport over the Indian subcontinent using the regional climate model, RegCM4.1. *Atmospheric Research*, 134, 64–76. <https://doi.org/10.1016/J.ATMOSRES.2013.07.019>
- Dey, S., & Di Girolamo, L. (2011). A decade of change in aerosol properties over the Indian subcontinent. *Geophysical Research Letters*, 38(14), 137–150. <https://doi.org/10.1029/2011GL048153>
- Dey, S., & Girolamo, L. Di. (2010). A climatology of aerosol optical and microphysical properties over the Indian subcontinent from 9 years (2000–2008) of Multiangle Imaging Spectroradiometer (MISR) data. *Journal of Geophysical Research: Atmospheres*, 115(D15), 15204. <https://doi.org/10.1029/2009JD013395>
- Dey, S., & Girolamo, L. Di. (2011). A decade of change in aerosol properties over the Indian subcontinent. *Geophysical Research Letters*, 38(14). <https://doi.org/10.1029/2011GL048153>
- Dey, S., Tripathi, S. N., Singh, R. P., & Holben, B. N. (2004). Influence of dust storms on the aerosol optical properties over the Indo-Gangetic basin. *Journal of Geophysical Research: Atmospheres*, 109(D20), 20211. <https://doi.org/10.1029/2004JD004924>
- Eck, T. F., Holben, B. N., Reid, J. S., Dubovik, O., Smirnov, A., O'Neill, N. T., Slutsker, I., & Kinne, S. (1999). Wavelength dependence of the optical depth of biomass burning, urban, and desert dust aerosols. *Journal of Geophysical Research: Atmospheres*, 104(D24), 31333–31349. <https://doi.org/10.1029/1999JD900923>
- Ellsworth J. Welton, Kenneth J. Voss, Patricia K. Quinn, Piotr J. Flatau, Krzysztof Markowicz, James R. Campbell, James D. Spinhirne, Howard R. Gordon, & Johnson, J. E. (2002). Measurements of aerosol vertical profiles and optical properties during INDOEX 1999 using micropulse lidars. *Journal of Geophysical Research: Atmospheres*, 107(D19), INX2 18-1. <https://doi.org/10.1029/2000JD000038>
- Fernald, F. G., Herman, B. M., & Reagan, J. A. (1972). Determination of Aerosol Height Distributions by Lidar. *Journal of Applied Meteorology*, 11(3), 482–489. [https://doi.org/10.1175/1520-0450\(1972\)011<0482:doahdb>2.0.co;2](https://doi.org/10.1175/1520-0450(1972)011<0482:doahdb>2.0.co;2)
- Forster, P., Ramaswamy, V., Artaxo, P., Berntsen, T., Betts, R., Fahey, D. W., Haywood, J., Lean, J., Lowe, D. C., Myhre, G., Nganga, J., Prinn, R., Raga, G., Schulz, M., & Dorland, R. Van. (2007). The Physical Science Basis. Contribution of Working Group I. *Fourth Assessment Report of the Intergovernmental Panel on Climate Change*, 10. <http://www.ipcc.ch/ipccreports/ar4-wg1.htm>
- Franke, K., Ansmann, A., Müller, D., Althausen, D., Wagner, F., & Scheele, R. (2001). One-year observations of particle lidar ratio over the tropical Indian Ocean with Raman lidar. *Geophysical Research Letters*, 28(24), 4559–4562. <https://doi.org/10.1029/2001GL013671>
- Ganguly, D., Ginoux, P., Ramaswamy, V., Winker, D. M., Holben, B. N., & Tripathi, S. N. (2009). Retrieving the composition and concentration of aerosols over the Indo-Gangetic basin using CALIOP and AERONET data. *Geophysical Research Letters*, 36(13). <https://doi.org/10.1029/2009GL038315>
- Gautam, R., Hsu, N. C., Lau, K. M., & Kafatos, M. (2009). Aerosol and rainfall variability over the Indian monsoon region: Distributions, trends and coupling. *Annales Geophysicae*, 27(9), 3691–3703. <https://doi.org/10.5194/ANGE0-27-3691-2009>

- Gautam, Ritesh, Hsu, N. C., & Lau, K.-M. (2010). Premonsoon aerosol characterization and radiative effects over the Indo-Gangetic Plains: Implications for regional climate warming. *Journal of Geophysical Research: Atmospheres*, *115*(D17), 17208. <https://doi.org/10.1029/2010JD013819>
- Gautam, S. (2020). The Influence of COVID-19 on Air Quality in India: A Boon or Inutile. *Bulletin of Environmental Contamination and Toxicology* *2020* *104*:6, *104*(6), 724–726. <https://doi.org/10.1007/S00128-020-02877-Y>
- Gogoi, M. M., Bhuyan, P. K., & Krishna Moorthy, K. (2008). Estimation of the effect of long-range transport on seasonal variation of aerosols over northeastern India. *Annales Geophysicae*, *26*(6), 1365–1377. <https://doi.org/10.5194/ANGEO-26-1365-2008>
- Graf, H. F. (2004). The Complex Interaction of Aerosols and Clouds. *Science*, *303*(5662), 1309–1311. <https://doi.org/10.1126/SCIENCE.1094411>
- Guan, H., Esswein, R., Lopez, J., Bergstrom, R., Warnock, A., Follette-Cook, M., Fromm, M., & Iraci, L. T. (2010). A multi-decadal history of biomass burning plume heights identified using aerosol index measurements. *Atmospheric Chemistry and Physics*, *10*(14), 6461–6469. <https://doi.org/10.5194/ACP-10-6461-2010>
- Guieu, C., Azhar, M. Al, Aumont, O., Mahowald, N., Levy, M., Ethé, C., & Lachkar, Z. (2019). Major Impact of Dust Deposition on the Productivity of the Arabian Sea. *Geophysical Research Letters*, *46*(12), 6736–6744. <https://doi.org/10.1029/2019GL082770>
- Haywood, J., & Boucher, O. (2000). Estimates of the direct and indirect radiative forcing due to tropospheric aerosols: A review. *Reviews of Geophysics*, *38*(4), 513–543. <https://doi.org/10.1029/1999RG000078>
- Hegde, P., Pant, P., Naja, M., Dumka, U. C., & Sagar, R. (2007). South Asian dust episode in June 2006: Aerosol observations in the central Himalayas. *Geophysical Research Letters*, *34*(23), 23802. <https://doi.org/10.1029/2007GL030692>
- Hodzic, A., Chepfer, H., Vautard, R., Chazette, P., Beekmann, M., Bessagnet, B., Chatenet, B., Cuesta, J., Drobinski, P., Goloub, P., Haefelin, M., & Morille, Y. (2004). Comparison of aerosol chemistry transport model simulations with lidar and Sun photometer observations at a site near Paris. *Journal of Geophysical Research: Atmospheres*, *109*(D23), 1–19. <https://doi.org/10.1029/2004JD004735>
- Holben, B. N., Eck, T. F., Slutsker, I., Tanré, D., Buis, J. P., Setzer, A., Vermote, E., Reagan, J. A., Kaufman, Y. J., Nakajima, T., Lavenu, F., Jankowiak, I., & Smirnov, A. (1998). AERONET—A Federated Instrument Network and Data Archive for Aerosol Characterization. *Remote Sensing of Environment*, *66*(1), 1–16. [https://doi.org/10.1016/S0034-4257\(98\)00031-5](https://doi.org/10.1016/S0034-4257(98)00031-5)
- Holz, R. E., Ackerman, S. A., Nagle, F. W., Frey, R., Dutcher, S., Kuehn, R. E., Vaughan, M. A., & Baum, B. (2009). Global Moderate Resolution Imaging Spectroradiometer (MODIS) cloud detection and height evaluation using CALIOP. *Journal of Geophysical Research Atmospheres*, *114*(8). <https://doi.org/10.1029/2008JD009837>
- Hsu, N. C., Gautam, R., Sayer, A. M., Bettenhausen, C., Li, C., Jeong, M. J., Tsay, S. C., & Holben, B. N. (2012). Global and regional trends of aerosol optical depth over land and ocean using SeaWiFS measurements from 1997 to 2010. *Atmospheric Chemistry and Physics*, *12*(17), 8037–8053. <https://doi.org/10.5194/ACP-12-8037-2012>
- Hu, Y., Winker, D., Vaughan, M., Lin, B., Omar, A., Trepte, C., Flittner, D., Yang, P., Nasiri, S. L., Baum, B., Holz, R., Sun, W., Liu, Z., Wang, Z., Young, S., Stamnes, K., Huang, J., & Kuehn, R. (2009). CALIPSO/CALIOP Cloud Phase Discrimination Algorithm. *Journal of Atmospheric and Oceanic Technology*, *26*(11), 2293–2309. <https://doi.org/10.1175/2009JTECHA1280.1>
- Huneus, N., Chevallier, F., & Boucher, O. (2012). Estimating aerosol emissions by assimilating observed aerosol optical depth in a global aerosol model. *Atmospheric Chemistry and Physics*, *12*(10), 4585–4606. <https://doi.org/10.5194/ACP-12-4585-2012>
- Hunt, W. H., Winker, D. M., Vaughan, M. A., Powell, K. A., Lucker, P. L., & Weimer, C. (2009).

- CALIPSO Lidar Description and Performance Assessment. *Journal of Atmospheric and Oceanic Technology*, 26(7), 1214–1228. <https://doi.org/https://doi.org/10.1175/2009JTECHA1223.1>
- Jayaraman, A., Gadhavi, H., Ganguly, D., Misra, A., Ramachandran, S., & Rajesh, T. A. (2006). Spatial variations in aerosol characteristics and regional radiative forcing over India: Measurements and modeling of 2004 road campaign experiment. *Atmospheric Environment*, 40(34), 6504–6515. <https://doi.org/10.1016/J.ATMOSENV.2006.01.034>
- Jethva, H., Satheesh, S. K., & Srinivasan, J. (2005). Seasonal variability of aerosols over the Indo-Gangetic basin. *Journal of Geophysical Research: Atmospheres*, 110(D21), 1–15. <https://doi.org/10.1029/2005JD005938>
- Kahn, R. A., Gaitley, B. J., Garay, M. J., Diner, D. J., Eck, T. F., Smirnov, A., & Holben, B. N. (2010). Multiangle Imaging Spectroradiometer global aerosol product assessment by comparison with the Aerosol Robotic Network. *Journal of Geophysical Research: Atmospheres*, 115(D23). <https://doi.org/10.1029/2010JD014601>
- Kahn, R. A., Gaitley, B. J., Martonchik, J. V., Diner, D. J., Crean, K. A., & Holben, B. (2005). Multiangle Imaging Spectroradiometer (MISR) global aerosol optical depth validation based on 2 years of coincident Aerosol Robotic Network (AERONET) observations. *Journal of Geophysical Research: Atmospheres*, 110(D10), 1–16. <https://doi.org/10.1029/2004JD004706>
- Kahn, R. A., Li, W.-H., Moroney, C., Diner, D. J., Martonchik, J. V., & Fishbein, E. (2007). Aerosol source plume physical characteristics from space-based multiangle imaging. *Journal of Geophysical Research: Atmospheres*, 112(D11). <https://doi.org/10.1029/2006JD007647>
- Kahn, R., Petzold, A., Wendisch, M., Bierwirth, E., Dinter, T., Esselborn, M., Fiebig, M., Heese, B., Knippertz, P., MÜLLER, D., Schladitz, A., & Hoyningen-HUENE, W. Von. (2017). Desert dust aerosol air mass mapping in the western Sahara, using particle properties derived from space-based multi-angle imaging. <Http://Dx.Doi.Org/10.1111/j.1600-0889.2008.00398.X>, 61(1), 239–251. <https://doi.org/10.1111/J.1600-0889.2008.00398.X>
- Kar, J., Vaughan, M. A., Lee, K. P., Tackett, J. L., Avery, M. A., Garnier, A., Getzewich, B. J., Hunt, W. H., Josset, D., Liu, Z., Lucker, P. L., Magill, B., Omar, A. H., Pelon, J., Rogers, R. R., Toth, T. D., Trepte, C. R., Vernier, J. P., Winker, D. M., & Young, S. A. (2018). CALIPSO lidar calibration at 532 nm: Version 4 nighttime algorithm. *Atmospheric Measurement Techniques*, 11(3), 1459–1479. <https://doi.org/10.5194/AMT-11-1459-2018>
- Kaskaoutis, D. G., Kharol, S. K., Sinha, P. R., Singh, R. P., Badarinath, K. V. S., Mehdi, W., & Sharma, M. (2011). Contrasting aerosol trends over South Asia during the last decade based on MODIS observations. *Atmospheric Measurement Techniques Discussions*, 4(4), 5275–5323. <https://doi.org/10.5194/amtd-4-5275-2011>
- Kaskaoutis, D. G., Kumar, S., Sharma, D., Singh, R. P., Kharol, S. K., Sharma, M., Singh, A. K., Singh, S., Singh, A., & Singh, D. (2014). Effects of crop residue burning on aerosol properties, plume characteristics, and long-range transport over northern India. *Journal of Geophysical Research*, 119(9), 5424–5444. <https://doi.org/10.1002/2013JD021357>
- Kedia, S., & Ramachandran, S. (2009). Variability in aerosol optical and physical characteristics over the Bay of Bengal and the Arabian Sea deduced from Ångström exponents. *Journal of Geophysical Research: Atmospheres*, 114(D14). <https://doi.org/10.1029/2009JD011950>
- Kedia, S., Ramachandran, S., Holben, B. N., & Tripathi, S. N. (2014). Quantification of aerosol type, and sources of aerosols over the Indo-Gangetic Plain. *Atmospheric Environment*, 98, 607–619. <https://doi.org/10.1016/J.ATMOSENV.2014.09.022>
- Kharol, S. K., Badarinath, K. V. S., Sharma, A. R., Mahalakshmi, D. V., Singh, D., & Prasad, V. K. (2012). Black carbon aerosol variations over Patiala city, Punjab, India—A study during agriculture crop residue burning period using ground measurements and satellite data. *Journal of Atmospheric and Solar-Terrestrial Physics*, 84–85, 45–51. <https://doi.org/10.1016/J.JASTP.2012.05.013>
- Kim, H., & Paulson, S. E. (2013). Real refractive indices and volatility of secondary organic aerosol

- generated from photooxidation and ozonolysis of limonene,  $\alpha$ -pinene and toluene. *Atmospheric Chemistry and Physics*, 13(15), 7711–7723. <https://doi.org/10.5194/ACP-13-7711-2013>
- Kim, M. H., Omar, A. H., Tackett, J. L., Vaughan, M. A., Winker, D. M., Trepte, C. R., Hu, Y., Liu, Z., Poole, L. R., Pitts, M. C., Kar, J., & Magill, B. E. (2018). The CALIPSO version 4 automated aerosol classification and lidar ratio selection algorithm. *Atmospheric Measurement Techniques*, 11(11), 6107–6135. <https://doi.org/10.5194/AMT-11-6107-2018>
- Koch, D., & Del Genio, A. D. (2010). Black carbon semi-direct effects on cloud cover: Review and synthesis. *Atmospheric Chemistry and Physics*, 10(16), 7685–7696. <https://doi.org/10.5194/ACP-10-7685-2010>
- Krishna Moorthy, K., Suresh Babu, S., & Satheesh, S. K. (2007). Temporal heterogeneity in aerosol characteristics and the resulting radiative impact at a tropical coastal station &ndash; Part 1: Microphysical and optical properties. *Annales Geophysicae*, 25(11), 2293–2308. <https://doi.org/10.5194/ANGEO-25-2293-2007>
- KS, V., A, M., T, B., M, S.-H., DM, B., RK, M., & MT, L. (2020). Vertical distribution of smoke aerosols over upper Indo-Gangetic Plain. *Environmental Pollution (Barking, Essex : 1987)*, 257. <https://doi.org/10.1016/J.ENVPOL.2019.113377>
- Kulkarni, P., & Sreekanth, V. (2020). Spaceborne lidar retrieved composite and speciated aerosol extinction profiles and optical depths over India: A decade of observations. *Atmospheric Pollution Research*, 11(5), 946–962. <https://doi.org/10.1016/j.apr.2020.02.007>
- Kumar, S. P., Muraleedharan, P. M., Prasad, T. G., Gauns, M., Ramaiah, N., Souza, S. N. de, Sardesai, S., & Madhupratap, M. (2002). Why is the Bay of Bengal less productive during summer monsoon compared to the Arabian Sea? *Geophysical Research Letters*, 29(24), 88–1. <https://doi.org/10.1029/2002GL016013>
- Lakshmi, N. B., Nair, V. S., & Babu, S. S. (2017). Vertical Structure of Aerosols and Mineral Dust Over the Bay of Bengal From Multisatellite Observations. *Journal of Geophysical Research: Atmospheres*, 122(23), 12,845–12,861. <https://doi.org/10.1002/2017JD027643>
- Langmann, B. (2007). A model study of smoke-haze influence on clouds and warm precipitation formation in Indonesia 1997/1998. *Atmospheric Environment*, 41(32), 6838–6852. <https://doi.org/10.1016/J.ATMOENV.2007.04.050>
- Laprise, R. (2008). Regional climate modelling. *Journal of Computational Physics*, 227(7), 3641–3666. <https://doi.org/10.1016/J.JCP.2006.10.024>
- Lau, K.-M., Ramanathan, V., Wu, G.-X., Li, Z., Tsay, S. C., Hsu, C., Sikka, R., Holben, B., Lu, D., Tartari, G., Chin, M., Koudelova, P., Chen, H., Ma, Y., Huang, J., Taniguchi, K., & Zhang, R. (2008). The Joint Aerosol–Monsoon Experiment: A New Challenge for Monsoon Climate Research. *Bulletin of the American Meteorological Society*, 89(3), 369–384. <https://doi.org/10.1175/BAMS-89-3-369>
- Lau, K. M., Kim, M. K., & Kim, K. M. (2006). Asian summer monsoon anomalies induced by aerosol direct forcing: The role of the Tibetan Plateau. *Climate Dynamics*, 26(7–8), 855–864. <https://doi.org/10.1007/s00382-006-0114-z>
- Levy, R. C., Remer, L. A., Kleidman, R. G., Mattoo, S., Ichoku, C., Kahn, R., & Eck, T. F. (2010). Global evaluation of the Collection 5 MODIS dark-target aerosol products over land. *Atmospheric Chemistry and Physics*, 10(21), 10399–10420. <https://doi.org/10.5194/ACP-10-10399-2010>
- Levy, Robert C., Remer, L. A., Mattoo, S., Vermote, E. F., & Kaufman, Y. J. (2007). Second-generation operational algorithm: Retrieval of aerosol properties over land from inversion of Moderate Resolution Imaging Spectroradiometer spectral reflectance. *Journal of Geophysical Research: Atmospheres*, 112(D13). <https://doi.org/10.1029/2006JD007811>
- Li, J., Carlson, B. E., Dubovik, O., & Lacis, A. A. (2014). Recent trends in aerosol optical properties derived from AERONET measurements. *Atmospheric Chemistry and Physics*, 14(22), 12271–12289. <https://doi.org/10.5194/ACP-14-12271-2014>

- Liu, Z., Vaughan, M., Winker, D., Kittaka, C., Getzewich, B., Kuehn, R., Omar, A., Powell, K., Trepte, C., & Hostetler, C. (2009a). The CALIPSO lidar cloud and aerosol discrimination: Version 2 algorithm and initial assessment of performance. *Journal of Atmospheric and Oceanic Technology*, 26(7), 1198–1213. <https://doi.org/10.1175/2009JTECHA1229.1>
- Liu, Z., Vaughan, M., Winker, D., Kittaka, C., Getzewich, B., Kuehn, R., Omar, A., Powell, K., Trepte, C., & Hostetler, C. (2009b). The CALIPSO Lidar Cloud and Aerosol Discrimination: Version 2 Algorithm and Initial Assessment of Performance. *Journal of Atmospheric and Oceanic Technology*, 26(7), 1198–1213. <https://doi.org/10.1175/2009JTECHA1229.1>
- Luo, H., Jiang, B., Li, F., & Lin, W. (2019). Simulation of the effects of sea-salt aerosols on the structure and precipitation of a developed tropical cyclone. *Atmospheric Research*, 217, 120–127. <https://doi.org/10.1016/J.ATMOSRES.2018.10.018>
- Madineni, V. R., Dasari, H. P., Karumuri, R., Viswanadhapalli, Y., Perumal, P., & Hoteit, I. (2021). Natural processes dominate the pollution levels during COVID-19 lockdown over India. *Scientific Reports* 2021 11:1, 11(1), 1–14. <https://doi.org/10.1038/s41598-021-94373-4>
- Mangla, R., J, I., & Chakra, S. S. (2020). Inter-comparison of multi-satellites and Aeronet AOD over Indian Region. *Atmospheric Research*, 240, 104950. <https://doi.org/10.1016/J.ATMOSRES.2020.104950>
- Masand, M., Sivakala, K. K., Menghani, E., Thinesh, T., Anandham, R., Sharma, G., Sivakumar, N., Jebakumar, S. R. D., & Jose, P. A. (2018). Biosynthetic Potential of Bioactive Streptomycetes Isolated From Arid Region of the Thar Desert, Rajasthan (India). *Frontiers in Microbiology*, 0(APR), 687. <https://doi.org/10.3389/FMICB.2018.00687>
- Masson-Delmotte, V., Zhai, P., Pörtner, H.-O., Roberts, D., Skea, J., Shukla, P. R., Pirani, A., Moufouma-Okia, W., Péan, C., Pidcock, R., Connors, S., Matthews, J. B. R., Chen, Y., Zhou, X., Gomis, M. I., Lonnoy, E., Maycock, T., Tignor, M., & Waterfield, T. (2019). *Global warming of 1.5°C An IPCC Special Report on the impacts of global warming of 1.5°C above pre-industrial levels and related global greenhouse gas emission pathways, in the context of strengthening the global response to the threat of climate change, sustainable development, and efforts to eradicate poverty Edited by Science Officer Science Assistant Graphics Officer Working Group I Technical Support Unit.* [www.environmentalgraphiti.org](http://www.environmentalgraphiti.org)
- Mehta, M. (2015). A study of aerosol optical depth variations over the Indian region using thirteen years (2001–2013) of MODIS and MISR Level 3 data. *Atmospheric Environment*, 109, 161–170. <https://doi.org/10.1016/J.ATMOSENV.2015.03.021>
- Mehta, M., Hooda, W., & Prakash, C. (2021). A Satellite View of the Changes in Summer-time Aerosol Vertical Distribution Before and During Covid-19 Lockdown Conditions in India. *Current Science*, 120(12), 1818–1819.
- Mehta, M., Khushboo, R., Raj, R., & Singh, N. (2020). Spaceborne observations of aerosol vertical distribution over Indian mainland (2009–2018). *Atmospheric Environment*, 244(December 2019), 117902. <https://doi.org/10.1016/j.atmosenv.2020.117902>
- Mehta, M., Khushboo, R., Raj, R., & Singh, N. (2021). Spaceborne observations of aerosol vertical distribution over Indian mainland (2009–2018). *Atmospheric Environment*, 244, 117902. <https://doi.org/10.1016/J.ATMOSENV.2020.117902>
- Mehta, M., Sharma, V., & Doley, G. J. (2018). *Aerosol Optical Depth Variation During a Recent Dust Event in North India.* 567–571. [https://doi.org/10.1007/978-981-10-5792-2\\_44](https://doi.org/10.1007/978-981-10-5792-2_44)
- Mehta, M., Singh, N., & Anshumali. (2018a). Global trends of columnar and vertically distributed properties of aerosols with emphasis on dust, polluted dust and smoke - inferences from 10-year long CALIOP observations. *Remote Sensing of Environment*, 208(February), 120–132. <https://doi.org/10.1016/j.rse.2018.02.017>
- Mehta, M., Singh, N., & Anshumali. (2018b). Global trends of columnar and vertically distributed properties of aerosols with emphasis on dust, polluted dust and smoke - inferences from 10-year long CALIOP observations. *Remote Sensing of Environment*, 208, 120–132.

<https://doi.org/10.1016/J.RSE.2018.02.017>

- Mehta, M., Singh, N., & Solanki, R. (2019). Changing aerosol loadings over Central Himalayan region (2007–2016) – A satellite perspective. *Atmospheric Environment*, 207(September 2018), 117–128. <https://doi.org/10.1016/j.atmosenv.2019.03.024>
- Mehta, M., Singh, R., Singh, A., Singh, N., & Anshumali. (2016a). Recent global aerosol optical depth variations and trends - A comparative study using MODIS and MISR level 3 datasets. *Remote Sensing of Environment*, 181, 137–150. <https://doi.org/10.1016/j.rse.2016.04.004>
- Mehta, M., Singh, R., Singh, A., Singh, N., & Anshumali. (2016b). Recent global aerosol optical depth variations and trends — A comparative study using MODIS and MISR level 3 datasets. *Remote Sensing of Environment*, 181, 137–150. <https://doi.org/10.1016/J.RSE.2016.04.004>
- Menon, S., Hansen, J., Nazarenko, L., & Luo, Y. (2002). Climate effects of black carbon aerosols in China and India. *Science*, 297(5590), 2250–2253. <https://doi.org/10.1126/SCIENCE.1075159>
- Middleton, N. J. (1986). Dust storms in the Middle East. *Journal of Arid Environments*, 10(2), 83–96. [https://doi.org/10.1016/S0140-1963\(18\)31249-7](https://doi.org/10.1016/S0140-1963(18)31249-7)
- Mielonen, T., Arola, A., Komppula, M., Kukkonen, J., Koskinen, J., De Leeuw, G., & Lehtinen, K. E. J. (2009). Comparison of CALIOP level 2 aerosol subtypes to aerosol types derived from AERONET inversion data. *Geophysical Research Letters*, 36(18), 1–5. <https://doi.org/10.1029/2009GL039609>
- Miller, R. L., Tegen, I., & Perlwitz, J. (2004). Surface radiative forcing by soil dust aerosols and the hydrologic cycle. *Journal of Geophysical Research: Atmospheres*, 109(D4), 4203. <https://doi.org/10.1029/2003JD004085>
- Mishra, A. K., & Shibata, T. (2012a). Climatological aspects of seasonal variation of aerosol vertical distribution over central Indo-Gangetic belt (IGB) inferred by the space-borne lidar CALIOP. *Atmospheric Environment*, 46, 365–375. <https://doi.org/10.1016/J.ATMOSENV.2011.09.052>
- Mishra, A. K., & Shibata, T. (2012b). Synergistic analyses of optical and microphysical properties of agricultural crop residue burning aerosols over the Indo-Gangetic Basin (IGB). *Atmospheric Environment*, 57, 205–218. <https://doi.org/10.1016/J.ATMOSENV.2012.04.025>
- Mishra, M. K., & Rathore, P. S. (2021a). Impact of Nationwide COVID-19 Lockdown on Indian Air Quality in Terms of Aerosols as Observed from the Space. *Aerosol and Air Quality Research*, 21(4), 200461. <https://doi.org/10.4209/AAQR.2020.07.0461>
- Mishra, M. K., & Rathore, P. S. (2021b). Impact of Nationwide COVID-19 Lockdown on Indian Air Quality in Terms of Aerosols as Observed from the Space. *Aerosol and Air Quality Research*, 21(4), 200461. <https://doi.org/10.4209/AAQR.2020.07.0461>
- MO, A., D, R., P, A., AA, C., GP, F., KM, L., & MA, S.-D. (2004). Smoking rain clouds over the Amazon. *Science (New York, N.Y.)*, 303(5662), 1337–1342. <https://doi.org/10.1126/SCIENCE.1092779>
- Molod, A., Takacs, L., Suarez, M., & Bacmeister, J. (2015). Development of the GEOS-5 atmospheric general circulation model: Evolution from MERRA to MERRA2. *Geoscientific Model Development*, 8(5), 1339–1356. <https://doi.org/10.5194/GMD-8-1339-2015>
- Molod, Andrea, Takacs, L., Suarez, M., Bacmeister, J., Song, I.-S., Eichmann, A., & Suarez, M. J. (2012). *Technical Report Series on Global Modeling and Data Assimilation, Volume 28 The GEOS-5 Atmospheric General Circulation Model: Mean Climate and Development from MERRA to Fortuna*. <http://www.sti.nasa.gov>
- Mona, L., Amodeo, A., D'Amico, G., Giunta, A., Madonna, F., & Pappalardo, G. (2012). Multi-wavelength Raman lidar observations of the Eyjafjallajökull volcanic cloud over Potenza, southern Italy. *Atmospheric Chemistry and Physics*, 12(4), 2229–2244. <https://doi.org/10.5194/ACP-12-2229-2012>
- Moorthy, K. K., Babu, S. S., Manoj, M. R., & Satheesh, S. K. (2013). Buildup of aerosols over the Indian Region. *Geophysical Research Letters*, 40(5), 1011–1014. <https://doi.org/10.1002/GRL.50165>

- Moorthy, K. K., Beegum, S. N., Babu, S. S., Smirnov, A., John, S. R., Kumar, K. R., Narasimhulu, K., Dutt, C. B. S., & Nair, V. S. (2010). Optical and physical characteristics of Bay of Bengal aerosols during W-ICARB: Spatial and vertical heterogeneities in the marine atmospheric boundary layer and in the vertical column. *Journal of Geophysical Research: Atmospheres*, *115*(D24), 24213. <https://doi.org/10.1029/2010JD014094>
- Moorthy, K. K., Nair, V. S., Babu, S. S., & Satheesh, S. K. (2009). Spatial and vertical heterogeneities in aerosol properties over oceanic regions around India: Implications for radiative forcing. *Quarterly Journal of the Royal Meteorological Society*, *135*(645), 2131–2145. <https://doi.org/10.1002/QJ.525>
- Müller, D., Ansmann, A., Mattis, I., Tesche, M., Wandinger, U., Althausen, D., & Pisani, G. (2007). Aerosol-type-dependent lidar ratios observed with Raman lidar. *Journal of Geophysical Research: Atmospheres*, *112*(D16), 16202. <https://doi.org/10.1029/2006JD008292>
- Nabavi, S. O., Haimberger, L., & Samimi, C. (2016). Climatology of dust distribution over West Asia from homogenized remote sensing data. *Aeolian Research*, *21*, 93–107. <https://doi.org/10.1016/J.AEOLIA.2016.04.002>
- Nair, V. S., Moorthy, K. K., & Babu, S. S. (2013). Influence of continental outflow and ocean biogeochemistry on the distribution of fine and ultrafine particles in the marine atmospheric boundary layer over Arabian Sea and Bay of Bengal. *Journal of Geophysical Research: Atmospheres*, *118*(13), 7321–7331. <https://doi.org/10.1002/JGRD.50541>
- Nair, V. S., Satheesh, S. K., Moorthy, K. K., Babu, S. S., Nair, P. R., & George, S. K. (2010). Surprising observation of large anthropogenic aerosol fraction over the “near-pristine” southern Bay of Bengal: Climate implications. *Journal of Geophysical Research: Atmospheres*, *115*(D21), 21201. <https://doi.org/10.1029/2010JD013954>
- Natesan, U., & Subramanian, S. P. (1991). *Comparison Of Wind Speeds Over Arabian Sea And Bay Of Bengal Derived From Geosat Altimeter Data*. OnePetro.
- Navas-Guzmán, F., Bravo-Aranda, J. A., Guerrero-Rascado, J. L., Granados-Muñoz, M. J., & Alados-Arboledas, L. (2013). Statistical analysis of aerosol optical properties retrieved by Raman lidar over Southeastern Spain. <Http://Dx.Doi.Org/10.3402/Tellusb.V65i0.21234>, *65*(1). <https://doi.org/10.3402/TELLUSB.V65I0.21234>
- Nebojsa Nakicenovic and Rob Swart (Eds.). (2000). *Emissions Scenarios — IPCC*. Cambridge University Press, UK. <https://www.ipcc.ch/report/emissions-scenarios/>
- Omar, A. H., Winker, D. M., Tackett, J. L., Giles, D. M., Kar, J., Liu, Z., Vaughan, M. A., Powell, K. A., & Trepte, C. R. (2013). CALIOP and AERONET aerosol optical depth comparisons: One size fits none. *Journal of Geophysical Research: Atmospheres*, *118*(10), 4748–4766. <https://doi.org/10.1002/JGRD.50330>
- Omar, Ali H., Winker, D. M., Kittaka, C., Vaughan, M. A., Liu, Z., Hu, Y., Trepte, C. R., Rogers, R. R., Ferrare, R. A., Lee, K. P., Kuehn, R. E., & Hostetler, C. A. (2009). The CALIPSO automated aerosol classification and lidar ratio selection algorithm. *Journal of Atmospheric and Oceanic Technology*, *26*(10), 1994–2014. <https://doi.org/10.1175/2009JTECHA1231.1>
- Omar, Ali H., Won, J.-G., Winker, D. M., Yoon, S.-C., Dubovik, O., & McCormick, M. P. (2005). Development of global aerosol models using cluster analysis of Aerosol Robotic Network (AERONET) measurements. *Journal of Geophysical Research: Atmospheres*, *110*(D10), 1–14. <https://doi.org/10.1029/2004JD004874>
- Pandey, A., Patel, S., Pervez, S., Tiwari, S., Yadama, G., Chow, J. C., Watson, J. G., Biswas, P., & Chakrabarty, R. K. (2017). Aerosol emissions factors from traditional biomass cookstoves in India: Insights from field measurements. *Atmospheric Chemistry and Physics*, *17*(22), 13721–13729. <https://doi.org/10.5194/ACP-17-13721-2017>
- Pandey, S. K., & Vinoj, V. (2021). Surprising Changes in Aerosol Loading over India amid COVID-19 Lockdown. *Aerosol and Air Quality Research*, *21*(3), 200466. <https://doi.org/10.4209/AAQR.2020.07.0466>

- Pandithurai, G., Dipu, S., Dani, K. K., Tiwari, S., Bisht, D. S., Devara, P. C. S., & Pinker, R. T. (2008). Aerosol radiative forcing during dust events over New Delhi, India. *Journal of Geophysical Research: Atmospheres*, 113(D13). <https://doi.org/10.1029/2008JD009804>
- Pant, P., Hegde, P., Dumka, U. C., Sagar, R., Satheesh, S. K., Moorthy, K. K., Saha, A., & Srivastava, M. K. (2006). Aerosol characteristics at a high-altitude location in central Himalayas: Optical properties and radiative forcing. *Journal of Geophysical Research: Atmospheres*, 111(D17). <https://doi.org/10.1029/2005JD006768>
- Parvathi, V., Suresh, I., Lengaigne, M., Izumo, T., & Vialard, J. (2017). Robust Projected Weakening of Winter Monsoon Winds Over the Arabian Sea Under Climate Change. *Geophysical Research Letters*, 44(19), 9833–9843. <https://doi.org/10.1002/2017GL075098>
- Pathak, B., Subba, T., Dahutia, P., Bhuyan, P. K., Moorthy, K. K., Gogoi, M. M., Babu, S. S., Chutia, L., Ajay, P., Biswas, J., Bharali, C., Borgohain, A., Dhar, P., Guha, A., De, B. K., Banik, T., Chakraborty, M., Kundu, S. S., Sudhakar, S., & Singh, S. B. (2016). Aerosol characteristics in north-east India using ARFINET spectral optical depth measurements. *Atmospheric Environment*, 125, 461–473. <https://doi.org/10.1016/J.ATMOSENV.2015.07.038>
- Pathakoti, M., Muppalla, A., Hazra, S., Dangeti, M., Shekhar, R., Jella, S., Mullapudi, S. S., Andugulapati, P., & Vijayasundaram, U. (2020a). An assessment of the impact of a nation-wide lockdown on air pollution – a remote sensing perspective over India. *Atmospheric Chemistry and Physics Discussions*, 1–16. <https://doi.org/10.5194/ACP-2020-621>
- Pathakoti, M., Muppalla, A., Hazra, S., Dangeti, M., Shekhar, R., Jella, S., Mullapudi, S. S., Andugulapati, P., & Vijayasundaram, U. (2020b). An assessment of the impact of a nation-wide lockdown on air pollution – a remote sensing perspective over India. *Atmospheric Chemistry and Physics Discussions*, 1–16. <https://doi.org/10.5194/acp-2020-621>
- Pierangelo, C., Chédin, A., Heilliette, S., Jacquinet-Husson, N., & Armante, R. (2004). Dust altitude and infrared optical depth from AIRS. *Atmospheric Chemistry and Physics*, 4(7), 1813–1822. <https://doi.org/10.5194/ACP-4-1813-2004>
- PJ, R., DM, B., JS, H., DS, B., PK, K., CY, C., & RY, K. (2006). Ranibizumab for neovascular age-related macular degeneration. *The New England Journal of Medicine*, 355(14), 1419–1431. <https://doi.org/10.1056/NEJMOA054481>
- Powell, K. A., Hostetler, C. A., Vaughan, M. A., Lee, K.-P., Trepte, C. R., Rogers, R. R., Winker, D. M., Liu, Z., Kuehn, R. E., Hunt, W. H., & Young, S. A. (2009). CALIPSO Lidar Calibration Algorithms. Part I: Nighttime 532-nm Parallel Channel and 532-nm Perpendicular Channel. *Journal of Atmospheric and Oceanic Technology*, 26(10), 2015–2033. <https://doi.org/https://doi.org/10.1175/2009JTECHA1242.1>
- Prasad, A. K., Singh, S., Chauhan, S. S., Srivastava, M. K., Singh, R. P., & Singh, R. (2007). Aerosol radiative forcing over the Indo-Gangetic plains during major dust storms. *Atmospheric Environment*, 41(29), 6289–6301. <https://doi.org/10.1016/J.ATMOSENV.2007.03.060>
- Prijith, S. S., Aloysius, M., & Mohan, M. (2013). Global aerosol source/sink map. *Atmospheric Environment*, 80, 533–539. <https://doi.org/10.1016/J.ATMOSENV.2013.08.038>
- Prijith, S. S., Suresh Babu, S., Lakshmi, N. B., Satheesh, S. K., & Krishna Moorthy, K. (2016). Meridional gradients in aerosol vertical distribution over Indian Mainland: Observations and model simulations. *Atmospheric Environment*, 125, 337–345. <https://doi.org/10.1016/J.ATMOSENV.2015.10.066>
- Prijith, S. S., Srinivasulu, J., & Sesha Sai, M. V. R. (2021). Dominance of natural aerosols over India in pre-monsoon: inferences from the lockdown effects. 120(2).
- Prijith, Sudhakaran Syamala, Rao, P. V. N., Mohan, M., Sai, M. V. R. S., & Ramana, M. V. (2018). Trends of absorption, scattering and total aerosol optical depths over India and surrounding oceanic regions from satellite observations: role of local production, transport and atmospheric dynamics. *Environmental Science and Pollution Research* 2018 25:18, 25(18), 18147–18160. <https://doi.org/10.1007/S11356-018-2032-0>

- PRODUCTS - CALIPSO Standard Browse Images - Version V4.x. (n.d.). Retrieved September 5, 2021, from [https://www-calipso.larc.nasa.gov/products/lidar/browse\\_images/std\\_v4\\_index.php](https://www-calipso.larc.nasa.gov/products/lidar/browse_images/std_v4_index.php)
- Proestakis, E., Amiridis, V., Marinou, E., Georgoulas, A. K., Solomos, S., Kazadzis, S., Chimot, J., Che, H., Alexandri, G., Biniotoglou, I., Daskalopoulou, V., Kourtidis, K. A., De Leeuw, G., & Van Der A, R. J. (2018). Nine-year spatial and temporal evolution of desert dust aerosols over South and East Asia as revealed by CALIOP. *Atmospheric Chemistry and Physics*, *18*(2), 1337–1362. <https://doi.org/10.5194/acp-18-1337-2018>
- Prospero, J. M., Prospero, J. M., Ginoux, P., Torres, O., Nicholson, S. E., & Gill, T. E. (2002). Environmental characterization of global sources of atmospheric soil dust derived from the NIMBUS7 TOMS absorbing aerosol product, Rev. *REVIEWS OF GEOPHYSICS*, *40*(1), 1002. <http://citeseerx.ist.psu.edu/viewdoc/summary?doi=10.1.1.137.1744>
- Putaud, J. P., Van Dingenen, R., Alastuey, A., Bauer, H., Birmili, W., Cyrus, J., Flentje, H., Fuzzi, S., Gehrig, R., Hansson, H. C., Harrison, R. M., Herrmann, H., Hitztenberger, R., Hüglin, C., Jones, A. M., Kasper-Giebl, A., Kiss, G., Koussa, A., Kuhlbusch, T. A. J., ... Raes, F. (2010). A European aerosol phenomenology – 3: Physical and chemical characteristics of particulate matter from 60 rural, urban, and kerbside sites across Europe. *Atmospheric Environment*, *44*(10), 1308–1320. <https://doi.org/10.1016/J.ATMOSENV.2009.12.011>
- Quijano, A. L., Sokolik, I. N., & Toon, O. B. (2000). Radiative heating rates and direct radiative forcing by mineral dust in cloudy atmospheric conditions. *Journal of Geophysical Research: Atmospheres*, *105*(D10), 12207–12219. <https://doi.org/10.1029/2000JD900047>
- Ram, K., Sarin, M. M., & Hegde, P. (2010). Long-term record of aerosol optical properties and chemical composition from a high-altitude site (Manora Peak) in Central Himalaya. *Atmospheric Chemistry and Physics*, *10*(23), 11791–11803. <https://doi.org/10.5194/ACP-10-11791-2010>
- Ramachandran, S., & Cherian, R. (2008). Regional and seasonal variations in aerosol optical characteristics and their frequency distributions over India during 2001–2005. *Journal of Geophysical Research: Atmospheres*, *113*(D8), 8207. <https://doi.org/10.1029/2007JD008560>
- Ramachandran, S., & Kedia, S. (2010). Black carbon aerosols over an urban region: Radiative forcing and climate impact. *Journal of Geophysical Research: Atmospheres*, *115*(D10), 10202. <https://doi.org/10.1029/2009JD013560>
- Ramanathan, V., Crutzen, P. J., Kiehl, J. T., & Rosenfeld, D. (2001). Atmosphere: Aerosols, climate, and the hydrological cycle. *Science*, *294*(5549), 2119–2124. <https://doi.org/10.1126/SCIENCE.1064034>
- Ramanathan, V., Li, F., Ramana, M. V., Praveen, P. S., Kim, D., Corrigan, C. E., Nguyen, H., Stone, E. A., Schauer, J. J., Carmichael, G. R., Adhikary, B., & Yoon, S. C. (2007). Atmospheric brown clouds: Hemispherical and regional variations in long-range transport, absorption, and radiative forcing. *Journal of Geophysical Research: Atmospheres*, *112*(D22), 22–43. <https://doi.org/10.1029/2006JD008124>
- Ramanathan, V., & Ramana, M. V. (2005). Persistent, Widespread, and Strongly Absorbing Haze Over the Himalayan Foothills and the Indo-Gangetic Plains. *Pure and Applied Geophysics* *2005* *162*:8, *162*(8), 1609–1626. <https://doi.org/10.1007/S00024-005-2685-8>
- Randles, C. A., & Ramaswamy, V. (2008). Absorbing aerosols over Asia: A Geophysical Fluid Dynamics Laboratory general circulation model sensitivity study of model response to aerosol optical depth and aerosol absorption. *Journal of Geophysical Research: Atmospheres*, *113*(D21), 21203. <https://doi.org/10.1029/2008JD010140>
- Randles, C. A., Silva, A. M. da, Buchard, V., Colarco, P. R., Darmenov, A., Govindaraju, R., Smirnov, A., Holben, B., Ferrare, R., Hair, J., Shinzuka, Y., & Flynn, C. J. (2017). The MERRA-2 Aerosol Reanalysis, 1980 Onward. Part I: System Description and Data Assimilation Evaluation. *Journal of Climate*, *30*(17), 6823–6850. <https://doi.org/10.1175/JCLI-D-16-0609.1>
- Remer, L. A., Kaufman, Y. J., Tanré, D., Mattoo, S., Chu, D. A., Martins, J. V., Li, R.-R., Ichoku, C., Levy, R. C., Kleidman, R. G., Eck, T. F., Vermote, E., & Holben, B. N. (2005). The MODIS Aerosol Algorithm, Products, and Validation. *Journal of the Atmospheric Sciences*, *62*(4), 947–973.

<https://doi.org/10.1175/JAS3385.1>

- Remer, Lorraine A., Remer, L. A., Tanré, D., & Kaufman, Y. J. (2006). *Algorithm for remote sensing of tropospheric aerosol from MODIS: Collection 005*. 2229--2259.  
<http://citeseerx.ist.psu.edu/viewdoc/summary?doi=10.1.1.385.6530>
- Rolph, G., Stein, A., & Stunder, B. (2017). Real-time Environmental Applications and Display sYstem: READY. *Environmental Modelling & Software*, *95*, 210–228.  
<https://doi.org/10.1016/J.ENVSOFT.2017.06.025>
- Rosenfeld, D., Lohmann, U., Raga, G. B., O'Dowd, C. D., Kulmala, M., Fuzzi, S., Reissell, A., & Andreae, M. O. (2008). Flood or drought: How do aerosols affect precipitation? *Science*, *321*(5894), 1309–1313.  
<https://doi.org/10.1126/SCIENCE.1160606>
- Rummukainen, M., Rockel, B., Bärring, L., Christensen, J. H., & Reckermann, M. (2015). Twenty-First-Century Challenges in Regional Climate Modeling. *Bulletin of the American Meteorological Society*, *96*(8), ES135–ES138. <https://doi.org/10.1175/BAMS-D-14-00214.1>
- Sarra, A. di, Iorio, T. Di, Cacciani, M., Fiocco, G., & Fuà, D. (2001). Saharan dust profiles measured by lidar at Lampedusa. *Journal of Geophysical Research: Atmospheres*, *106*(D10), 10335–10347.  
<https://doi.org/10.1029/2000JD900734>
- Satheesh, S. K., & Krishna Moorthy, K. (2005). Radiative effects of natural aerosols: A review. *Atmospheric Environment*, *39*(11), 2089–2110. <https://doi.org/10.1016/J.ATMOENV.2004.12.029>
- Satheesh, S. K., Moorthy, K. K., Babu, S. S., Vinoj, V., & Dutt, C. B. S. (2008). Climate implications of large warming by elevated aerosol over India. *Geophysical Research Letters*, *35*(19).  
<https://doi.org/10.1029/2008GL034944>
- Satheesh, S. K., & Srinivasan, J. (2002). Enhanced aerosol loading over Arabian Sea during the pre-monsoon season: Natural or anthropogenic? *Geophysical Research Letters*, *29*(18), 21–1.  
<https://doi.org/10.1029/2002GL015687>
- Satheesh, S. K., Vinoj, V., & Moorthy, K. K. (2006). Vertical distribution of aerosols over an urban continental site in India inferred using a micro pulse lidar. *Geophysical Research Letters*, *33*(20).  
<https://doi.org/10.1029/2006GL027729>
- Schult, I., Feichter, J., & Cooke, W. F. (1997). Effect of black carbon and sulfate aerosols on the Global Radiation Budget. *Journal of Geophysical Research: Atmospheres*, *102*(D25), 30107–30117.  
<https://doi.org/10.1029/97JD01863>
- Schulz, M., Textor, C., Kinne, S., Balkanski, Y., Bauer, S., Bernsten, T., Berglen, T., Boucher, O., Dentener, F., Guibert, S., Isaksen, I. S. A., Iversen, T., Koch, D., Kirkevåg, A., Liu, X., Montanaro, V., Myhre, G., Penner, J. E., Pitari, G., ... Takemura, T. (2006). Radiative forcing by aerosols as derived from the AeroCom present-day and pre-industrial simulations. *Atmospheric Chemistry and Physics*, *6*(12), 5225–5246. <https://doi.org/10.5194/ACP-6-5225-2006>
- Schuster, G. L., Vaughan, M., MacDonnell, D., Su, W., Winker, D., Dubovik, O., Lapyonok, T., & Trepte, C. (2012). Comparison of CALIPSO aerosol optical depth retrievals to AERONET measurements, and a climatology for the lidar ratio of dust. *Atmospheric Chemistry and Physics*, *12*(16), 7431–7452.  
<https://doi.org/10.5194/ACP-12-7431-2012>
- Seinfeld, J. H., & Pandis, S. N. (2016). *Atmospheric Chemistry and Physics: From Air Pollution to Climate Change, 3rd Edition*. Wiley-Blackwell.
- Shao, Y., Wyrwoll, K. H., Chappell, A., Huang, J., Lin, Z., McTainsh, G. H., Mikami, M., Tanaka, T. Y., Wang, X., & Yoon, S. (2011). Dust cycle: An emerging core theme in Earth system science. *Aeolian Research*, *2*(4), 181–204. <https://doi.org/10.1016/J.AEOLIA.2011.02.001>
- Sharma, A. R., Kharol, S. K., Badarinath, K. V. S., & Singh, D. (2010). Impact of agriculture crop residue burning on atmospheric aerosol loading - A study over Punjab State, India. *Annales Geophysicae*, *28*(2), 367–379. <https://doi.org/10.5194/ANGE0-28-367-2010>

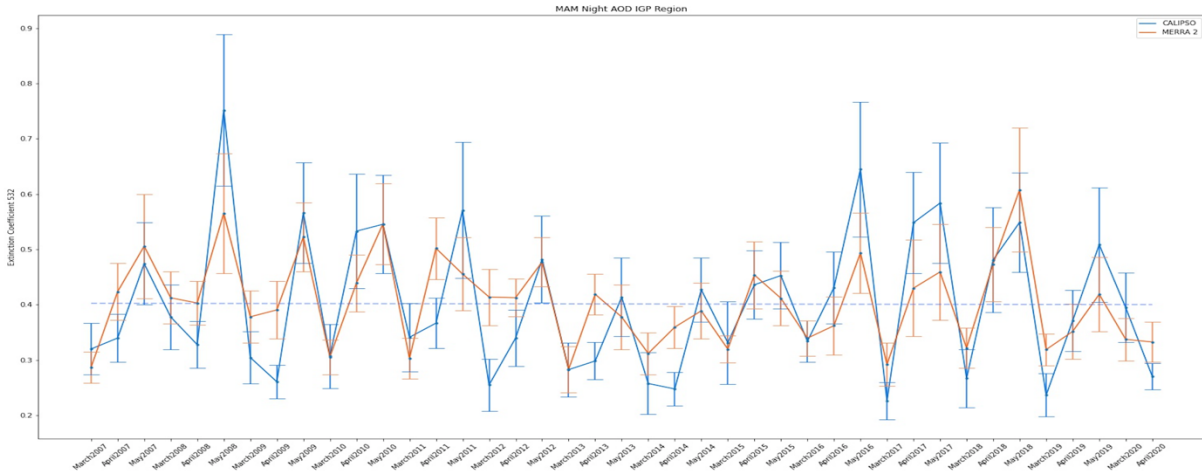
- Sharma, D., Singh, D., & Kaskaoutis, D. G. (2012). Impact of two intense dust storms on aerosol characteristics and radiative forcing over Patiala, Northwestern India. *Advances in Meteorology*, 2012. <https://doi.org/10.1155/2012/956814>
- Shen, F., Zhang, Q., Ma, J., Li, Z., & Hong, J. (2021). Identification of polluted clouds and composition analysis based on GF-5 DPC data. *Journal of Quantitative Spectroscopy and Radiative Transfer*, 269. <https://doi.org/10.1016/J.JQSRT.2021.107659>
- Singh, R. P., Dey, S., Tripathi, S. N., Tare, V., & Holben, B. (2004). Variability of aerosol parameters over Kanpur, northern India. *Journal of Geophysical Research: Atmospheres*, 109(D23), 1–14. <https://doi.org/10.1029/2004JD004966>
- Solanki, R., & Singh, N. (2014). LiDAR observations of the vertical distribution of aerosols in free troposphere: Comparison with CALIPSO level-2 data over the central Himalayas. *Atmospheric Environment*, 99, 227–238. <https://doi.org/10.1016/J.ATMOENV.2014.09.083>
- Srinivas, B., Sarin, M. M., & Kumar, A. (2011). Impact of anthropogenic sources on aerosol iron solubility over the Bay of Bengal and the Arabian Sea. *Biogeochemistry* 2011 110:1, 110(1), 257–268. <https://doi.org/10.1007/S10533-011-9680-1>
- Srivastava, A. K., Tiwari, S., Devara, P. C. S., Bisht, D. S., Srivastava, M. K., Tripathi, S. N., Goloub, P., & Holben, B. N. (2011). Pre-monsoon aerosol characteristics over the Indo-Gangetic Basin: Implications to climatic impact. *Annales Geophysicae*, 29(5), 789–804. <https://doi.org/10.5194/ANGEO-29-789-2011>
- Srivastava, R. (2017). Trends in aerosol optical properties over South Asia. *International Journal of Climatology*, 37(1), 371–380. <https://doi.org/10.1002/JOC.4710>
- Stein, A. F., Draxler, R. R., Rolph, G. D., Stunder, B. J. B., Cohen, M. D., & Ngan, F. (2015). NOAA's hybrid atmospheric transport and dispersion modeling system. In *Bulletin of the American Meteorological Society* (Vol. 96, Issue 12, pp. 2059–2077). American Meteorological Society. <https://doi.org/10.1175/BAMS-D-14-00110.1>
- Stephens, G. L., Vane, D. G., Boain, R. J., Mace, G. G., Sassen, K., Wang, Z., Illingworth, A. J., O'Connor, E. J., Rossow, W. B., Durden, S. L., Miller, S. D., Austin, R. T., Benedetti, A., & Mitrescu, C. (2002). THE CLOUDSAT MISSION AND THE A-TRAIN: A New Dimension of Space-Based Observations of Clouds and Precipitation. *Bulletin of the American Meteorological Society*, 83(12), 1771–1790. <https://doi.org/10.1175/BAMS-83-12-1771>
- Stull, R. B. (1988). Mean Boundary Layer Characteristics. *An Introduction to Boundary Layer Meteorology*, 1–27. [https://doi.org/10.1007/978-94-009-3027-8\\_1](https://doi.org/10.1007/978-94-009-3027-8_1)
- Sun, E., Xu, X., Che, H., Tang, Z., Gui, K., An, L., Lu, C., & Shi, G. (2019). Variation in MERRA-2 aerosol optical depth and absorption aerosol optical depth over China from 1980 to 2017. *Journal of Atmospheric and Solar-Terrestrial Physics*, 186, 8–19. <https://doi.org/10.1016/J.JASTP.2019.01.019>
- Sun, Y., Wang, Z., Dong, H., Yang, T., Li, J., Pan, X., Chen, P., & Jayne, J. T. (2012). Characterization of summer organic and inorganic aerosols in Beijing, China with an Aerosol Chemical Speciation Monitor. *Atmospheric Environment*, 51, 250–259. <https://doi.org/10.1016/J.ATMOENV.2012.01.013>
- Sundström, A.-M., Nousiainen, T., & Petäjä, T. (2009). On the Quantitative Low-Level Aerosol Measurements Using Ceilometer-Type Lidar. *Journal of Atmospheric and Oceanic Technology*, 26(11), 2340–2352. <https://doi.org/10.1175/2009JTECHA1252.1>
- Tegen, I., & Miller, R. (1998). A general circulation model study on the interannual variability of soil dust aerosol. *Journal of Geophysical Research: Atmospheres*, 103(D20), 25975–25995. <https://doi.org/10.1029/98JD02345>
- Thomas, A., Kanawade, V. P., Sarangi, C., & Srivastava, A. K. (2021). Effect of COVID-19 shutdown on aerosol direct radiative forcing over the Indo-Gangetic Plain outflow region of the Bay of Bengal. *Science of The Total Environment*, 782, 146918. <https://doi.org/10.1016/J.SCITOTENV.2021.146918>
- Thompson, S. L., Ramaswamy, V., & Covey, C. (1987). Atmospheric effects of nuclear war aerosols in

- general circulation model simulations: Influence of smoke optical properties. *Journal of Geophysical Research: Atmospheres*, 92(D9), 10942–10960. <https://doi.org/10.1029/JD092ID09P10942>
- Tindale, N. W., & Pease, P. P. (1999). Aerosols over the Arabian Sea: Atmospheric transport pathways and concentrations of dust and sea salt. *Deep Sea Research Part II: Topical Studies in Oceanography*, 46(8–9), 1577–1595. [https://doi.org/10.1016/S0967-0645\(99\)00036-3](https://doi.org/10.1016/S0967-0645(99)00036-3)
- Tomasi, C., Fuzzi, S., & Kokhanovsky, A. (2017). *Atmospheric Aerosols*. <https://doi.org/10.1002/9783527336449>
- Tripathi, S. N., Srivastava, A. K., Dey, S., Satheesh, S. K., & Krishnamoorthy, K. (2007). The vertical profile of atmospheric heating rate of black carbon aerosols at Kanpur in northern India. *Atmospheric Environment*, 41(32), 6909–6915. <https://doi.org/10.1016/J.ATMOENV.2007.06.032>
- Twomey, S. (1974). Pollution and the planetary albedo. *Atmospheric Environment (1967)*, 8(12), 1251–1256. [https://doi.org/10.1016/0004-6981\(74\)90004-3](https://doi.org/10.1016/0004-6981(74)90004-3)
- Vaughan, M. A., Powell, K. A., Kuehn, R. E., Young, S. A., Winker, D. M., Hostetler, C. A., Hunt, W. H., Liu, Z., McGill, M. J., & Getzewich, B. J. (2009). Fully automated detection of cloud and aerosol layers in the CALIPSO lidar measurements. *Journal of Atmospheric and Oceanic Technology*, 26(10), 2034–2050. <https://doi.org/10.1175/2009JTECHA1228.1>
- Vaughan, M., Garnier, A., Josset, D., Avery, M., Lee, K. P., Liu, Z., Hunt, W., Pelon, J., Hu, Y., Burton, S., Hair, J., Tackett, J. L., Getzewich, B., Kar, J., & Rodier, S. (2019). CALIPSO lidar calibration at 1064nm: Version 4 algorithm. *Atmospheric Measurement Techniques*, 12(1), 51–82. <https://doi.org/10.5194/AMT-12-51-2019>
- Vinjamuri, K. S., Mhawish, A., Banerjee, T., Sorek-Hamer, M., Broday, D. M., Mall, R. K., & Latif, M. T. (2020). Vertical distribution of smoke aerosols over upper Indo-Gangetic Plain. *Environmental Pollution*, 257, 113377. <https://doi.org/10.1016/j.envpol.2019.113377>
- Wang, Hua, Sun, Z., Li, H., Gao, Y., Wu, J., & Cheng, T. (2018). Vertical-distribution Characteristics of Atmospheric Aerosols under Different Thermodynamic Conditions in Beijing. *Aerosol and Air Quality Research*, 18(11), 2775–2787. <https://doi.org/10.4209/AAQR.2018.03.0078>
- Wang, Huijun, & He, S. (2012). Weakening relationship between East Asian winter monsoon and ENSO after mid-1970s. *Chinese Science Bulletin* 2012 57:27, 57(27), 3535–3540. <https://doi.org/10.1007/S11434-012-5285-X>
- Winker, D. M., Pelon, J., Coakley, J. A., Ackerman, S. A., Charlson, R. J., Colarco, P. R., Flamant, P., Fu, Q., Hoff, R. M., Kittaka, C., Kubar, T. L., Treut, H. Le, McCormick, M. P., Mégie, G., Poole, L., Powell, K., Trepte, C., Vaughan, M. A., & Wielicki, B. A. (2010). The CALIPSO Mission: A Global 3D View of Aerosols and Clouds. *Bulletin of the American Meteorological Society*, 91(9), 1211–1230. <https://doi.org/10.1175/2010BAMS3009.1>
- Winker, D. M., Tackett, J. L., Getzewich, B. J., Liu, Z., Vaughan, M. A., & Rogers, R. R. (2013). The global 3-D distribution of tropospheric aerosols as characterized by CALIOP. *Atmospheric Chemistry and Physics*, 13(6), 3345–3361. <https://doi.org/10.5194/ACP-13-3345-2013>
- Winker, David M., Hunt, W. H., & McGill, M. J. (2007). Initial performance assessment of CALIOP. *Geophysical Research Letters*, 34(19). <https://doi.org/10.1029/2007GL030135>
- Winker, David M., Pelon, J. R., & McCormick, M. P. (2003). CALIPSO mission: spaceborne lidar for observation of aerosols and clouds. *Lidar Remote Sensing for Industry and Environment Monitoring III*, 4893, 1–11. <https://doi.org/10.1117/12.466539>
- Winker, David M., Vaughan, M. A., Omar, A., Hu, Y., Powell, K. A., Liu, Z., Hunt, W. H., & Young, S. A. (2009a). Overview of the CALIPSO mission and CALIOP data processing algorithms. *Journal of Atmospheric and Oceanic Technology*, 26(11), 2310–2323. <https://doi.org/10.1175/2009JTECHA1281.1>
- Winker, David M., Vaughan, M. A., Omar, A., Hu, Y., Powell, K. A., Liu, Z., Hunt, W. H., & Young, S. A. (2009b). Overview of the CALIPSO Mission and CALIOP Data Processing Algorithms. *Journal of Atmospheric and Oceanic Technology*, 26(11), 2310–2323. <https://doi.org/10.1175/2009JTECHA1281.1>

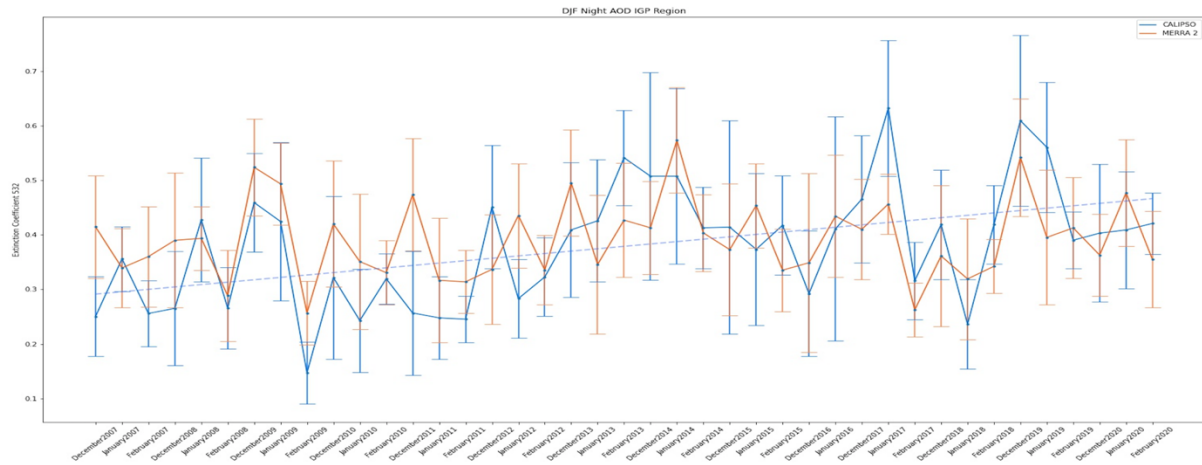
- Young, A. (1995). The Tyranny of Numbers: Confronting the Statistical Realities of the East Asian Growth Experience. *The Quarterly Journal of Economics*, 110(3), 641–680.  
<https://doi.org/10.2307/2946695>
- Young, S. A., & Vaughan, M. A. (2009a). The retrieval of profiles of particulate extinction from cloud-aerosol lidar infrared pathfinder satellite observations (CALIPSO) data: Algorithm description. *Journal of Atmospheric and Oceanic Technology*, 26(6), 1105–1119.  
<https://doi.org/10.1175/2008JTECHA1221.1>
- Young, S. A., & Vaughan, M. A. (2009b). The Retrieval of Profiles of Particulate Extinction from Cloud-Aerosol Lidar Infrared Pathfinder Satellite Observations (CALIPSO) Data: Algorithm Description. *Journal of Atmospheric and Oceanic Technology*, 26(6), 1105–1119.  
<https://doi.org/10.1175/2008JTECHA1221.1>
- Yu, H., Kaufman, Y. J., Chin, M., Feingold, G., Remer, L. A., Anderson, T. L., Balkanski, Y., Bellouin, N., Boucher, O., Christopher, S., DeCola, P., Kahn, R., Koch, D., Loeb, N., Reddy, M. S., Schulz, M., Takemura, T., & Zhou, M. (2006). A review of measurement-based assessments of the aerosol direct radiative effect and forcing. *Atmospheric Chemistry and Physics*, 6(3), 613–666.  
<https://doi.org/10.5194/ACP-6-613-2006>
- Zarzycki, C. M., & Bond, T. C. (2010). How much can the vertical distribution of black carbon affect its global direct radiative forcing? *Geophysical Research Letters*, 37(20).  
<https://doi.org/10.1029/2010GL044555>
- Zieger, P., Fierz-Schmidhauser, R., Weingartner, E., & Baltensperger, U. (2013). Effects of relative humidity on aerosol light scattering: Results from different European sites. *Atmospheric Chemistry and Physics*, 13(21), 10609–10631. <https://doi.org/10.5194/ACP-13-10609-2013>

## APPENDIX - I

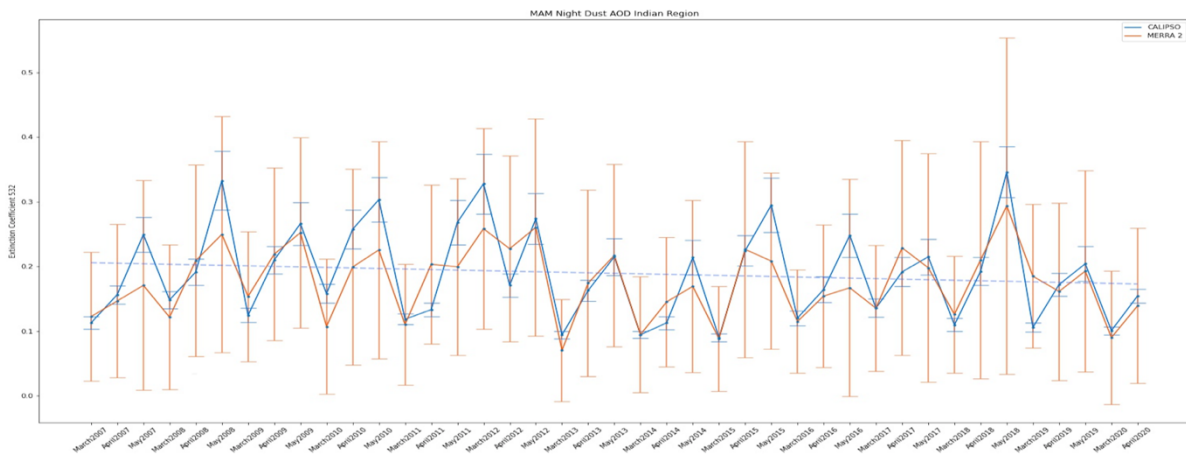
Some of the significant trend plots (in reference to section 5.6) for a comparative assessment of AOD estimated by CALIOP sensor and MERRA 2 reanalysis dataset.



**A1 1** MAM nighttime trend (total) IGP region



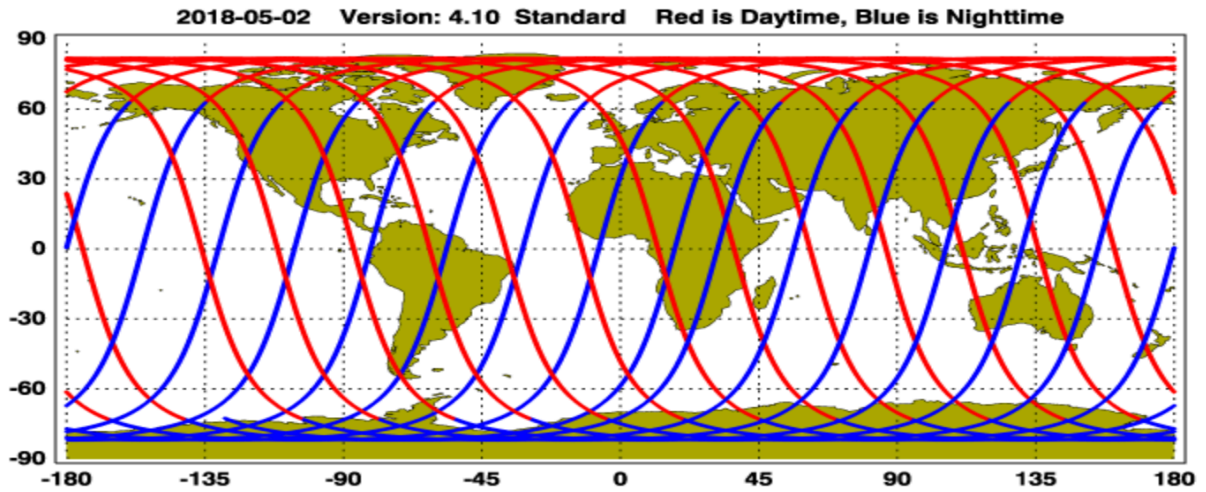
**A1 2** DJF nighttime trend (total) IGP region



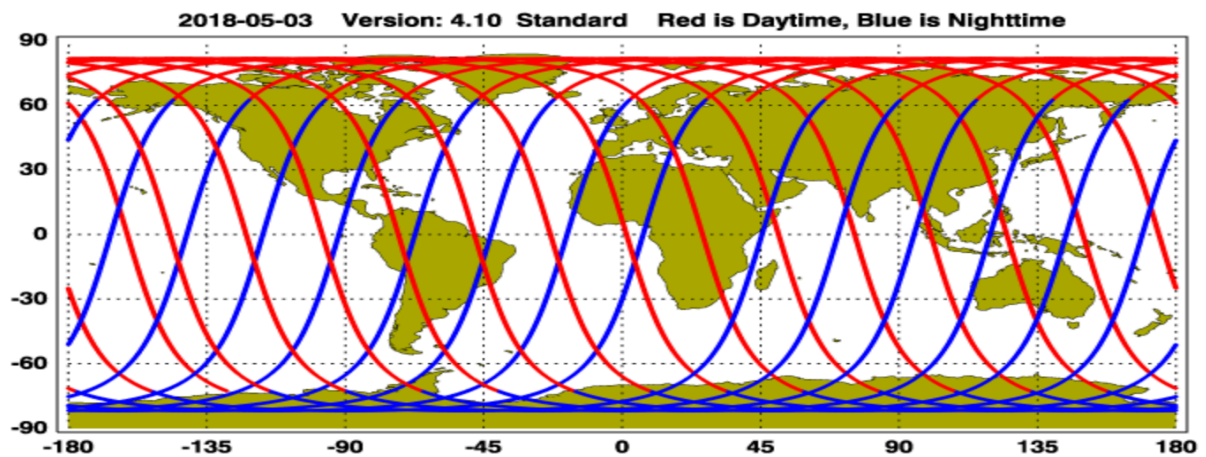
**A1 3** MAM nighttime dust trend Indian region

## APPENDIX - II

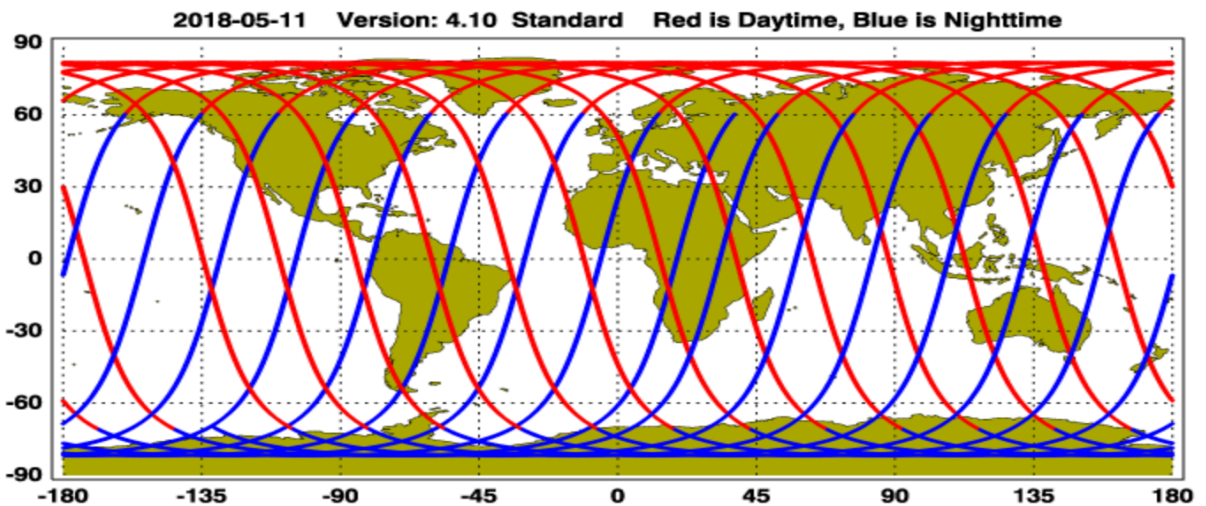
The following supplementary data is in reference to showcase the bias between dust and smoke extinction in total as well case smoke case study section 5.9. (*PRODUCTS - CALIPSO Standard Browse Images - Version V4.X, n.d.*)



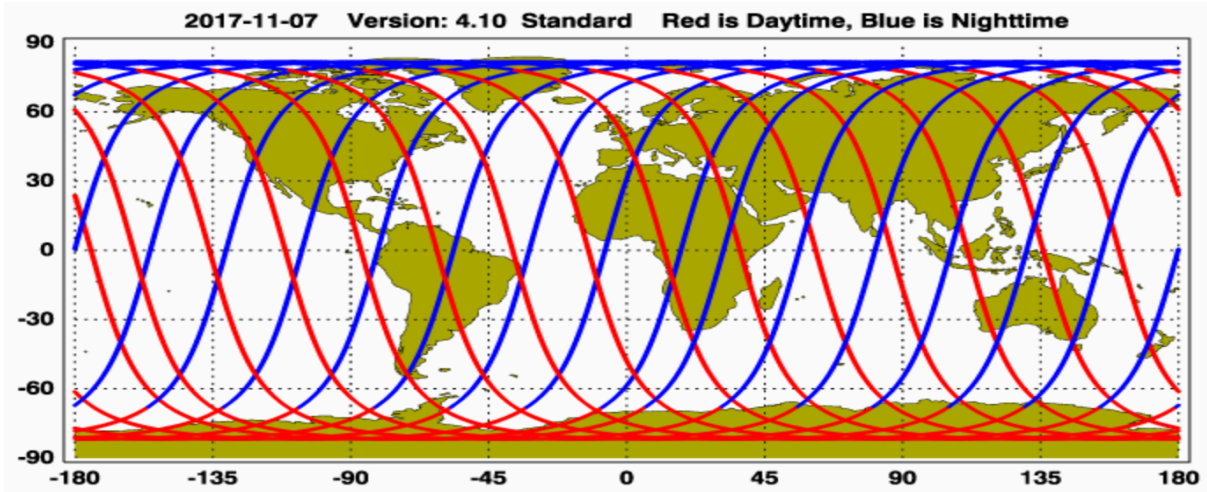
A2 1 CALIPSO orbital pass on 2 May 2018 (Dust storm-1)



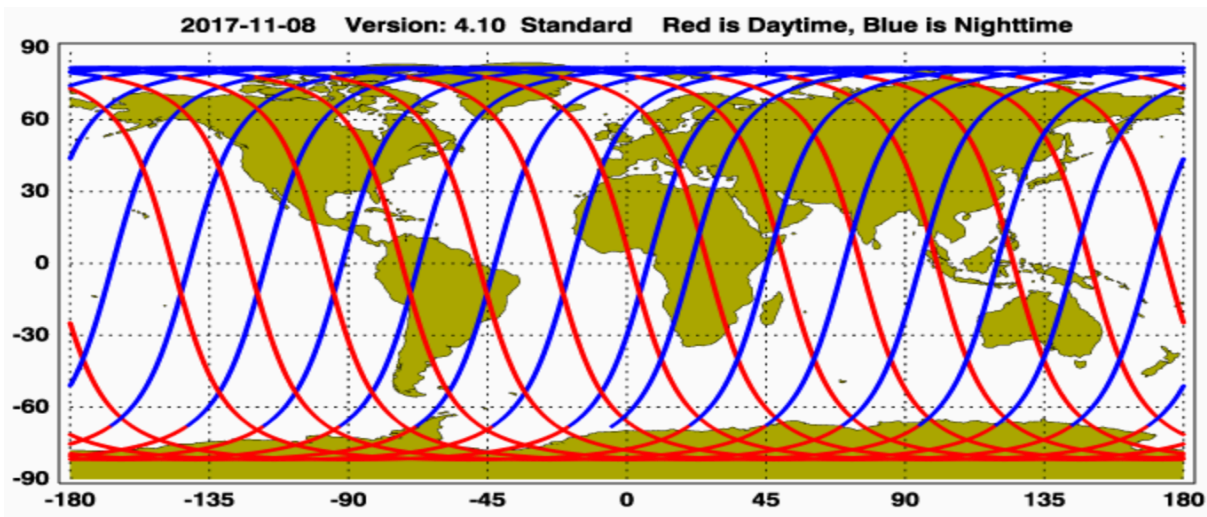
A2 2 CALIPSO orbital pass on 3 May 2018 (Dust storm-1)



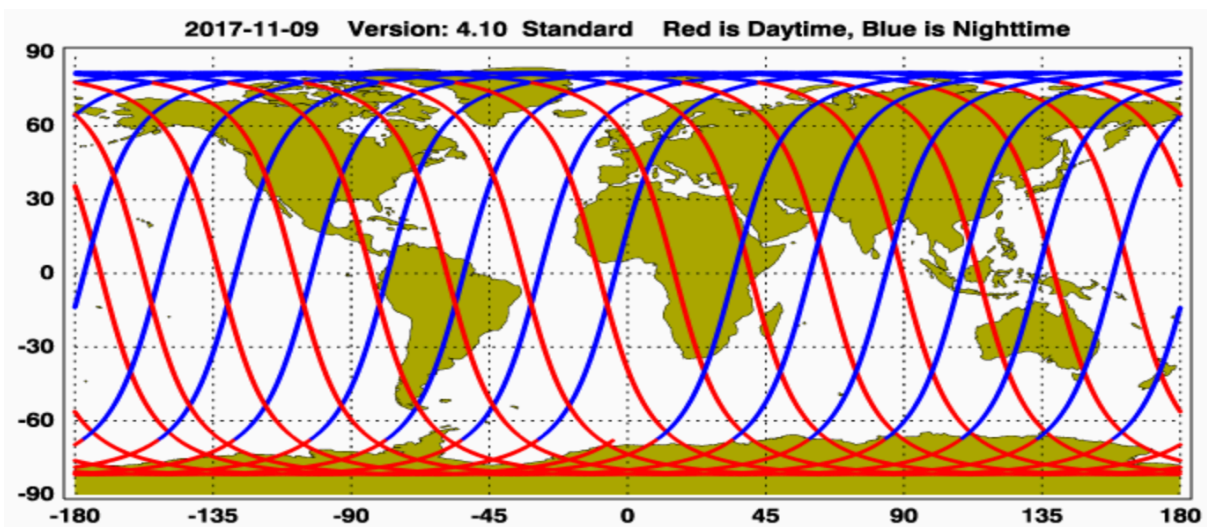
A2 3 CALIPSO orbital pass on 11 May 2018 (Dust storm-2)



A2 4 CALIPSO orbital pass on 7 November 2017 (Smog)



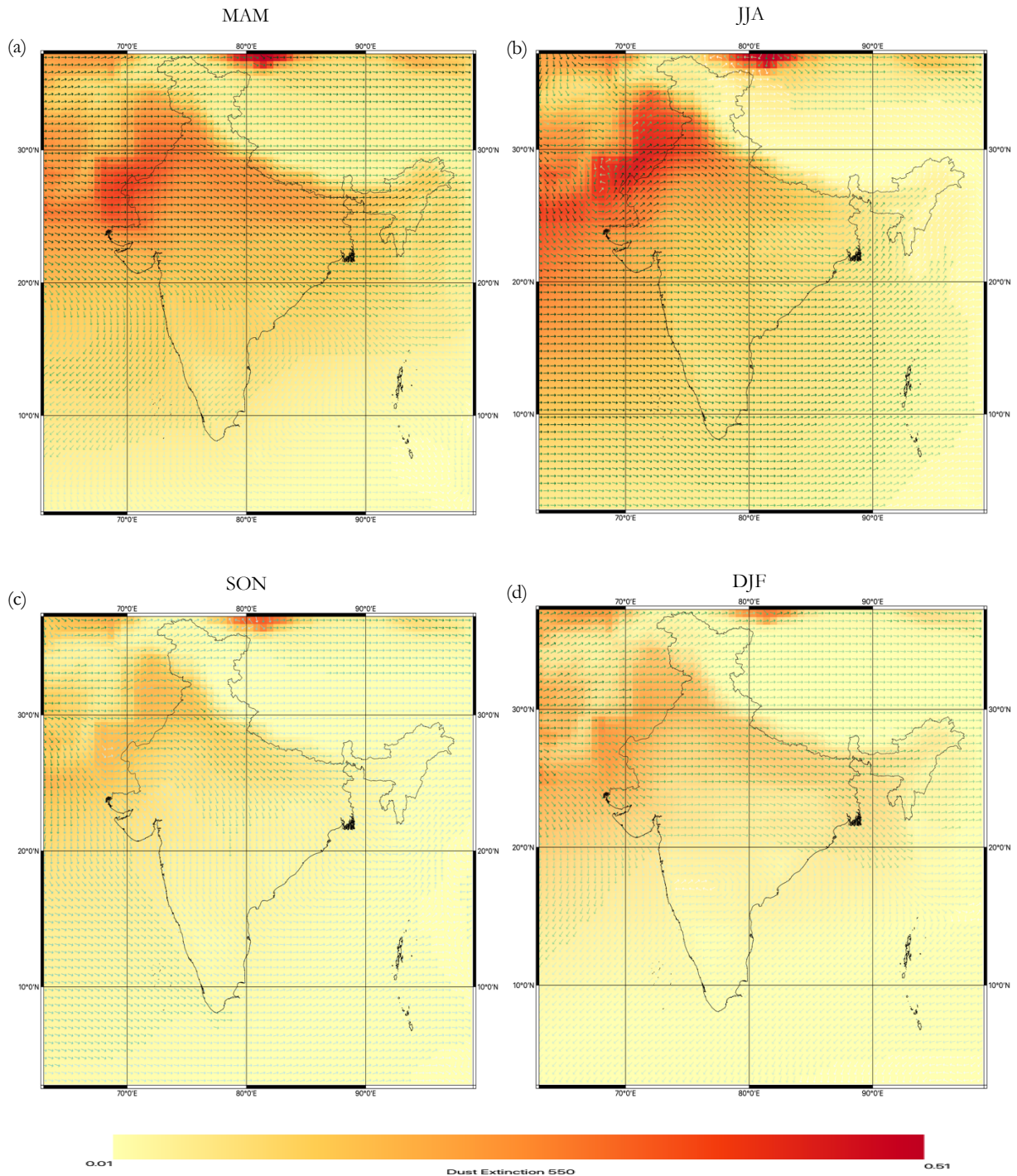
A2 5 CALIPSO orbital pass on 8 November 2017 (Smog)



A2 6 CALIPSO orbital pass on 9 November 2017 (Smog)

## APPENDIX - III

The seasonal AOD derived from MERRA 2 is mapped with the seasonal dust flux. The color of the arrow mark represents the dust emission ( $\text{kg m}^{-1} \text{s}^{-1}$ ) at the source. The maps are in a comparative study of dust in section 5.1.2. Large dust emission and flux are seen during pre-monsoon, especially in JJA. It is noticed that the emission sources in MAM were higher in northern India and are well spatially distributed in Northern India. While in JJA dust is high, dust emissions are in the central-north and north-western part of India. Winter was found to have low AOD due to low dust flux.



A3 1 Seasonal dust extinction at 550 nm and dust flux(a) MAM (b) JJA (c) SON (d) DJF

## APPENDIX - IV

Data Sources/ Acknowledgements:

Dataset	Source
<b>Koppen Classification</b>	(Beck et al., 2018)
<b>Wind data</b>	Global Modeling and Assimilation Office (GMAO) (2015), MERRA-2 tavgM_2d_slv_Nx: 2d,Monthly mean,Time-Averaged,Single-Level,Assimilation,Single-Level Diagnostics V5.12.4, Greenbelt, MD, USA, Goddard Earth Sciences Data and Information Services Center (GES DISC), Accessed: 15-07-2021, <a href="https://doi.org/10.5067/AP1B0BA5PD2K">10.5067/AP1B0BA5PD2K</a>
<b>Precipitation data</b>	Global Modeling and Assimilation Office (GMAO) (2015), MERRA-2 tavgM_2d_flux_Nx: 2d,Monthly mean,Time-Averaged,Single-Level,Assimilation,Surface Flux Diagnostics V5.12.4, Greenbelt, MD, USA, Goddard Earth Sciences Data and Information Services Center (GES DISC), Accessed: 15-07-2021, <a href="https://doi.org/10.5067/0JRLVL8YV2Y4">10.5067/0JRLVL8YV2Y4</a>
<b>Dust Flux data</b>	Global Modeling and Assimilation Office (GMAO) (2015), MERRA-2 tavgM_2d_flux_Nx: 2d,Monthly mean,Time-Averaged,Single-Level,Assimilation,Surface Flux Diagnostics V5.12.4, Greenbelt, MD, USA, Goddard Earth Sciences Data and Information Services Center (GES DISC), Accessed: 15-08-2021, <a href="https://doi.org/10.5067/0JRLVL8YV2Y4">10.5067/0JRLVL8YV2Y4</a>
<b>Aerosol Optical Depth data</b>	Global Modeling and Assimilation Office (GMAO) (2015), MERRA-2 tavgM_2d_aer_Nx: 2d,Monthly mean,Time-averaged,Single-Level,Assimilation,Aerosol Diagnostics V5.12.4, Greenbelt, MD, USA, Goddard Earth Sciences Data and Information Services Center (GES DISC), Accessed: 10-07-2021, <a href="https://doi.org/10.5067/FH9A0MLJPC7N">10.5067/FH9A0MLJPC7N</a>
<b>CALIPSO</b>	( <i>CALIPSO - Data File Ordering Web Tool - By Data Month</i> , n.d.)
<b>HYSPLIT</b>	(Rolph et al., 2017; Stein et al., 2015)

I gratefully acknowledge NASA Langley Research Centre Atmospheric Science Data Centre for the CALIPSO data, GES-DISC Interactive Online Visualization and Analysis Infrastructure (Giovanni) for providing the MERRA-2 data and NOAA Air Resources Laboratory (ARL) for the provision of the HYSPLIT transport and dispersion model and/or READY website.